Thermal and Hydraulic Characterization of Arrays of Hook-Shaped Fins and Cavities for Enhancing Convective Heat Transfer

Omar Khaled Mohamed Khaled

A THESIS SUBMITTED TO THE FACULTY OF GRADUATE STUDIES
IN PARTIAL FULFILLMENT OF THE REQUIREMENTS
FOR THE DEGREE OF MASTER OF APPLIED SCIENCE

GRADUATE PROGRAM IN MECHANICAL ENGINEERING
YORK UNIVERSITY
TORONTO, ONTARIO
August 2022

© Omar Khaled, 2022

ABSTRACT

A popular method for augmenting convective heat transfer from surfaces is altering the flow field by adding extended features (fins) and/or cavities (dimples). The size, shape, interfin spacings and configuration of these arrays play a crucial role in their performance. Many studies have investigated ways to leverage novel manufacturing techniques to create different fin shapes to improve thermal-fluidic performance. NUCAP Industries has developed a technology that creates a unique array of hook-shaped raised features (hooks) and cavities (dimples) on metal surfaces (GRIPMetal). However, understanding the associated thermal and hydraulic performances of these newly developed arrays represents a distinct technical gap. Consequently, the primary objective of this work is to develop models and design tools that will allow engineers to design these GRIPMetal arrays with the optimum performance fitted into each application. This will be addressed through three specific objectives with a synergistic combination of experimentations and numerical simulations. First, the enhancement in heat transfer and the associated pressure drop for rectangular channels fitted with typical GRIPMetal designs is accurately quantified through experimentations. Two distinct testing facilities were designed, open-circuit wind tunnel and closed fluid loop, and constructed to carry out these experiments employing air and water as working fluids. The outcome of these experiments demonstrated that the presence of GRIPMetal arrays in rectangular channels promotes the convective heat transfer when compared to flat surfaces, however, with an inevitable increase in the required pumping power. The magnitude of the enhancement depends on the flow rate, tunnel height with respect to the hooks height but not the interfin spacings between hooks and their size. Nevertheless, more comprehensive investigations are required to complete the performance map of these arrays. Second, the overall Nusselt numbers and friction factors were calculated for the arrays, and empirical correlations were developed through nonlinear multivariable regression to act as design tools for fitting these arrays into real-life applications. Finally, a numerical model is developed using a commercially available CFD software package to simulate the flow across these arrays. The model will aid in providing better insight of the fluid flow and heat transfer characteristics associated with these unique arrays. Then consequently, optimizing their performance by exploring a wider range of geometrical configurations. The model was validated against the data obtained from the closed fluid loop. The model underpredicted the heat transfer from the array, while it overpredicted the incurred pressure

drop; predictions worsen at higher Reynolds numbers. This is attributed to the incorrect resolving of the boundary layer and the lower estimation of turbulence intensity in the array as well as the distinction between the actual manufactured array geometry and the developed computational model. A spatial variation in the heat transfer coefficient of the array was concluded from the velocity and temperature distributions of the fluid flow.

ACKNOWLEDGMENTS

In the name of Allah, the Beneficent, the Merciful

All praise is due to Allah, the Lord of the Worlds

This fulfilment of this thesis would have been impossible without the support of my supervisor, committee members, colleagues, family, and friends. I would like to take this opportunity to express my genuine gratitude to all of them for their continuous support.

First, I would like to express my sincere appreciation to my supervisor, Professor Roger Kempers for his support, guidance, and motivation throughout the previous two years. He is my primary resource for getting helpful insights and for answering my research questions. I have gained so much technical knowledge from Prof. Kempers, as well as how to be well-organized and work hard, efficient, and smart. I have been fortunate and honored to be one of his lab members. Thank you for your investment in my personal growth!

I also gratefully acknowledge the support of NUCAP Industries team; John Swift, Nghi Pham and Ray Arbesman in fabricating the testing samples and extracting the dimensional parameters of the arrays.

The work of this thesis would not have been possible without the help of my colleague, mentor and friend, Dr. Ahmed Elkholy. He was among the first to welcome me in Canada, he gave me a lab tour, introduced all equipment/facilities/resources in our lab to me, never hesitated to answer any of my questions, discussed with me every imaginable subject in my research, provided me with tips and so much advice to the best of his knowledge and experience. I look forward to working with you again, and I will always remember the past two years with gratitude for all that you have done for me.

I would like to thank Professor Hossam Sadek for his continuous presence and help at York University, and Yehia Ibrahim without whom I would not have come to York University in the first place.

I am grateful to my colleague and friend in TF-lab, Sinan Olcun, for his continuous support, help and discussions throughout my studies.

I would also like to thank my friends Khaled Youssef, Ahmed Azzam, Menna Elsayed, Aya Elsayed, Mohamed Abdelhamid, Ismail Elkomy, Milad Shakeri Bonab and Kapil Narwal in the mechanical engineering department at York University for making the once an enjoyable place to work and for making Canada feel like home.

I would finally like to thank my beloved wife, Reem Ibrahim, and my parents for their support, patience, and love. They deserve all the credit for the encouragement in carrying out this work. Without all of you, I would not be where I am today, and as such, I am forever grateful.

TABLE OF CONTENTS

LIST OF TABLES

LIST OF FIGURES

NOMENCLATURE

A_b	Base area subjected to the heat flux (m²)
C_h	Clearance between two adjacent rows of hooks (mm)
C	Tip clearance (m)
C_d	Drag coefficient of an array of hooks
C_p	Specific heat capacity of air at the average bulk temperature (J/kgK)
D_h	Hydraulic diameter (m)
f_{Dh}	Friction factor based on the hydraulic diameter
f_h	Friction factor based on the hook height
f_o	Friction factor of flat plate
h_{lm}	Convective heat transfer coefficient based on logarithmic mean temperature (W/m²K)
h_{bulk}	Convective heat transfer coefficient based on average temperature difference (W/m²K)
h	Hook height (mm)
H	Test section channel height (m)
h_{lm}	Heat transfer coefficient (W/m²K)
h_{bulk}	Heat transfer coefficient (W/m²K)
k	Thermal conductivity of air at the average bulk temperature (W/mK)
L_f	Length of the test section (m)
L_c	Characteristic length (m)
L_h	Hook length (mm)
L_g	Groove length (mm)
Nu_{Dh}	Nusselt number based on the hydraulic diameter
Nu_h	Nusselt number based on hook height
Nu_o	Nusselt number of flat plate
ΔP	Pressure drop across the heat sink (Pa)
Pr	Prandtl number of fluid at the average bulk temperature
Q_{loss}	Heat loss rate (W)
Q_{elec}	Electrical input power (W)

R_{loss}	Heat loss resistance (K/W)
Re_a	Reynolds number based on the array velocity
Re	Reynolds number based on inlet velocity
Re^*	Modified Reynolds number for rectangular channels
S_T	Spanwise spacing (mm)
S_L	Streamwise spacing (mm)
ΔT_{lm}	Logarithmic mean temperature difference (K)
ΔT_{bulk}	Average temperature difference between the surface and the air (K)
T_i	Fluid inlet bulk temperature (°C)
T_o	Fluid outlet bulk temperature (°C)
$T_{s,avg}$	Test section average surface temperature (°C)
$T_{s,i}$	Test section inlet surface temperature (°C)
$T_{s,o}$	Test section outlet surface temperature (°C)
T_{amb}	Ambient temperature (°C)
V_a	Array velocity (m/s)
V_{in}	Mean inlet velocity (m/s)
$\dot{V}$	Flow rate (m^3/s)
W_h	Hook width (mm)
W	Test section channel width (mm)
ρ	Density of the of fluid at the average bulk temperature (kg/m^3)
μ	Dynamic viscosity of fluid at the average bulk temperature (Pas)
η	Thermal performance factor

Chapter 1 INTRODUCTION

1.1 Power electronics cooling

According to the International Energy Agency (IEA) and the US Energy Information Administration (EIA), the global energy consumption has almost tripled since 1975, although the world's population has just increased by 75~80 %. In 2019, the total consumption of the world reached 23,788 TWh. This can be attributed to the advent of the digital revolution, also known as "Third Industrial Revolution", that occurred in the latter half of the 20th century, in which traditional manufacturing and industrial processes have been largely automated, leading to significantly higher energy demands. Also, the growth in the global access of electricity led to the electrification of most aspects of our daily life. All these details exert a considerable burden on the energy production sectors globally.

The technology of power electronics such as insulated gate bipolar transistors (IGBTs), gate turn-off thyristors (GTOs), … etc. can potentially reduce the overall energy consumption and/or increase the efficiency of electrical energy usage. Power electronics can be applied in a broad spectrum of fields such as: renewable energy, smart electrical grid, industrial drives, HVAC, communication, automotive and electrical appliances. However, one of the challenges facing the advancement in power electronics is their thermal management due to the relatively high heat flux dissipating from these electronics and their continuing miniaturization [1–3].

There have been many efforts for mitigating the burden of power electronics cooling through i) developing innovative thermal management techniques and/or ii) enhancement of heat transfer mechanisms. Heat transfer augmentation techniques can be classified into passive and active methods. In active methods, the enhancement is achieved using an external effect, such as electric and magnetic fields, and fluid or surface vibration. Conversely, in passive methods such as surface modification [4–7] microchannels [8,9] and nanofluids, the augmentation is carried out without the need of an external effect.

1.2 Motivation of Research and General Objectives

In passive enhancement techniques, convective heat transfer can be enhanced by altering the flow structure through the addition of arrays of raised features (fins) and/or cavities (dimples) in different configurations and cross-sectional geometries in the flow field. These features serve to both increase the heat transfer surface area and improve fluid mixing through wake shedding and separation of boundary layer resulting in enhancing of the convective heat transfer [10]. These arrays can be implemented in heat sinks and cold plates with air or water as the working fluid.

Arrays of pin fins and/or dimples have been subjected to extensive investigations in the last few decades to not only achieve more enhanced heat transfer but also reduce the pumping power as much as possible. Often, secondary to these thermal-hydraulic objectives, are application-specific requirements such as compactness, cost, mechanical strength, and manufacturability. The most common array was the cylindrical pin fin array for its superior heat transfer performance and ease of manufacturing [11]. In the beginning, the pin fins had relatively large height to diameter ratio (h/D) i.e. $h/D > 4$, however, more recently, with the benefit of microfabrication technologies the geometrical features of the pin fins were shrunk to be just few millimeters and even further to the microscale for cooling applications within compact spaces, such as electronics and turbine cooling [12]. Owing to the high pressure drop of the array of cylindrical pin fins, many efforts were exerted as an attempt to optimize the performance of these arrays by examining novel pin fin cross-sections, different configurations and combining pin fins and dimples in single array.

From this basis, NUCAP Industries has developed a technology to fabricate a novel array of hook-shaped fins and dimples on metal surfaces (trademarked as GRIPMetal) that has shown potential to emerge as an excellent convective heat transfer enhancement technique by offering increased heat transfer surface area and improving the mixing of the fluid. However, the main challenge to design optimized, application-specific cooling technologies which leverage these novel arrays is the lack of appropriate design tools or correlations that can predict heat transfer rates as a function of flow conditions and geometric parameters of the array. In addition, there is a poor fundamental understanding of the thermal and hydraulic behavior of these arrays. Therefore, the overarching objective of this work is to develop models and design tools that will allow engineers to design these GRIPMetal arrays with the optimum performance fitted into each application. This will be

addressed through three specific objectives with a synergistic combination of experimentations and numerical simulations as follows:

i. Accurately quantify the enhancement in heat transfer and the accompanied pressure drop for rectangular channels fitted with typical GRIPMetal designs employing different working fluids.
ii. Develop design tools such as correlations and/or charts which can be used to design GRIPMetal-enhanced surfaces for specific heat exchange requirements.
iii. Develop and validate numerical models which can be used to optimize GRIPMetal performance by exploring a wider range of geometrical configurations and provide a better understanding of fluid flow and heat transfer associated with these unique features.

1.3 Thesis Layout

This thesis is divided into six chapters. Following this brief introduction and relevant background information in Chapter 1, Chapter 2 provides a comprehensive review of the relevant literature that includes the investigations of fin arrays and a description of the most recent advances in the development of new fin/dimples geometries to enhance the performance of these arrays for convective heat transfer. In addition, a detailed description of the proposed GRIPMetal arrays with the definition and values of their geometrical parameters.

Chapter 3 details an experimental investigation of the heat transfer and pressure drop characteristics of rectangular channels with GRIPMetal surfaces and compares their performance to flat plate and existing short pin fin correlations. The tests were conducted through a bespoke open circuit wind tunnel. The tested channels had the arrays applied to their two opposing major walls at different spacings between the hooks tip and the opposing endwall (feature tip clearance). This chapter has been submitted to *Applied Thermal Engineering* as "Thermal Enhancement of Rectangular Channels using Hook-Shaped Fins and Dimples" and is under review.

Chapter 4 describes the design and the fabrication of a high-accuracy closed water loop which has wide operating-range. It allows for flow visualization and the characterization of convective heat transfer coefficient and pressure drop of any surfaces for their application in liquid cooling. This apparatus was used to investigate the heat transfer and pressure drop characteristics of rectangular

channels with the same arrays. In this experiment the arrays of hooks were only applied to single wall of the channel at different tip clearances than tested in Chapter 3. This apparatus was employed to study the effect of changing the fluid properties (represented in Prandtl number) on the thermal-hydraulic performance.

Chapter 5 presents the details of the numerical model developed using SOLIDWORKS Flow Simulation software package and the validation procedure of the model against the experimental results from Chapter 4.

Finally, Chapter 6 summarizes the main conclusions and outcomes of this thesis and outlines some directions for future work.

Chapter 2 Literature Review

This chapter presents a critical review of the relevant literature related to convective heat transfer enhancement using arrays of fins. The first section of this chapter details the distinction between short and long pin fins. This is followed by sections focusing on the theoretical work that has been published with regards to the thermal and the hydrodynamic performances of various geometries of fin arrays. The final section will explain the arrangement of the proposed arrays, their manufacturing, and dimensions.

2.1 Short and Long Fins

Pin fins added to the flow field have been used as a potential technique to enhance heat transfer from surfaces [13–16]. Pin fins can be classified into short and long fins, with short pin fins classified as having pin-height-to-diameter ratios, *h/D*, of between 0.5 and 4, while long pin fins have *h/D* of more than 4.

Flow over long cylindrical fins (infinite tubes) i.e. $h/D > 4$ was first studied by [17–19]. Heat transfer from these long pin fins was observed to be from the cylindrical surfaces of the fins themselves rather than transfer the endwalls. In contrast to long fins arrays where heat transfer from endwalls is relatively negligible, the short pin fins arrays exhibit endwall heat transfer that is comparable to the heat transfer from the fins themselves [20–22]. The heat transfer from these endwalls depends strongly on the geometry of the pin fins and their distribution [23]. Although it was shown that short pin fins heat transfer is typically lower than that of long pin fins [20,24–26], short pin fins are commonly used for cooling applications in compact spaces such as gas turbines, cooling of electronics, and aerospace applications [27].

The addition of short pin fins enhances the heat transfer of surfaces in two ways: i) they increase the heat transfer surface area, ii) they produce horseshoe vortices on the upstream endwall of the pin fin and wake vortices downstream which subsequently generate high turbulence and mixing [28]. Horseshoe vortices break up the boundary layer on the endwalls and produce high shear stress beneath it that produces high heat transfer region upstream of the pin fin [23]. For short pin fins, the additional area contribution to heat transfer improvement is relatively low and the fluid mixing

component is the dominant factor. Consequently, the correlations that represent the heat transfer and the pressure drop for the long pin fins are not suitable for the short pin fins [20].

In the last few decades, heat transfer and pressure drop performance of the flow over arrays of short pin fins have been the subject of extensive investigation to better understand their flow characteristics. Experiments have been conducted to get insight into the role of i) pin fins arrangement in the array, ii) spanwise and streamwise spacings between the fins, iii) tip clearances and iv) different shapes of pin fin cross-section on the fluid mixing and hence the heat transfer and pressure drop characteristics.

2.2 Effect of Geometrical Arrangement

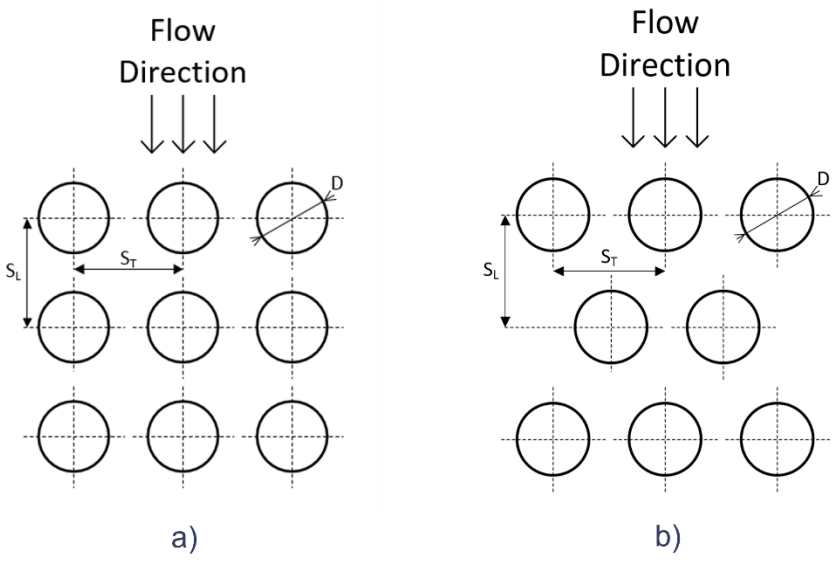

Figure 2-1 Schematic of different types of arrays; a) In-line b) Staggered

Pin fins arrays might be staggered, or in-line as shown in Figure 2-1. The flow behaviour across them is different and consequently, they exhibit different thermal and hydrodynamic performances. Sparrow et al. [29] showed that a staggered arrangement of fins generally has better heat transfer capabilities and greater pressure drop penalty than in-line arrays; this difference increases as the pin-height-to-diameter ratio, *h/D*, increases. Then he concluded that in-line array transfers more heat at fixed pumping power and surface area, while the staggered array minimizes the surface area at a fixed flow rate. Chyu [21] conducted experiments using naphthalene

sublimation mass transfer technique rather than heat transfer to study the effect of pin fin array configurations (in-line and staggered) on heat transfer and pressure drop. The heat transfer coefficients for the arrays were obtained through the analogy between heat transfer and mass transfer. His results reveals that the array-averaged heat transfer for staggered arrays is higher than that of in-line array by 13%. In addition, the friction factor for the staggered array is found to be 1.5~2 times that for the in-line array. Also, the streamwise row-by-row heat transfer variation shows the general trend of heat transfer coefficient is to increase reaching a maximum, and then decreases toward a fully developed value. This maximum occurs at those rows having the first direct wake shedding, i.e., second row for the in-line array and third row for the staggered array.

2.3 Effect of Streamwise and Spanwise Spacings

Metzger et al. [25] experimentally investigated the variation of heat transfer for short pin fins arrays with different streamwise spacings (S_L/D = 2.5 & S_L/D = 1.5). Their results showed that the average heat transfer is higher for the smaller streamwise pin spacing by 5 %. Lawson et al. [30] and Ferster et al. [31] demonstrated that heat transfer augmentation depends more on the streamwise spacing, S_L, than the spanwise spacing, S_T, while the opposite is true for pressure drop. They also concluded that to increase heat transfer with the lowest pressure drop penalty, streamwise spacings should be minimized and spanwise spacing should be maximized. This was consistent with the findings of Lyall et al. [32] which indicate that increasing the spanwise spacing decreases the pressure drop for a single row array.

2.4 Effect of Tip Clearance

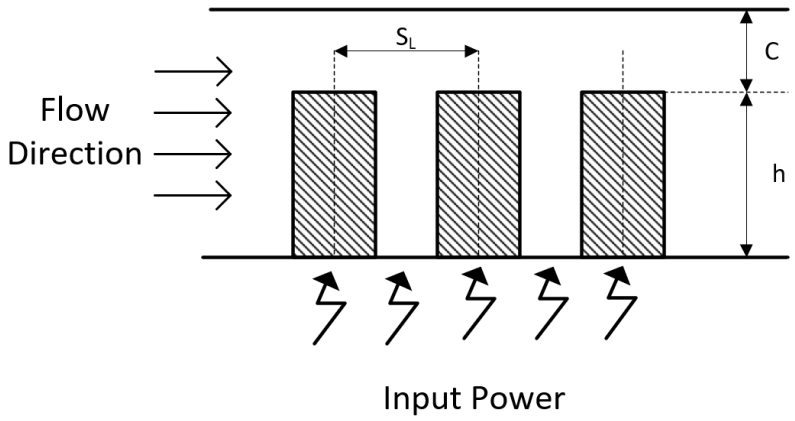

Figure 2-2 Flow over pin-fin channel with tip clearance

Sparrow and Kadle [33] were the first to investigate the effect of introducing a tip clearance on the heat transfer of a longitudinal fin array. They concluded that for clearance-to-fin-height ratios, *C/h*, of 0.1, 0.2 and 0.3, the heat transfer decreased by 15%, 26%, and 36%, respectively, when compared with the no-clearance case. Garimella and Eibeck [34] tested the effect of tip clearance-to-fin-height ratio on the heat transfer and pressure drop characteristics of rectangular pin fins. Their results show that heat transfer decreases with increasing tip clearance and becomes independent of *Re* at high values of *C/h*. Jubran et al. [35] experimentally investigated the effect of inter-fin spacing and tip clearance on the heat transfer from in-line and staggered circular pin fin arrays. They discovered that the staggered array has a greater heat transfer rate, regardless of the value of the tip clearance, and increasing the tip clearance to equal the fin height results in a 40% reduction in heat transfer compared with the no-clearance case. The effect of tip clearance atop of in-line short square pin fins array on the heat transfer is experimentally investigated by Chyu et al. [36] They found that the pin fin heat transfer is 14% and 9% higher for $C/h = 0.25$ and 0.5, respectively when compared to $C/h = 0$ case. While it is 4% and 36% lower for $C/h = 1$ and 2, respectively. Although the heat transfer from the whole array (pin fins + endwalls) when $C/h = 0.25$ is only 7% lower than $C/h = 0$ case, the introduction of a gap might reduce the pressure drop point incurred by the array. Thus, enhancing the overall performance of the array. Moores and Joshi [37] examined the effect of tip clearance for a liquid-cooled array of circular pins fins. They

concluded that low tip clearance values (C/h = 0 to 0.25) enhance heat transfer due to the additional heat transfer area added from the tips. Siw et al. [38] experimentally studied a staggered array of pin fins with different tip clearances of C/h = 0, 1/3, and 1. Unlike the previous mentioned studies the pin fins were applied to both endwalls. Their results showed that the C/h = 1/3 exhibit the highest heat transfer augmentation among all the cases, which is 15% higher than C/h = 0. Accompanied with this, there was a reduction in the pressure drop by approximately 30–35% for C/h = 1/3 when compared to C/h = 0.

The authors of [36–39] suggest that tip clearances generate three-dimensional vortices at the tips that promote mixing, and provide additional heat transfer area, thereby enhancing heat transfer. More recently, Tabkhi et al. [40] experimentally and numerically showed that the presence of tip clearance significantly enhances heat transfer in the wake region through improving the three dimensionality of the vortices downstream of the fin and shortening the wake region.

2.5 Effect of Cross-Sectional Shape

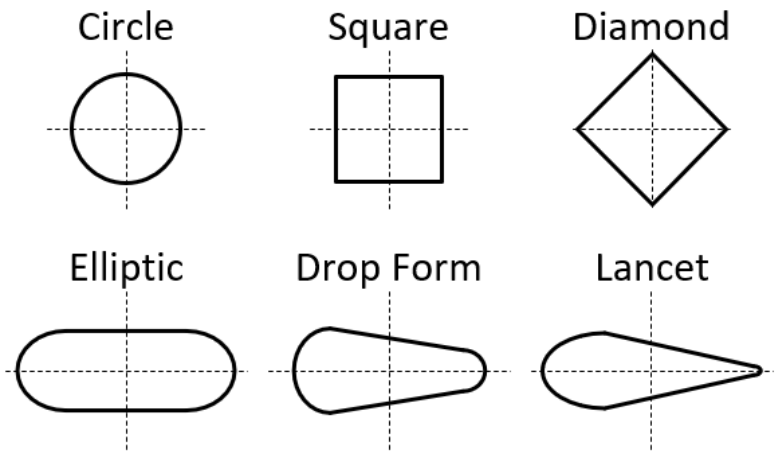

Figure 2-3 Typical pin fins cross-sectional shapes

Much effort has also gone into exploring the cross-sectional shapes of pin fins to optimize the performance of these arrays beyond those of circular pins. Metzger et al. [41] experimentally compared the heat transfer and pressure drop characteristics of circular and oblong pin fins with

varying angles of attack. They showed that the heat transfer of oblong pin fins is higher than that of the circular pins by a maximum of 20% but at the expense of having double the pressure drop. Similarly, Chyu et al. [42] studied an array of cubic/diamond fins using the naphthalene sublimation technique and heat/mass transfer analogy. They found that heat transfer for cubic pin fins array is 40% and 80% higher than that of the diamond and the circular arrays, respectively. Utilizing the same naphthalene sublimation technique, Li et al. [43] and Chen et al. [44] characterized the heat transfer and pressure drop from rectangular channel fitted with an array of elliptic and drop-shaped pin fins, respectively. Their results showed that the heat transfer from the elliptic pin fins array and the drop-shaped pin fins array are slightly higher than the circular pin fin array tested by Metzger et al. [25],while their pressure drop is 42~55 % lower. Sahiti et al. [45] numerically investigated the influence of several pin fin cross sections (NACA airfoil, drop shape, lancet, elliptic, circular, and square) on the heat transfer performance for both staggered and in-line arrays. Their results showed that either the elliptic or the drop-form pin fins are superior to the others depending on the geometrical parameters of the array (pin length, transverse and longitudinal spacings, and coverage ratio). Also, the heat transfer and pressure drop of six different pin fin cross sections (circular, elliptic, oblong, drop-form, NACA, and lancet) in a staggered array were compared experimentally by Xi et al. [46]. They concluded that the circular pin fin had the largest heat transfer but also had the maximum pressure drop penalty when compared with other shapes. The elliptical pin fins showed a superior thermal performance to the others because of their relatively very low pressure drop and moderate heat transfer.

2.6 Concept of Dimples/Hybrid Pin Fin-Dimple Arrays

Arrays of dimples are emerging as a promising passive heat transfer enhancement technique due to their relatively low pressure drop penalty. The dimpled surface was inspired by its usage on golf balls to decrease the flow resistance. Chyu et al. [47] experimentally compared the heat transfer performance from a dimpled rectangular channel and a smooth flat plate. The dimples were circular, and teardrop shaped. Both shapes showed higher heat transfer than that of the smooth plate by a factor of 2.5. The effect of changing dimple shapes on the heat transfer and pressure drop was also experimentally and numerically investigated by Rao et al [48]. Their results showed that heat transfer enhancement is greatly influenced by dimple shape. For instance, the

enhancement for a teardrop-shaped dimple ranged from 1.89 to 2, depending on the *Re* when compared to a smooth flat plate. This enhancement is 18% greater than that of conventional spherical dimples and 28% greater than that of elliptical ones. On the other hand, the pressure drop did not exhibit any dependency on the shape except for the teardrop-shaped dimple for which the friction factor was 1.6–2.3 times the smooth flat plate friction factor. Xie et al. [49] numerically compared the heat transfer characteristics of a rectangular channel with array of hemispherical/teardrop dimples and protrusions. Their results showed that the flow covers the teardrop surface easily and impinge on the rear part with higher energy when compared to the hemispherical surface. This results in 5~10 % more augmentation in the heat transfer for the -shaped arrays than the hemispherical arrays. More recently, Gao et al. [50] experimentally studied both the liquid and vapor flow of R134a over a dimpled flat plate in a rectangular channel. The comparison between the obtained results and a correlation for a flat plate with the same aspect ratio showed that the presence of dimples resulted in multiplying both the friction factor and the Nusselt number by a factor of up to 15.7 and 8.6, respectively. Moon et al. [51] studied the heat transfer and pressure drop characteristics of an array of circular dimples at different channel heights. Their results showed that heat transfer augmentation due to these dimples with respect to a smooth flat plate is approximately constant and equal to 2.1. In addition, both pressure drop and heat transfer are independent of channel height. Rao et al. [52] introduced the concept of hybrid pin fin–dimple arrays which aims to enhance the heat transfer from pin fin arrays through the addition of dimples in the array. They experimentally compared the thermal and the hydraulic performances of pin fin–dimple and pin fin arrays and investigated the effect of dimple depth on the performance. They showed that the presence of dimples improved the heat transfer by up to 19%, depending on the dimple depth and *Re* number, while the friction factor is lowered by 17.6% more for the shallower dimples than for the pin fin arrays.

2.7 Technological Opportunity: GRIPMetal

To summarize the literature, the thermal-hydraulic performance of short pin fins arrays can be enhanced by altering the cross-sectional shape of pin fins, introducing tip clearances, and implementing the concept of hybrid pin/dimple arrays. However, because arrays of short pin fins are millimeter scale, most of these arrays require intensive, complex, time-consuming, and

unreasonably expensive manufacturing processes. From this perspective, NUCAP Industries Inc. has developed a proprietary skiving process which creates unique hook-shaped fins and corresponding dimples/cavities on metal surfaces (trademarked as GRIPMetal). These hook-shaped arrays represent an attractive surface enhancement technique because they are quick and simple to manufacture, have a relatively lower cost and, most importantly, are readily and commercially available in the market. Due to the nature of the skiving process, these fins have a hook shape, heretofore referred to as hooks. These hooks offer increased surface area, enhance the mixing of the fluid, and promote boundary layer separation and three dimensionality of the flow field, which increases convective heat transfer. Also, their dimples increase the endwall mixing of the fluid by generating strong vortex flows.

Arrays of these hooks can be applied to the walls of longitudinal fins of heat sinks or heat exchangers to enhance their heat transfer performance. In addition, a cold plate enhanced with such features could also be an attractive cooling technology for modern power electronics such as IGBTs

2.8 Hook Geometry

The arrays of hooks are manufactured by a skiving process in which they are partially removed material from the metal's surface. Thus, downstream or upstream of each hook there is a dimple/cavity from which the hooks were formed; thus, these dimples have an equal volume to the hooks. Depending on the depth of the tool, its angle of attack, and the stroke length, different hook sizes and arrays can be formed on the surface of a plate. A unit cell of hooks array, shown in Figure 2-4, consists of two groups of hooks and each group has two adjacent hooks. Hooks 1 and 2 are separated by a clearance, C_h, and placed in a staggered arrangement with a streamwise pitch S_L. Hooks 3 and 4 are in the same arrangement as Hooks 1 and 2, but with a reversed orientation and at a spanwise pitch of S_T. Then, the array is formed by creating a rectangular pattern of unit cells in the streamwise and spanwise directions.

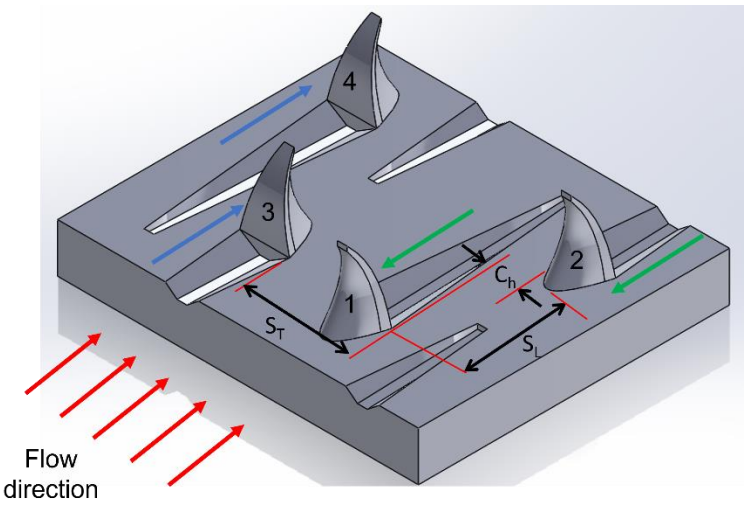

Figure 2-4: A unit cell of a GRIPMetal array of hooks

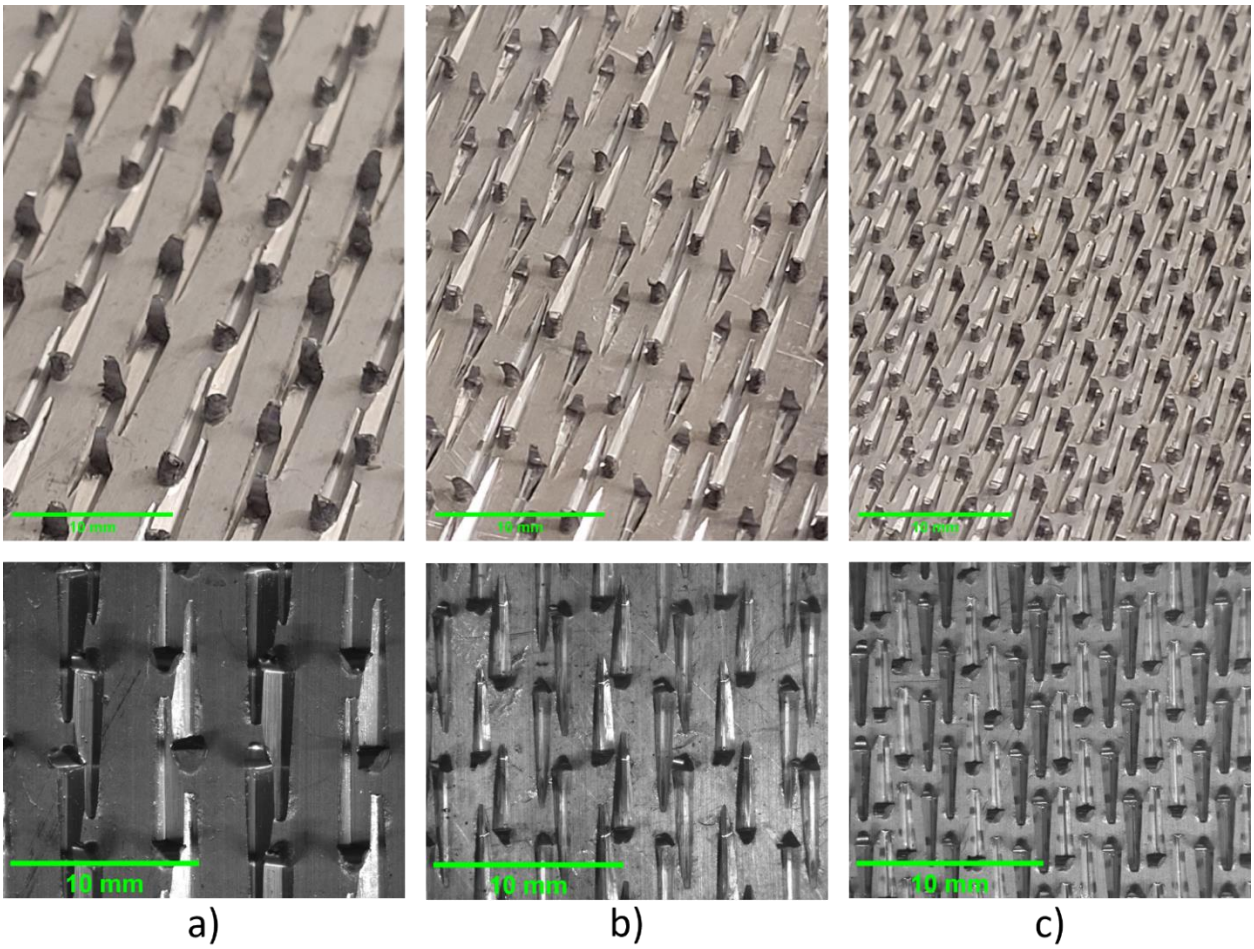

Figure 2-5: Normal and microscopic images for different arrays of hooks: a) Heavy hooks b) Standard hooks c) Mini hooks.

Figure 2-5 shows the three different arrays of hooks that were tested, along with a magnified image for each array. The microscopic images were captured using a Leica MZ10 F stereomicroscope (Leica Microsystems GmbH, Wetzlar, Germany). The averaged normalized values of each array's geometrical parameters (height of hooks, spanwise pitch, streamwise pitch, etc.) are reported in Table 2-1 and explained in Figure 2-6.

Table 2-1: Normalized values of the geometrical parameters for different arrays of hooks

#	Array Name	h (mm)	S_L/h	S_T/h	W_h/h	C_h/h	L_h/h	L_g/h
1	Standard	1.5	2.67	1.49	0.67	0.67	0.55	3.4
2	Mini	1	2.5	1.33	1	1	0.83	3.6
3	Heavy	2.25	1.78	1.69	0.71	0.44	0.67	3.33

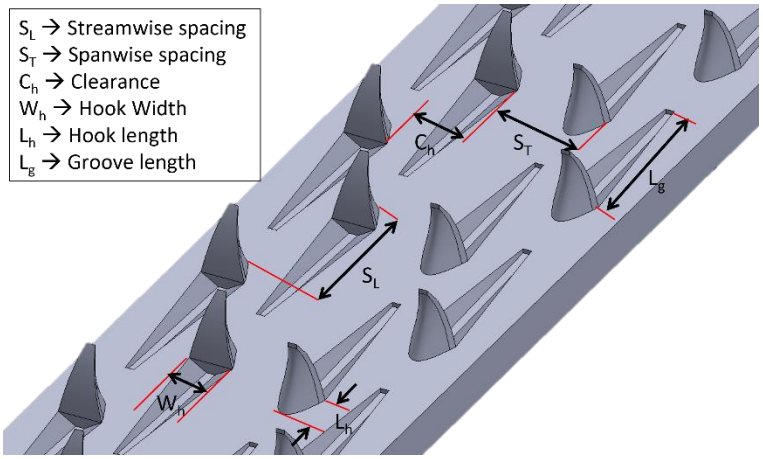

Figure 2-6: Explanation of the geometrical parameters depicted in Table 2-1

Chapter 3 Characterization of the Thermal – Hydraulic performance of Hook-Shaped Fins and Dimples Arrays

This chapter describes the experimental facility and the methodology followed to characterize the heat transfer and pressure drop of various arrays of hooks in a rectangular channel employing air as a working fluid. The rectangular channels in this experiment had the arrays applied to their two opposing major walls (bottom and top walls). The performance of one type of these arrays, Standard hooks array, is compared with that of a flat plate and existing short pin fin/ dimples data in the literature at various values of clearance between the hooks tip and the opposing endwall, *C*, from *h* to 4*h*, where *h* is the hooks height. Then at tip-clearance-to-hooks-height ratio, *C/h*, of 4, two other types of these arrays, named Heavy hooks and Mini hooks, are compared to the Standard hooks to evaluate the impact of changing the arrays geometrical parameters on the performance. Finally, the obtained data is used to develop correlations that can be used to facilitate the design of heat exchangers/heat sinks with these GRIPMetal arrays.

3.1 Experimental Setup (Wind Tunnel)

Forced convection experiments were carried out in an open circuit wind tunnel using compressed air. The tunnel consists of the sections shown in Figure 3-1. First, a diffuser section was connected by a hose to a pressure regulator placed on a compressed air line. This regulator sustains a constant inlet pressure to the tunnel during the experiments and, thus, a constant flowrate for a given Reynolds number. The diffuser had a diverging angle of 15° to minimize the turbulence and prevent flow separation from its walls. Second, a tube bundle section was attached to the diffuser for flow straightening, followed by an orifice setup for flow measuring. Finally, a contraction section was attached upstream of the developing section, which leads to the test section.

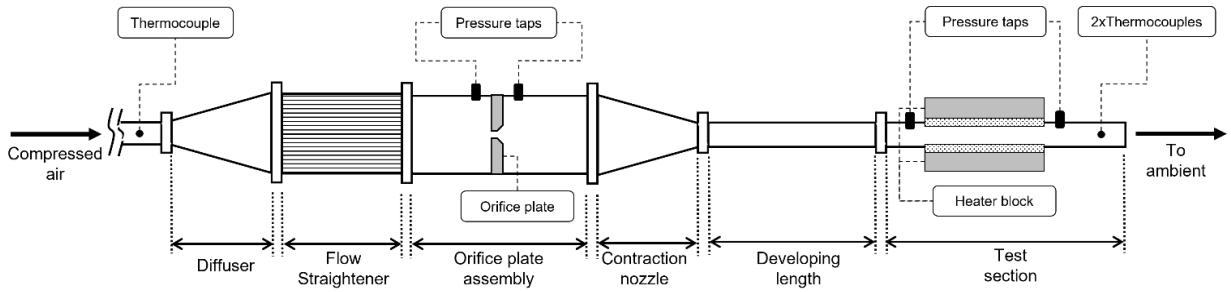

Figure 3-1: Wind tunnel assembly details (not to scale)

The test section is shown in Figure 3-2. Here, the surfaces were tested in pairs; the hooked surfaces formed onto aluminum plates which faced each other to form a rectangular flow channel. Each pair had a different array of hooks (i.e., different geometrical parameters skived on their surfaces), corresponding to the hook arrays in Table 2-1. The plates were 50.8 mm wide and 101.6 mm long and manufactured from 3.175 mm thick Al6061 alloys.

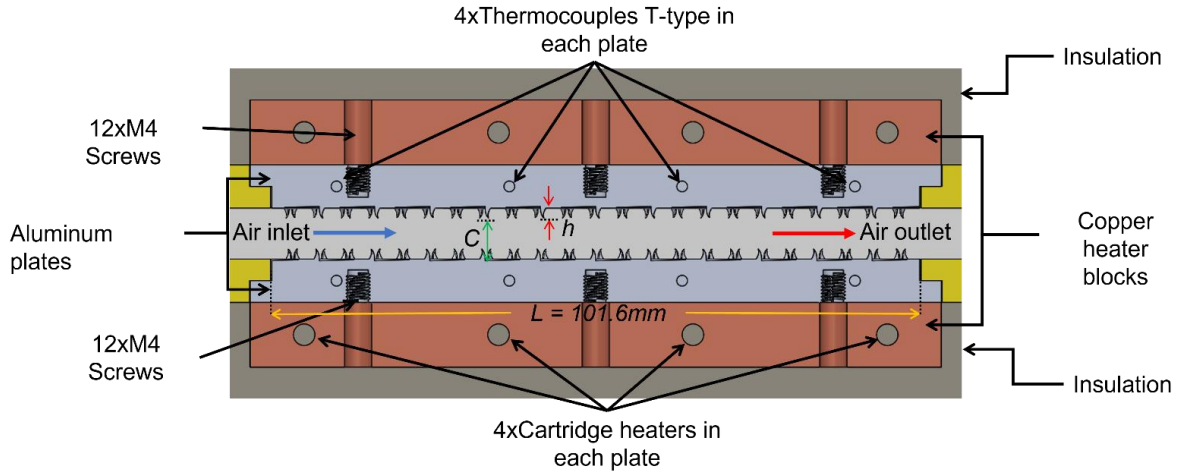

Figure 3-2: Detailed cross section of the test section

Two copper heater blocks each equipped with four 50 W cartridge heaters were mechanically fastened to the base test plates to provide the necessary heat flux. Contact resistance was mitigated by using a thin layer of thermal paste (k=8.5 W/mK) between the copper heater blocks and the aluminum test plates. All the remaining surfaces of the copper blocks were insulated with expanded polystyrene to minimize heat loss to the surroundings. Electrical power was provided to the heaters of each block independently and in equal amounts using a DC power supply (AIM-TTi CPX400DP). The electrical power was controlled such that there was a temperature rise in the

outlet air of 15 K with respect to the inlet (resulting in heat fluxes ranging from 0.19 to 1.9 W/cm²). This temperature difference allowed for sufficient accuracy in the temperature difference between the tested plates and the air and was low enough to minimize thermal property variations in the test section and heat losses to the ambient. The air inlet bulk temperature was approximately 25°C, while the wall temperature ranged from 30°C to 60°C, depending on the type of the surface being tested and the fluid flow rate.

Four 1.6 mm diameter T-type thermocouples were inserted into each aluminum plate 1.6 mm below the surface to measure the surface temperature distribution, as indicated in Figure 3-2. Due to the high thermal conductivity of the aluminum and relatively low heat fluxes, the surface temperature, T_s, of the plate was approximately equal to the thermocouple readings. An additional thermocouple measured inlet air temperature, T_i. At the outlet, two thermocouples, of 0.8 mm diameter, were used to measure the approximate bulk fluid outlet temperature, T_o, and their relative positions are shown in Figure 3-3.

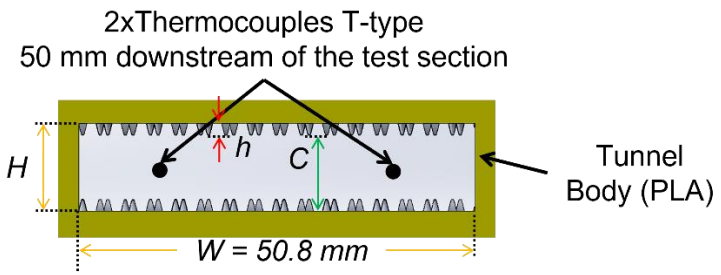

Figure 3-3: Detailed position of the bulk fluid outlet temperature thermocouples

The mass flow rate of the air was quantified using an orifice plate situated downstream of the flow straightener section with properly sized upstream and downstream pipe lengths based on ASME PRC19.5 recommendations and [53]. Pressure taps were located at a distance of 25.4 mm upstream and downstream of the orifice plate and were connected to differential pressure transducers, DPTs, (Amphenol All sensors BLVR series) to measure the pressure difference and calculate mass flow rate. For redundancy, variable area flowmeters were installed upstream of the wind tunnel and downstream of the pressure regulator to measure the volumetric flow rates. The readings from both methods were found to have negligible discrepancy within the measurement's uncertainties.

DPTs were also installed across the test section to measure the pressure drop. Four DPTs (Amphenol All sensors BLVR series) with different ranges of operating pressure were used, depending on the tested array and tunnels height. These DPTs were calibrated against an Omega PX409-001DWUI DPT which had an accuracy of 0.08% of the full scale.

Tests were conducted through a nominal Reynolds number based on the hydraulic diameter, *Re*, ranging from 4,000 to 20,000. Due to the nature of the implemented manufacturing technique, it is impractical to have the hooks of the two plates interdigitated. In addition, as discussed in the literature [37,40] the presence of tip clearance can potentially improve the performance of the array. Therefore, Standard hooks were tested at nominal tip-clearance-to-hooks-height ratio, $C/h = 0, 2, 4$ and 6.5. Then, the other two types of hooks, (i.e., Mini and Heavy hooks) were tested at $C/h = 4$ to evaluate the effect of changing the inter-fin spacings. This was achieved by changing the test section height, *H*, from 1.5 mm to 11.25 mm, according to the type of hooks being tested; this corresponds to an aspect ratio, *H/W*, from 0.03 to 0.22. For comparison, at each test section height, a pair of flat plates was tested.

3.2 Heat Loss Calibration

Before running any test, heat loss to the surroundings was quantified by performing a series of calibration runs with no airflow in the test section. A PID controller was tuned to produce the approximate range of plate temperatures of interest. When steady state was reached, the input power, the average plate temperature, $T_{s,avg}$, and ambient temperature, T_{amb}, were measured so that an overall thermal resistance for the heat loss, R_{loss}, could be anticipated according to

$$Q_{loss} = \frac{\left(T_{s,avg} - T_{amb}\right)}{R_{loss}}. \tag{3-1}$$

Consequently, while running a test, the heat loss from the test section was anticipated according to the measured plate and ambient temperatures using (3-1).

An energy balance was also performed on the test section to compare the energy gained by the air based on the measured temperature rise to that of the input energy introduced to the test section by the heaters minus the heat loss. The error between the two energy values was evaluated. The

average error was found to be 2.9% for all the tested channels except H = 11.25 mm with most of the cases having an error of less than 9%. The highest deviations were found to be for the H = 11.25 mm tunnel due to its relatively low fluid velocity that resulted in poor mixing of the fluid at the outlet and affected the outlet temperature measurements.

3.3 Data Reduction & Uncertainty Analysis

In the current study, it was noted that the streamwise wall temperature gradient did not follow the constant heat flux distribution; instead, the gradient tended to be more isothermal. This behavior was more pronounced at low Nusselt numbers (i.e., low values of *Re* and/or wide tunnels). This can be attributed to the relatively high conductivity of the copper heater block and the aluminum test sections which offer a heat flow path in the axial direction that is an attractive alternative to that offered by the relatively low convection of air [54–60]. This axial conduction in the wall carries substantial amounts of heat in the opposite direction of the fluid flow, which tends to level out the temperature distribution. Therefore, the fluid exhibits a drastic rise in bulk temperature in the first portion of the test section. This is consistent with the findings of Maranzana et al. [56] who state that the bulk temperature profile is not linear. Consequently, the bulk temperature profile between the inlet and the outlet can be approximated to attain an exponential behavior and logarithmic temperature difference ΔT_{lm} which is adopted and calculated as

$$\Delta T_{lm} = \frac{\left(T_{s,in} - T_i\right) - \left(T_{s,o} - T_o\right)}{ln\left(T_{s,in} - T_i\right) - ln\left(T_{s,o} - T_o\right)} \tag{3-2}$$

where $T_{s,in}$ and $T_{s,o}$ are, respectively, the inlet and outlet surface temperatures, obtained by linear extrapolation of the four thermocouple readings of each plate. While T_i and T_o are, respectively, the inlet and outlet air temperature. Then, the overall heat transfer coefficient of an array of hooks, h_{lm}, was calculated for each plate as

$$h_{lm} = \frac{Q_{elec} - Q_{loss}}{A_b \Delta T_{lm}} \tag{3-3}$$

where Q_{elec} denotes the input electrical power to the heaters and A_b is the nominal area (101.6 x 50.8 mm²). This form of h_{lm} reflects the heat transfer characteristics of the array as if there is a heat

source mounted on the flat side of the plate, such as electronic-chip or plate heat exchangers. Finally, the average between the two plates was calculated, noting that the discrepancy between the values of h_{lm} for the two plates were found to be less than 7%.

Another way of calculating the heat transfer coefficient employed in some studies [10,46,61,62] is to average the temperature difference between each thermocouple reading, $T_{s,i}$, for each plate and its corresponding local bulk air temperature, $T_{b,i}$ as

$$\Delta T_{bulk} = \frac{\sum_{i=1}^{4}\left(T_{s,i} - T_{b,i}\right)}{4} \tag{3-4}$$

such that $T_{b,i}$ is calculated by assuming a linear rise of the air temperature along the test section. Then, the heat transfer coefficient, h_{bulk}, is calculated the same as h_{lm}, but replacing ΔT_{lm} with ΔT_{bulk} such that

$$h_{bulk} = \frac{Q_{elec} - Q_{loss}}{A_b \Delta T_{bulk}}. \tag{3-5}$$

The average difference between the calculated values of the heat transfer coefficient using the two methods is 5%; thus, only the first one is reported in this study.

It is common to present heat transfer results in the dimensionless form of a Nusselt number, Nu,

$$Nu = \frac{h_{lm}\, L_c}{k} \tag{3-6}$$

where k is the thermal conductivity of air at bulk temperature, which is equal to 0.0257 W/mK, while L_c is the characteristic length, which is either the fin height, h, or the hydraulic diameter of the channel, D_h, computed as

$$D_h = \frac{2(HW)}{H + W} \tag{3-7}$$

where H and W are the height and the width of the test section channel.

To characterize the pressure drop, the friction factor f is calculated as

$$f = \frac{2\ \Delta P\ L_c}{L_f\ V_{in}^2\ \rho} \tag{3-8}$$

where ρ is the density of air at bulk temperature, which is equal to 1.174 kg/m^3, ΔP is the difference across the test section measured by the DPT, and V_{in} is the mean inlet velocity to the test section.

Finally, the Reynolds number, *Re*, is calculated as

$$Re = \frac{\rho\ V_{in}\ D_h}{\mu} \tag{3-9}$$

where μ is the dynamic viscosity at air bulk temperature, which is equal to 1.861e^{-5} Pas.

For a comprehensive assessment of both heat transfer and pressure drop characteristics of the hooks compared to those of the flat plate, the overall thermal performance η (proposed by Gee and Webb [63]) is evaluated as

$$\eta = \frac{\left(Nu_{D_h}/Nu_o\right)}{\left(f_{D_h}/f_o\right)^{1/3}} \tag{3-10}$$

where Nu_o and f_o are the Nusselt number and the friction factor based on D_h for flat surfaces, respectively, and Nu_{Dh} and f_{Dh} are the Nusselt number and the friction factor based on D_h for channels with hooks, respectively.

The uncertainty in each parameter is evaluated based on the propagation method proposed by Kline and McClintock [64]. It was found that the maximum uncertainty in *Re* was 17%. This occurred at low flow rates and narrow channels, while at higher flow rates and wide channels the uncertainty was lower than 4%. For *f*, the maximum uncertainty at wide channels and low flow rates was up to 60% and the minimum was 8%. Regarding the *Nu*, the maximum uncertainty was 3%.

3.4 Results

3.4.1 Comparison of Flat Plate to Correlations

Figure 3-4 compares heat transfer results for flat surfaces at different channel heights with two different correlations for turbulent heat transfer in a duct. The first correlation is the well-known Dittus–Boelter correlation [65] given by

$$Nu = 0.023\, Re^{0.8} Pr^{0.4}. \tag{3-11}$$

The correlation is then multiplied by a correction factor to account for the thermally developing flow [20,66] as

$$Nu = 0.023\, Re^{0.8} Pr^{0.4} \left[1.11 \left(\frac{Re^{0.2}}{\left({}^{L}/_{D_h} \right)^{0.8}} \right)^{0.275} \right] \tag{3-12}$$

for $L/L_d < 1$ and

$$Nu = 0.023\, Re^{0.8} Pr^{0.4} \left[1 + \frac{0.144\, Re^{0.25}}{{}^{L}/_{D_h}} \right] \tag{3-13}$$

for $L/L_d > 1$ and such that L_d is the developing length given by

$$L_d = 0.693\, Re^{0.25} D_h. \tag{3-14}$$

The second correlation for comparison is the Petukhov correlation, modified by Gnielinski [27,28]:

$$Nu = \left(\frac{{}^{f}/_{8} * (Re - 1000) * Pr}{1 + 12.7 \sqrt{{}^{f}/_{8}} * (Pr^{{}^{2}/_{3}} - 1)} \right) \left(1 + \frac{D_h}{L}^{{}^{2}/_{3}} \right) \tag{3-15}$$

where the friction factor, *f*, is calculated by Haaland correlation [69] given by

$$\frac{1}{\sqrt{f}} = -1.8\log\left(\left[\frac{\varepsilon/D_h}{3.7}\right]^{1.11} + \frac{6.9}{Re^*}\right) \tag{3-16}$$

such that *Re** is the modified Reynolds number proposed by Jones [70] to ensure a geometrical similarity between circular ducts and rectangular channels in calculating the friction factor given by

$$Re^* = \left[\frac{2}{3} + \frac{11H}{24W}\left(2 - \frac{H}{W}\right)\right] Re. \tag{3-17}$$

The experimental results for H=3 mm spacing agrees well with the corrected Dittus–Boelter correlation and deviates from the Gnielinski correlation by only 8% to 16%. For channels H=7.5 mm and 11.25 mm, the experimental *Nu* values are almost equal over the whole range of *Re* which is in good agreement with the corrected Dittus–Boelter correlation. We conjecture that this is mainly because the flow is thermally developing over the flat plates for those channels. The H=3 mm channel has a thermally developing region that ranges from 30% to 45% of the plate length depending on *Re*; hence, it shows lower *Nu* than the other channels.

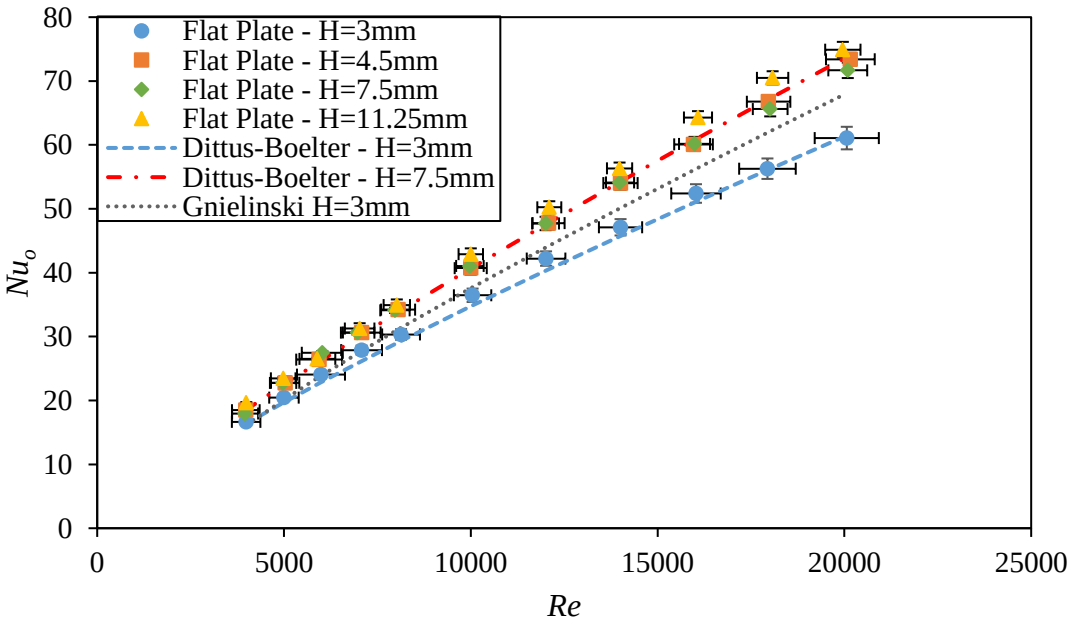

Figure 3-4: Comparison of current facility's flat plate Nu number with correlations (3-11) & (3-15)

Figure 3-5 compares the friction factor results for flat surfaces at two different channel heights with the Haaland correlation. The discrepancy between the experimental results and the correlation is 6%–11% within the *Re* range. For the H=4.5 mm channel, the correlation overpredicted the friction factor. While for the H= 3mm channel, the correlation underpredicted the friction factor. We attribute this to the relatively large uncertainties in the velocity measurements, the characteristic dimension of the relatively small channel, and the roughness of the channel walls. In addition, the very high-aspect ratio of the rectangular channels increases the friction factor beyond the flat-plate correlation. Overall, the heat transfer and pressure loss measurements for the flat plates are reasonable given the high-aspect ratio channel shape and thermally developing region for large spacings.

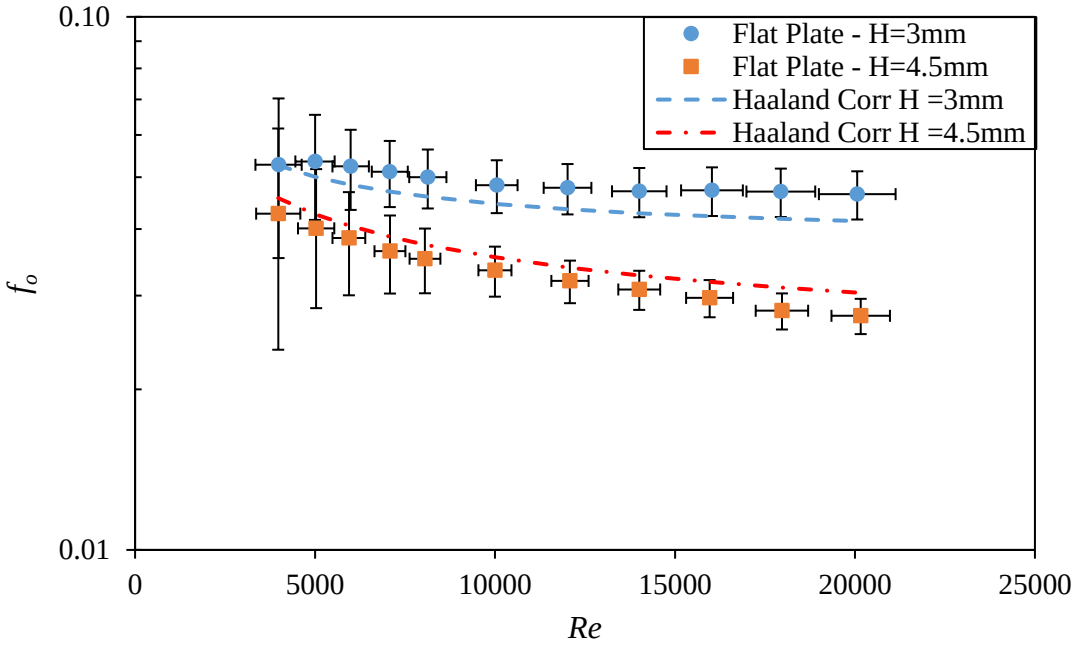

Figure 3-5: Comparison of current facility's flat plate friction factor with correlation (3-16)

3.4.2 Effect of Tip Clearance

The variation of Nusselt number of the GRIPMetal Standard hooks array with *Re* for the four tip clearances is shown in Figure 3-6.It is seen that Nu_h decreases with increasing tip-clearance-to-hooks-height ratio, *C/h*, at any given *Re*. This is primarily for two reasons: i) the increase in *C/h* is achieved by increasing the channel height, thus lowering the approach velocity at the same *Re*; ii)

increasing *C/h* creates a lower resistance path for the flow; consequently, more flow will bypass the array, resulting in the array being washed by lower velocity flow. For all cases, Nu_h follows an increasing trend with *Re*. It should also be noted that with increasing *C/h*, the Nu_h becomes less dependent on *Re*, and it tends to reach an asymptotic value. This indicates that at relatively high *C/h* the hooks represents boundary layer roughness that enhances the heat transfer; this is consistent with the findings of Garimella and Eibeck [34]

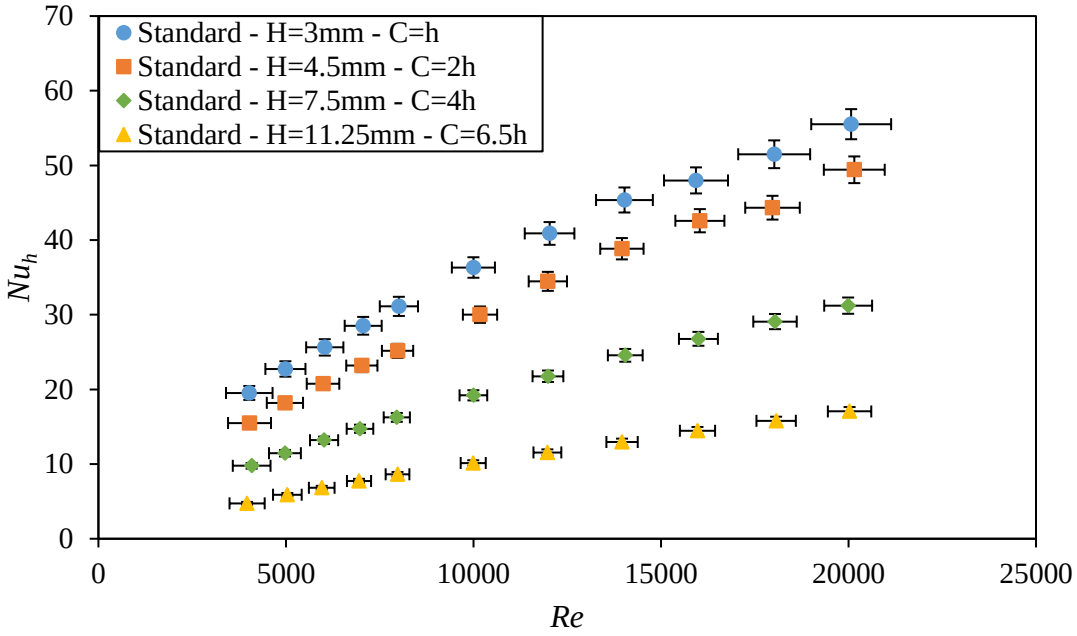

Figure 3-6:Nu_h vs Re for rectangular channels with array of Standard hooks at different values of C/h

Figure 3-7 shows the ratio between the hydraulic diameter Nusselt number, Nu_{Dh}, for GRIPMetal Standard hooks array and Nusselt number for flat plate, Nu_o, at different tip-clearance-to-hooks-height ratios. At each tip clearance, a comparison is carried out against the flat plate at the same channel height. Thus, the hydraulic diameter is the constant for any given channel. Therefore, this ratio represents the heat transfer augmentation factor due to the presence of the array of hooks. This augmentation is due to i) the addition of more heat transfer surface area which is 20~25% more than the flat plate area, and ii) the enhanced fluid mixing and the promoted boundary layer separation. This ratio is greater than unity for all tested channels, indicating that the presence of these arrays enhanced the heat transfer. Based on the literature, we conjecture that this enhancement can be attributed to the occurrence of the following phenomena in the flow field

[28,38,71–73]: i) the presence of horseshoe vortices at the hook–endwall junction upstream of the hook that enhances three-dimensional advection in the flow, ii) the existence of secondary flows due to the vortex pairs shedding from two transverse rims of the dimple which increases the turbulence mixing intensity near the endwall downstream of the dimple, iii) the flow attachment and impingement in the trailing rim of the dimple, and iv) the promotion of turbulence mixing in the main bulk flow due to the shear layers separated from the tip of the hooks.

Except for *C/h* = 6.5, this ratio is the highest at low *Re*; then, it decreases with increasing *Re* approaching an asymptotic value. This occurs as the flow regime over the flat plate changes from transition to fully turbulent, i.e., increasing the heat transfer capability of the flat plates. Maximum enhancement in heat transfer is found for the *C/h* = 2 and *C/h* = 4 cases, with a factor of 4.6 at low flow rates and 3.75 at higher flow rates. The *C/h* = 1 case shows a slightly lower augmentation factor than the two latter cases; the factor is 4.45 and 3.45 at low and high flow rates, respectively. For *C/h* = 6.5, the flow sees the array of hooks as boundary layer roughness, i.e., at such relatively high clearance the plate is acting more like a roughened plate than the benchmark flat plate. Consequently, the augmentation factor maintains a relatively constant value of 3, regardless of the *Re*. This represents the lowest enhancement for all tested tip clearances, as expected.

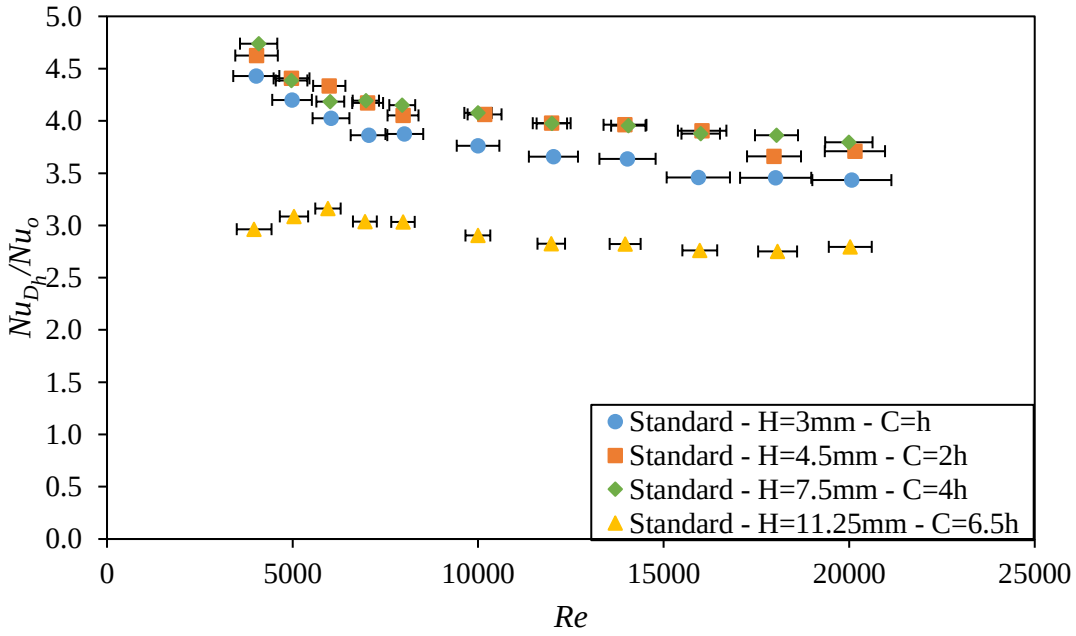

Figure 3-7: Nu_h / Nu_o vs Re for rectangular channels with array of Standard hooks at different values of C/h

Figure 3-8 depicts the friction factor, f_h, for GRIPMetal Standard hooks array with varying the tip clearance at different *Re*. Over the whole range of *Re*, the channel with $C/h = 1$ shows the greatest friction factor. This is logical because in this case the two opposing hooks are touching at the tips (i.e., no gap is present between the two hooks for flow). Therefore, the fluid is forced to flow entirely through the hooks array itself, which imposes very high restriction. In addition, the small channel height requires relatively high velocities to achieve the same *Re* when compared to other cases. As a result, the velocity of the flow within the array is very high, producing more frictional losses. That is why the friction factor for this case follows a declining trend with *Re* because the frictional losses are dominant. On the other hand, the f_h values for the remaining arrays are much lower than the $C/h = 1$ case and are independent of *Re*. Here, increasing the tip clearance produces a gap with lower resistance to the flow, which consequently lowers the average flow velocities at a given *Re*. In addition, the bypass flow results in a lower velocity flow through the array itself, hence decreasing the skin friction between the hooks and the fluid, and the inertial losses become more significant. The dominance of the inertial losses over the frictional losses is the primary cause of the flattening of these curves [74].

Figure 3-8 also shows the friction factor for a flat plate with a channel height of 11.25 mm, equivalent to the $C/h = 6.5$ case, calculated from Haaland's correlation (3-16), considering the roughness, ε, to be the hook height. The correlation is modified to account for the definition of f_h implemented in this study. The experimental results of f_h for the $C/h = 6.5$ case agree reasonably well with the values obtained from the empirical correlation. This further supports the conjecture that at such high values of *C/h*, the flow considers the array of hooks to be more like boundary layer roughness that increases the friction rather than as raised features.

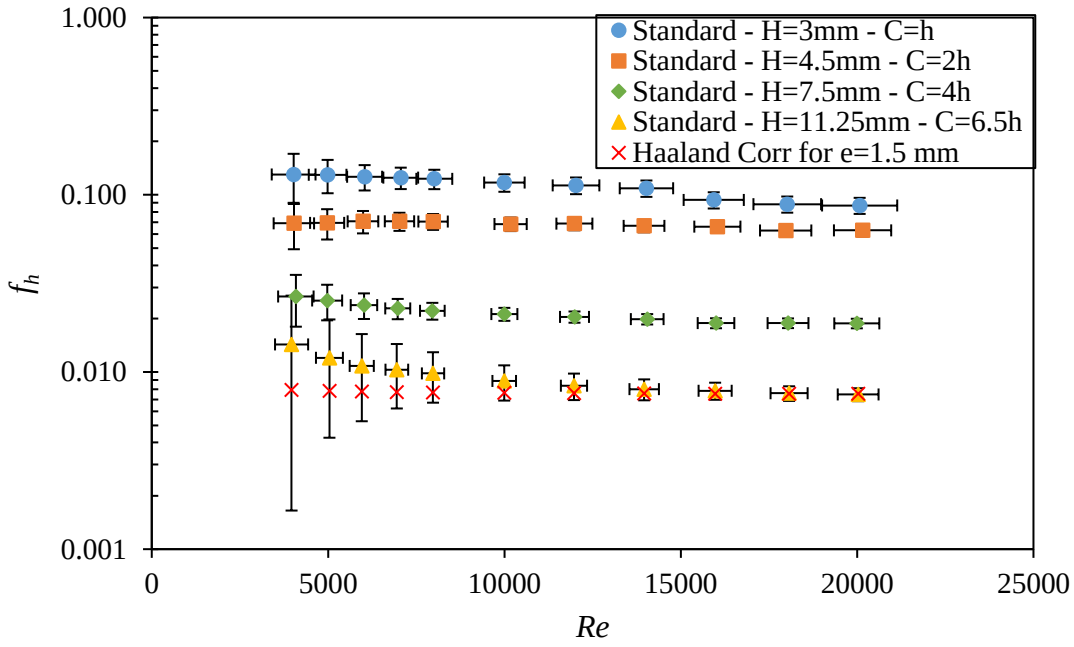

Figure 3-8: f_h vs Re for rectangular channels with array of Standard hooks at different values of C/h

For the final assessment of the performance at different values of tip-clearance-to-hooks-height ratio, the overall thermal performance factor, η, was evaluated (shown in Figure 3-9). According to the plot, within the studied *Re* range, η is independent of the value of *C/h*. In addition, as *Re* increases from 4,000 to 12,000, η gradually decreases from a value of 2.1 to 1.8, after which it also becomes independent of *Re*. Although the *C/h* = 6.5 showed a very low Nu_h compared with the other cases, having a friction factor that is comparable to a flat plate's resulted in the improvement of its thermal performance factor. Having a $\eta > 1$ illustrates that the heat transfer enhancement provided by these arrays outweighs the pressure drop penalty.

One should carefully choose among these tip clearances when implementing them in any given heat exchanger or heat sink application because having the same value of η can be deceiving. For instance, most electronics heat sinks or cold plates impose pressure drop constraints; thus, higher *C/h* values should be used, not lower ones. In this case, using a lower *C/h* value is not appropriate because it will incur a high pressure drop to the flow, lowering the *Re* and hence the Nu_h. On the other hand, choosing the high *C/h* value for its minimum pressure drop will yield a low heat transfer when applied in a particular heat exchanger and, hence, a higher surface temperature that might exceed design limitations.

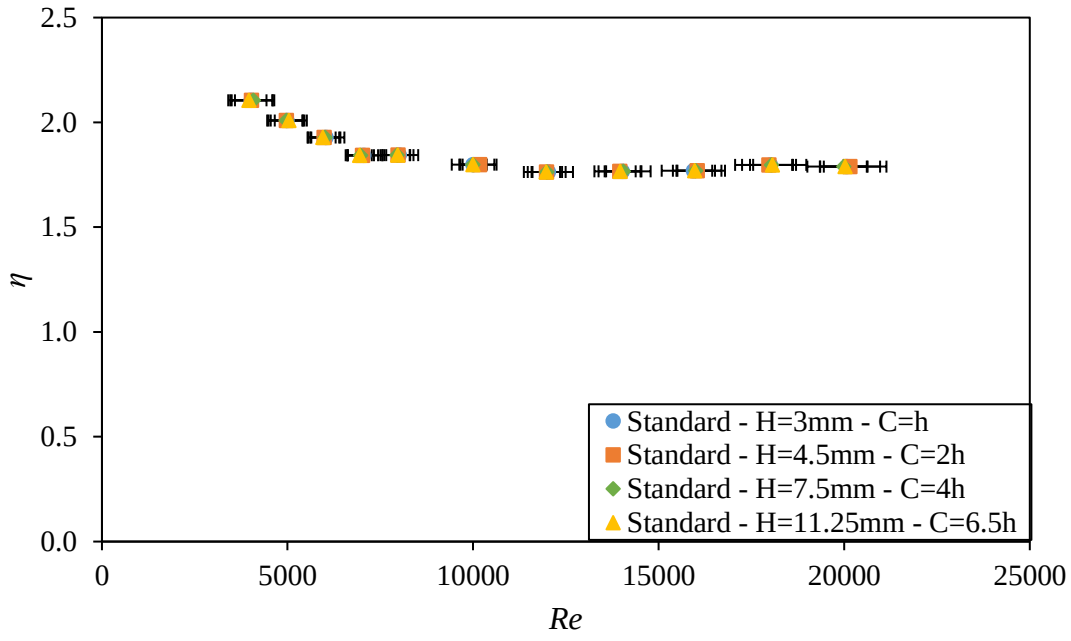

Figure 3-9: η vs Re for rectangular channels with array of Standard hooks at different values of C/h

3.4.3 Comparison with other Surface Enhancements

To the best of the authors' knowledge, no data on finned surfaces in the available literature captures the convective thermal-hydraulic performance of the present GRIPMetal arrays. This is because of i) the uniqueness of the proposed array in terms of the shape of the fin (hook-shaped) and its accompanying dimple, ii) the type of arrangement (i.e., changing orientation of the hooks and their dimple with respect to the flow from one column to another), and iii) the current rectangular channel is double-sided with arrays opposing each other. Nevertheless, comparisons of previously reported channels with state-of-the-art hybrid pin fin–dimple arrays [52] or dimple arrays [48,50] have been made to evaluate relative thermal-hydraulic performance.

Comparisons between hydraulic diameter based Nusselt number, Nu_{Dh}, and friction factor, f_{Dh} for a *Re* range of 8,000 to 20,000 were made. Figure 3-10 shows the comparison of Nu_{Dh} for channels of GRIPMetal Standard hooks array at C/h = 2 and 6.5 with the heat transfer data from [48,50,52]. Because the Nusselt number calculation in the present study is based on the nominal base area and not the heat transfer surface area, the reported Nusselt number for comparing studies was adjusted

accordingly. First, a comparison between the GRIPMetal Standard hooks rectangular channel of *C/h* = 2 and the rectangular channel with the hybrid pin fin–dimple array of [52] seems relevant because they both have almost the same aspect ratio. It is seen in Figure 3-10 that the GRIPMetal Standard hooks channel shows higher Nusselt number values than the other by 35%~55%, depending on *Re*. This can be contributed to the presence of a clearance between the two opposing hooks tips that induces severe vortex shedding and promotes turbulence in the main bulk flow because of the separated shear layers from those sharp hook tips [38]. Second, the dimples of the Standard hooks array can be approximated as the teardrop dimples investigated by Rao et al. [48]. Thus, the GRIPMetal Standard hooks channel of C/h = 6.5 was used for the comparison because it has an aspect ratio in the same magnitude as [48]. Also, the convex dimple studied by Gao et al. [50] was used for comparison because the dimples were applied to both endwalls of the channel as in the current study. From Figure 3-10 we can conclude that the GRIPMetal Standard hooks array exhibits higher convective heat transfer than the dimple arrays within the compared range of *Re*, which is in good agreement with findings of Rao et al. [52].

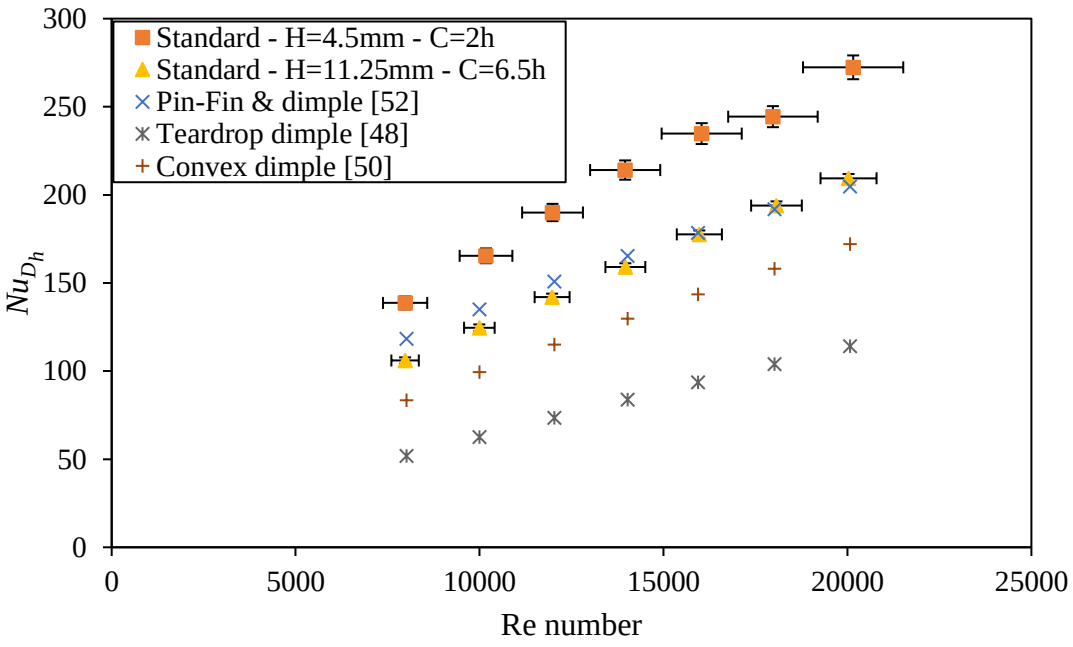

Figure 3-10: Comparison of Nu_h between rectangular channels with array of Standard hooks C/h = 2 and 6.5, pin fin and dimple arrays from the existing literature.

In Figure 3-11, f_{Dh} for channels of Standard hooks array at C/h = 2 and 6.5 is compared with the friction factors from previous studies. The friction factor of the channel C/h = 2 of the current study is lower than that of the channel with a hybrid pin fin–dimple array of [52] by about 45%. One possible explanation for this is the presence of a gap between the two opposing plates which offers a lower resistance path to the flow; this consequently lowers the pressure drop at a given *Re* when compared to the hybrid pin fin–dimple array that fills the whole channel. On the other hand, the GRIPMetal channel of C/h = 6.5 has a friction factor that is 2 times the friction factor of the teardrop dimples [48] and 5~8 times that of the convex dimples [50]. This is mainly because the presence of the hooks obstructs the flow, creating a low-pressure area downstream of the hook and a high-pressure area upstream due to the stagnation of the flow. Although the presence of the dimple downstream of the hooks reduces the intensity of the wakes downstream of the hooks and, thus, reduces the pressure drop, this effect still did not counteract the drag imposed by the hooks.

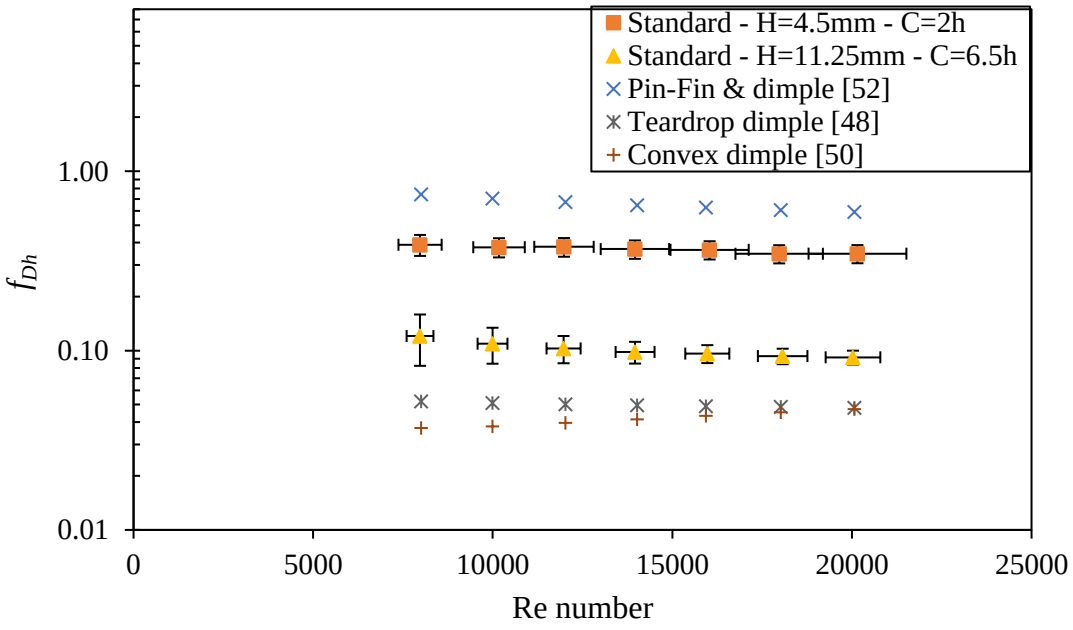

Figure 3-11: Comparison of f_h between rectangular channels with array of Standard hooks C/h = 2 and 6.5, pin fin and dimple arrays from the existing literature.

3.4.4 Nusselt Number Correlations

The Nusselt number, Nu_h, in Figure 3-6 was correlated through a nonlinear multiple variable regression analysis. The correlation took the following form as a function of *Re* and C/h:

$$Nu_h = a\, Re^b \left(C/h\right)^d Pr^{0.4} \tag{3-18}$$

where Pr is the Prandtl number of the air at the mean bulk temperature. Including Pr in the correlation will allow potential users to easily assess different fluids. An attempt was made to generate a single correlation for the four tested tip clearances; however, the correlation could not predict Nu_h accurately enough, especially for the C/h = 6.5 channel which had a root mean square error (RMSE) of 21%. Consequently, an alternate definition of the Reynolds number is considered to correlate the experimental data; that is referred to as the array Reynolds number, Re_a. The distinction between the array Reynolds number and Eq.(3-9) is the usage of the array velocity, V_a, as a reference velocity instead of the mean inlet velocity, V_{in}. This Re_a was previously defined by Garimella and Eibeck [34]. The motivation for using the array velocity V_a, is as follows. The presence of the tip clearance, C, divides the flow into two streams: i) the bypass stream and ii) the array stream and their ratio depends on the value of C (i.e., the ratio between the pressure drops of these streams). Thus, the actual velocity affecting the heat transfer from the array is not the mean inlet velocity but, rather, the velocity to which the hooks are exposed (i.e., array velocity, V_a).

Because most of the pressure drop in the channel is due to the drag encountered by the presence of the hooks, the drag is the determining factor for the ratio between the array velocity and the mean inlet velocity. As the tip clearance increases, more flow bypasses the array, resulting in lower drag coefficient and indicating a decrease in the array velocity. Hence, the mean inlet velocity and the array velocity are related to each other through the drag coefficient of the hooks as

$$V_a = V_{in} \sqrt{C_{d,i} / C_{d,C=h}} \tag{3-19}$$

where C_d is the drag coefficient of an array of hooks defined by

$$C_d = \frac{2\,\Delta P}{V_{in}^2\,\rho}. \tag{3-20}$$

Because the C/h = 1 case corresponds to the situation where there is no tip clearance between the two opposing plates (i.e., all the flow passes through the array), the drag coefficient of this channel,

$C_{d,C=h}$, is used as the reference coefficient. Figure 3-12 shows the drag coefficient for an array of Standard hooks with C/h = 1, 2, or 4 at different Re (the omission of C/h = 6.5 is discussed below).

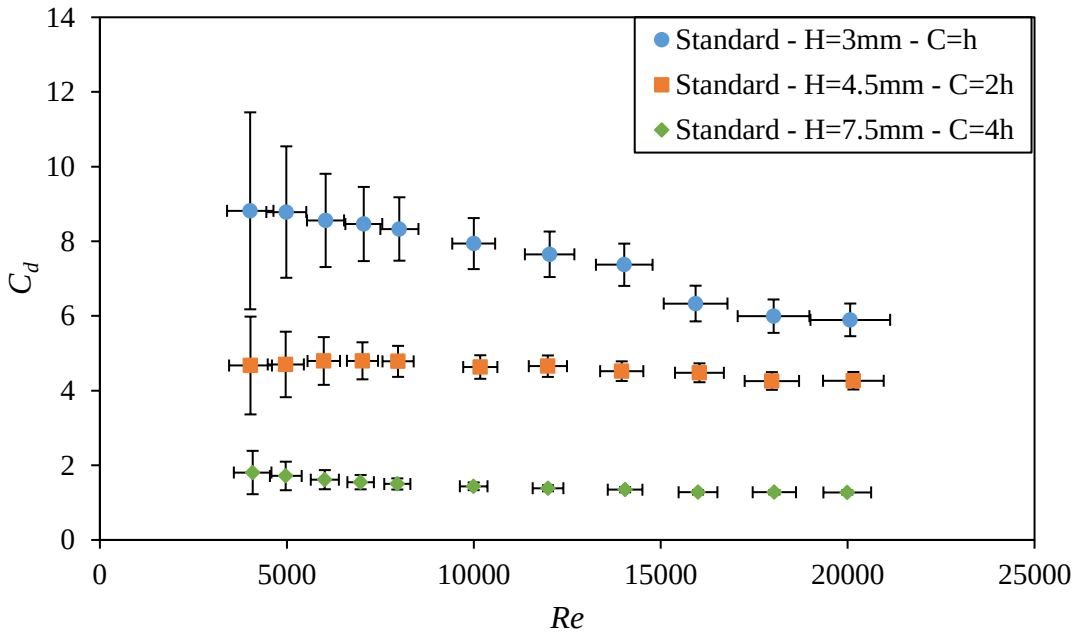

Figure 3-12: C_d vs Re for rectangular channels with array of Standard hooks at different values of C/h

After applying the definition of Re_a in the experimental data, the Nu_h for channels with C/h values of 1, 2, or 4 could be correlated to a single correlation. However, the prediction of Nu_h for C/h = 6.5 employing the Re_a definition did not produce an accurate correlation. This is because at such high values of tip clearance, the array affects the flow as surface roughness rather than as an array of raised features; thus, the array velocity V_a is no longer the effective velocity, and the heat transfer augmentation mechanism is different. Therefore, two sperate correlations were developed. The first,

$$Nu_h = 0.1063\, Re_a^{0.646}\left({}^{C}/_{h}\right)^{-0.05371} Pr^{0.4} \qquad \text{for } 1 \le {}^{C}/_{h} \le 4, \qquad (3\text{-}21)$$

is for channels with C/h values of 1, 2, or 4, implementing Re_a.

The other correlation,

$$Nu_h = 0.1542\, Re^{0.7301}\left(C/h\right)^{-1.286} Pr^{0.4} \qquad \text{for } 4 \le C/h \le 6.5, \tag{3-22}$$

is for the C/h =4 or 6.5 channels using *Re*. The presence of channel C/h = 4 in both correlations is to check the validity of (3-22) for intermediate values of *C/h* and to prove the adequacy of the proposed claims.

A comparison between the experimental data and the abovementioned correlations is depicted in Figure 3-13. The y-axis represents the Nu_h normalized by $Pr^{0.4}$ and $(C/h)^n$ in a log scale such that *n* is the exponent defined in correlations (3-21) and (3-22). The RMSE between predictions using these correlations and the experimental data is 3.7% and 2.4%, respectively. The collapse of the experimental data for channels with *C/h* values of 1, 2, or 4 on a single straight line helps justify the use of array velocity, V_a, as the physically significant reference velocity.

The value of Reynolds number's exponent of either 0.646 or 0.7301 shows that the convection through these arrays is dominated by strong turbulence and flow separation. The Reynolds number index for correlation (3-22) is higher, indicating that it exhibits lower dependency on the Reynolds number than (20). Also, it is approaching the 0.8 power dependence of the flat plate's heat transfer, supporting the claim that at high *C/h* values the flow is affected by these arrays as surface roughness.

The exponent of *C/h* for correlation (3-21) suggests that Nu_h for such arrays is not greatly affected by tip clearance; however, this is not the case because the effect of *C/h* is already included in the Re_a term. For correlation (3-22), the exponent *C/h* indicates that the effect of increasing *C/h* is to decrease the Nu_h; however, this effect declines with increasing *C/h*, indicates the possibility of using the same correlation for predicting the Nu_h for channels with *C/h* values greater than 6.5 with a reasonable accuracy.

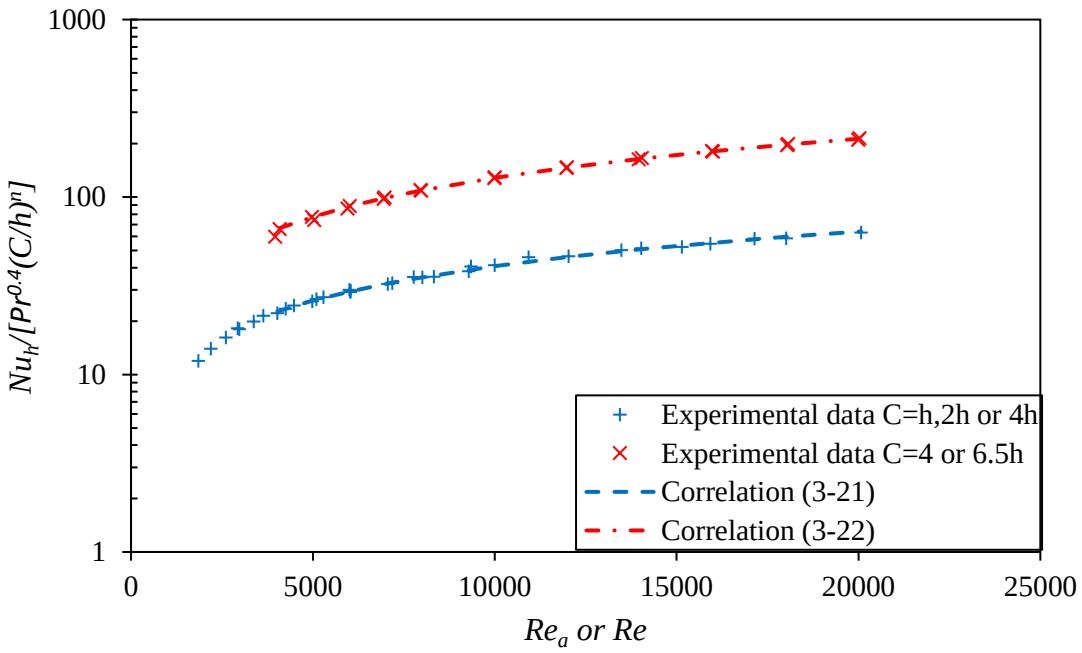

Figure 3-13: Comparison between correlations of Nu_h and experimental data for Standard hooks array

3.4.5 Friction Factor Correlations

In addition to the Nusselt number, the friction factor, f_h, shown in Figure 3-8 was correlated through performing nonlinear multiple variable regression analysis. Inspired by the friction factor correlations in the literature, the correlation took the following form as a function of *Re* and *C/h*:

$$f_h = \left[a \log Re + b\left(C/h\right)^d\right]^n. \tag{3-23}$$

Following the same procedure as above for correlating the Nu_h data, two separate correlations were developed for two different ranges of *C/h*. The first correlation,

$$f_h = \left[0.66 \log Re + 0.363\left(C/h\right)^{1.763}\right]^{-2} \qquad \text{for } 1 \le C/h \le 4, \tag{3-24}$$

is for channels with *C/h* values of 1, 2, or 4.

The other correlation,

$$f_h = 0.01\left[-\log Re + 11.5\left({}^{C}/_{h}\right)^{-0.451}\right] \qquad \text{for } 4 \le {}^{C}/_{h} \le 6.5, \qquad (3\text{-}25)$$

is for the *C/h* =4 or 6.5 channels.

The presence of channel *C/h* = 4 in both correlations is to check the validity of correlation (3-25) for intermediate values of *C/h*. Figure 3-14 shows a comparison of the experimental data of f_h with its corresponding predicted values implementing correlation (3-24) and (3-25). The RMSE between predictions using these correlations and the experimental data are 6.5% and 5.3%, respectively.

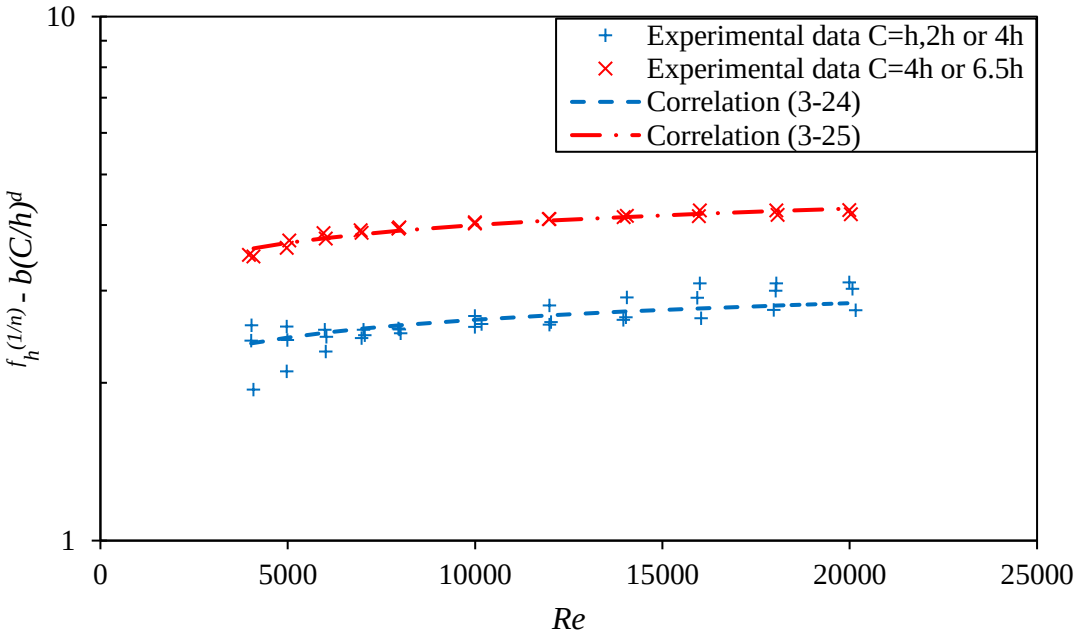

Figure 3-14: Comparison between correlations of f_h and experimental data for Standard hooks array

3.4.6 Effect of Hook Geometry

In this section, the effect of both the streamwise and spanwise spacings between the hooks and the hook size on the heat transfer and pressure drop characteristics is evaluated. To this end, two additional arrays of "Heavy" and "Mini" hooks (see geometrical parameters given in Table 2-1) were tested at tip-clearance-to-hooks-height ratio *C/h* = 4. Figure 3-15 shows the Nu_h for three

different arrays of Standard, Heavy and Mini hooks at C/h = 4 over the range of Re. As expected, the Nu_h increases with Re irrespective of the hook type. Results for the three types of hooks are shown to collapse onto a single straight line, with a slight difference between the Heavy hooks and the others of only about 3%. This indicates that at this C/h value and above, inter-fin spacings and hook shape have limited influence on the heat transfer of these arrays. It also shows that the choice of hook height as the characteristic length is appropriate. Thus, the correlations provided in Section 3.4.4 could be applied to the other types of hooks for $C/h \geq 4$.

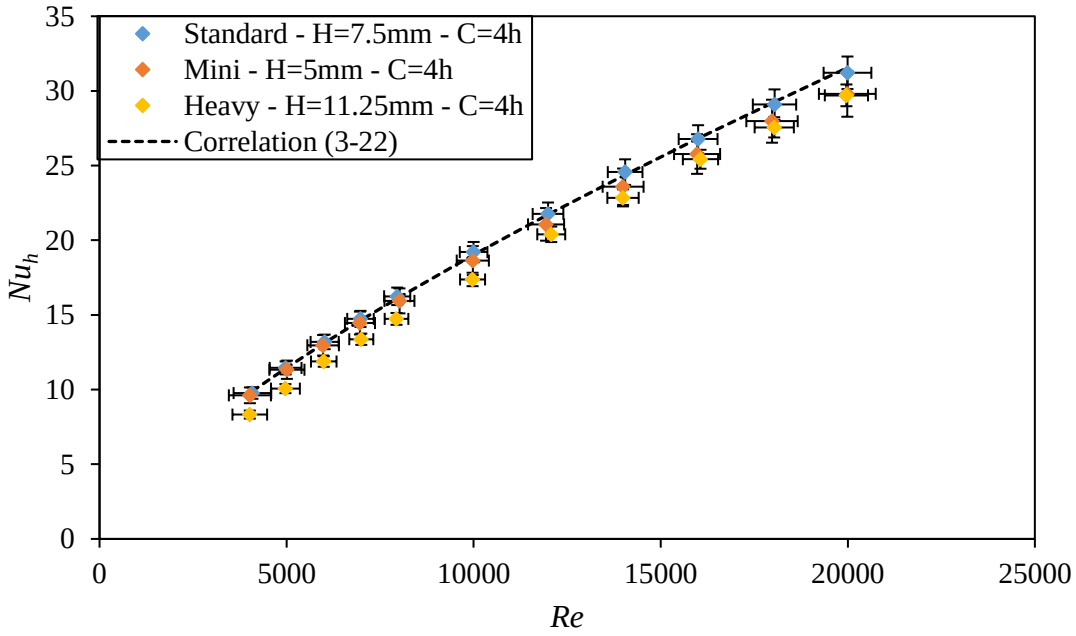

Figure 3-15: Nu_h vs Re for rectangular channels with arrays of different types of hooks at C/h = 4

On the other hand, Figure 3-16 represents the change of friction factor, f_h, for the three tested types of hooks at C/h = 4 with Re. It should be noted that, regardless of the value of Re, the Mini hooks array exhibits the greatest friction factor by a factor of 2.2 compared with the Standard hooks. This increase in f_h is attributed to two factors: First, to achieve C/h = 4 for Mini hooks, the channel height is reduced to 5 mm while the Standard and Heavy hooks require a height of 7.5 mm and 11.25 mm, respectively. This height results in a 33% reduction in the flow area compared to that of the Standard hooks case and, therefore, at any given Re, the approach velocity is the highest for Mini hooks. Second, the Mini hooks array has spanwise spacing that is almost half those of the

Standard and Heavy hooks arrays. As previously stated, and as found in [30–32], the pressure loss is greatly affected by spanwise spacing as a direct result of flow restriction between the hooks.

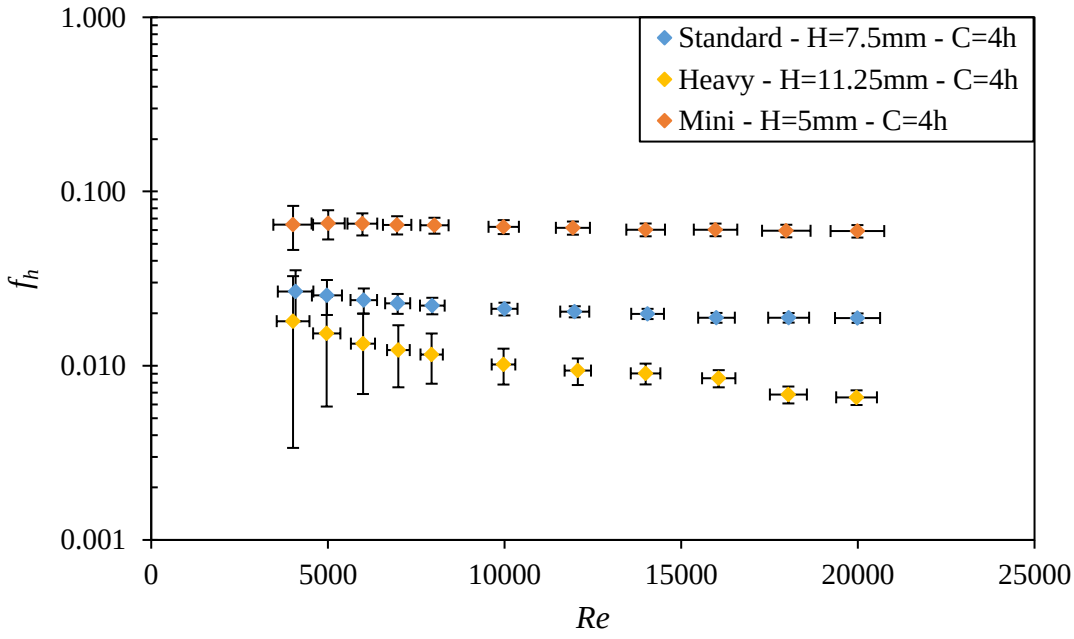

Figure 3-16: f_h vs Re for rectangular channels with arrays of different types of hooks at C/h = 4

3.5 Summary & Conclusions

In this experiment, the thermal and the hydrodynamic performances of GRIPMetal hooks arrays developed by NUCAP Industries Inc. was characterized and compared to that of flat plates. In addition to developing predictive correlations to serve as design tools for heat exchange applications. Such arrays are an attractive option for convective heat transfer enhancement due to their manufacturing simplicity and speed, low cost, and commercial availability in the market.

The effect of tip-clearance-to-hooks-height ratio, *C/h*, for an array of GRIPMetal Standard hooks with a nominal height, *h* = 1.5 mm, was investigated at values of 1, 2, 4 and 6.5. Then, two more arrays with hooks height, *h*, 1 mm and 2.25 mm, and different inter-fin spacings were tested at *C/h* = 4. Results were obtained at Reynolds numbers ranging from 4,000 to 20,000 using air as the working fluid. The results show that these hooks have good potential for practical air-side heat transfer enhancement and the following conclusions can be drawn:

- The array of Standard hooks improved the heat transfer capabilities of the rectangular channel when compared to flat plate depending on the value of tip-clearance-to-hooks-height ratio, *C/h*. Maximum enhancement in heat transfer was found to be for *C/h* = 2 and *C/h* = 4 cases with a factor of 4.6 at low flow rates and 3.75 at higher ratios. While for *C/h* = 6.5 the enhancement maintains a relatively constant factor of 3 regardless of the *Re*.
- The Nusselt number decreases with increasing tip-clearance-to-hooks-height ratio, *C/h*, at any given *Re* approaching an asymptotic value at higher *C/h* ratios, which is consistent with [18].
- The friction factor, f_h, of the channel with *C/h* = 1 is the greatest among all cases and it follows a declining trend with *Re*. However, for the remaining values of *C/h*, the friction factor is much lower and is independent of *Re*. This f_h - *Re* curve flattening is consistent with [38].
- The experimental results of f_h for the *C/h* = 6.5 case are coincident with the values obtained from Haaland's correlation [36]. This reinforces the claim that at such high values of *C/h*, the array of hooks act as boundary layer roughness rather than as raised features.
- The heat transfer performance of GRIPMetal Standard hooks array was found to be higher than performance data available in the literature for a hybrid staggered pin fin–dimple array, teardrop dimples staggered array, and convex dimple staggered array. On the other hand, GRIPMetal Standard hooks arrays exhibited higher pressure drop than both dimple arrays and lower than the hybrid staggered pin fin–dimple array.
- Two distinct correlations were developed for the Nu_h as a function of the array Reynolds number, Re_a, and tip-clearance-to-hooks-height ratio, *C/h*. Also, two correlations were obtained for the friction factor as a function of Reynolds number, *Re*, and tip-clearance-to-hooks-height ratio, *C/h*. These four correlations can be used as design tools to employ these hooks in any given application.
- The overall thermal performance factor, η, is independent of the value of *C/h* within the range of *Re* investigated. It steadily declines from 2.1 to 1.8 as *Re* increases from 4,000 to 12,000; then, it becomes independent of *Re*. These hooks have $\eta > 1$ which demonstrates that the heat transfer enhancement offsets the pressure drop penalty.
- Geometrical parameters of such arrays of hooks (i.e., hook height and streamwise and spanwise spacings between them) is found to have no effect on heat transfer characteristics at *C/h* = 4. Therefore, the developed correlations of Nu_h for Standard hooks can be used for the other two types for $C/h \geq 4$.

- The friction factor, f_h, of the Mini hooks array showed higher values than that of Standard and Heavy hooks arrays at any given *Re*. This can be attributed to i) the array's approach velocity is the highest for Mini hooks; and ii) the Mini hooks array has a spanwise spacing that is almost half that of the Standard and Heavy hooks arrays.

Chapter 4 Heat Transfer and Pressure Drop Characteristics of Hook-Shaped Fins and Dimples Arrays for Liquid Cooling Applications

In Chapter 3, an experiment was conducted using air as a working fluid to quantify the enhancement of the convective heat transfer coefficient of rectangular channel through employing different arrays of hooks to its major walls. The height of the channel was varied such that the tip-clearance-to-hooks-height ratio, *C/h*, ranges from 1 to 4. In this chapter, experiments were performed using a closed water loop apparatus to study the effect of changing fluid properties (specifically Prandtl number) on the performance of the GRIPMetal array. In this way, the applicability as employing these arrays as liquid cooled heat sinks and/or cold plates is evaluated as it is well-known that fins are usually placed in the flow field of gases, owing to their low thermal conductivity when compared to liquids. Furthermore, in this chapter the arrays of hooks were only applied to the bottom wall of the channel and the testing covers different range of tip-clearance-to-hooks-height ratio, *C/h*, than that of Chapter 3. This apparatus incorporates many key features, such as a transparent test section, ability to provide a wide range of flow rates, ability to vary the channel height. The loop was carefully designed to give more precise characterization of the convective heat transfer coefficient and pressure drop than the wind tunnel facility used in Chapter 3. Finally, owing to the high heat capacity of the water, and its relatively high convective heat transfer coefficient, an excellent energy balance between the input power and the rise in the fluid power can be achieved.

This chapter is divided into two parts; The first describes the design of the loop and the methodology followed to characterize the heat transfer and pressure drop. While the second details the results obtained for channel with Standard GRIPMetal hooks array at tip-clearance-to-hooks-height ratio, *C/h*, ranging from 0 to 1 and the comparison between these results and that of a flat plate and existing short pin fin/dimples data in the literature. Then at $C/h = 0$, two other types of these arrays, Heavy and Mini hooks, are compared to Standard hooks to evaluate the impact of changing the arrays geometrical parameters on the performance. Finally, resultant data is used to develop correlations that can be used to facilitate the design of other heat exchangers (e.g. cold plates) with GRIPMetal-enhanced surfaces.

4.1 Experimental Apparatus: Closed Water Loop

The schematic of the experimental facility used to characterize the thermal-hydraulic performance of the arrays of hooks is depicted in Figure 4-1. The setup is comprised of an instrumented closed water loop for supplying the flow to the test section housing fitted with an instrumented heater block for the evaluation of both the hydraulic and the thermal performance of heated surfaces. Different components of the loop are connected through 9.5 mm ID transparent nylon tubing and Swagelok fittings. Distilled water is circulated through the loop using a Fluid-O-Tech PA1011 Stainless Steel rotary vane pump coupled with a 1 Hp, 90 VDC motor. The motor speed is regulated by a controller to achieve the desired flow rate from the pump. The pump is followed by a pressure relief valve to protect the pump from failure in case of any sudden pressure build up. The flow rate was measured by an axial turbine flow meter (Omega BV2000TRN250B). An adequate developing length of straight tubing prior to the flowmeter was installed to ensure flowmeter measurement accuracy. A 5 μm water filter was installed as per flow meter specifications and to minimize the potential for particles to be introduced into the test section itself. The water temperature at both the inlet and outlet of the test section were measured with two calibrated 3 mm diameter sheathed four wire PT100-RTDs inserted parallel to the flow just upstream and downstream of the test section. A plate heat exchanger is placed downstream of the test section to cool down the water circulating in the loop to a constant temperature of 23.5 °C ± 1°C. The water temperature was chosen to match the ambient temperature as possible to minimize any heat exchange between them. A BOYD RC045 chiller with integral pump provided the coolant to the heat exchanger.

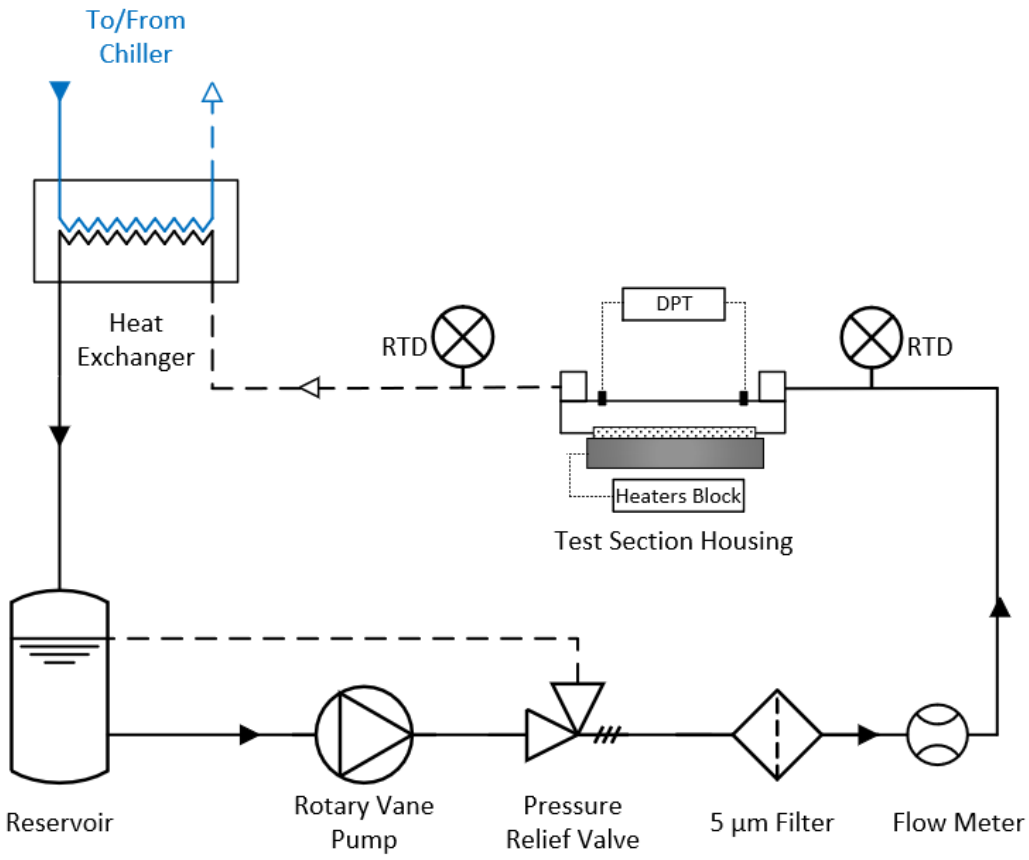

Figure 4-1 Schematic of the experimental water loop facility

A detailed layout of the test section housing is shown in Figure 4-2. The housing consists of three parts, top section, lower section, and a shim between them. clamped together by 28xM4 screws with EPDM O-rings situated in between the mating faces for sealing. All the three parts were manufactured from Al6061 alloys. The top section is an assembly of two plenums on the far left and the far right for water entry and exit from the housing, in addition to a transparent Polycarbonate cover in the middle that will be atop of the arrays being tested for flow visualization. This cover has two ports located 5 mm upstream and downstream of the test section for pressure measurements. Pressure drop across the test section was measured using either Omega PX409-030DWUV or PX409-001DWUV differential pressure transducers; each for different range of pressure drop. The two plenums and the cover were mechanically fastened to the top section through M3 screws with Neoprene gaskets beneath them for sealing. A PEEK insert was placed at the middle of the bottom section that acts as a housing for the test section to minimize the heat loss

from the test section to the housing. Three test surfaces, 50.8 mm x 100 mm, with different arrays of hooks, given in Table 2-1, were formed onto 11 mm thick Al6061 plates. Heat flux is provided through a copper heater block mechanically fastened to the test section using 6xM3 screws with a thin layer of thermal paste (k=8.5 W/mK) applied at the heater block-to-test section interface to minimize the contact resistance. Four 3.1 mm diameter and 50.8 mm length cartridge heaters (Dalton) 200 W each were embedded inside the copper block. Electrical power is supplied and controlled with a DC power supply (CPX400D, Aim TTi) and quantified using built-in voltage and current measurements. Power was varied according to the flow rate such that the temperature rise of the water is approximately 1 K (resulting in heat fluxes ranging from 2 to 15.75 W/cm²). Due to the limitation of the heaters wattage, the temperature rise of the water in some flow rates were less than 1 K, however, the temperature differences for all tested flow rates allowed for sufficient accuracy in the temperature difference between the tested plates and the water and was low enough to minimize thermal property variations in the test section and heat losses to the ambient. Four 4-wire PT100-RTDs were located 8 mm below the surface of the test sections for temperature measurements and the temperature of the surface is then determined through extrapolation utilizing 1-D Fourier conduction equation

$$T_s = T_{RTD} - \frac{Q_{in}}{A_b}\left[\frac{d}{k_{Al}}\right] \qquad 4\text{-}1)$$

where T_s and T_{RTD} are, respectively, the surface and RTD temperatures, Q_{in} denotes the input power to the test sections, A_b is the base area (100 x 50.8 mm²), d is the distance between the center of the RTDs and the surface (8 mm) and k is the thermal conductivity of Al6061 alloy, which is equal to 167 W/mK. One RTD is used to measure the ambient temperature surrounding the experiment to account for the heat loss. All RTDs are calibrated with respect to each other to minimize uncertainties in the measured temperature differences. The stack of the test section and copper heater block was placed on a base plate with alumina-silicate ceramic insulation beneath the heater block to minimize the heat loss. The base plate is then clamped to the bottom section through 12xM3 screws such that the test section is guided into the PEEK housing with an EPDM O-ring situated in between. The tightening torque of the screws is adjusted to ensure that the test section is flush with the PEEK and the bottom section, and the O-ring is squeezed enough for sealing.

The channel is then created using the test section surface, the bottom surface of the polycarbonate cover and the side walls of the shim inserted between the top and bottom sections of the housing. The height of the channel, i.e., tip-clearance-to-hooks-height ratio, is controlled by changing the shim thickness.

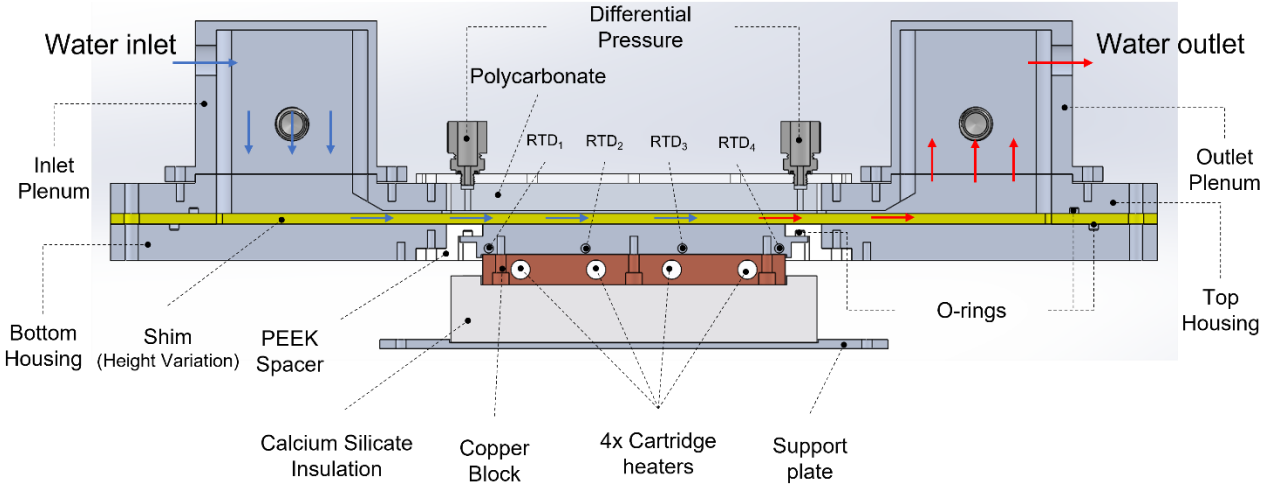

Figure 4-2 Detailed view of the test section housing

4.2 Heat Loss Calibration

Although the copper heater block was insulated from the bottom side and the aluminum plates were surrounded by PEEK insert to minimize any heat leak to the ambient or the housing, it is anticipated that there will be some heat loss. Consequently, before running any test, heat loss was quantified by performing a series of calibration runs with no water in the test section. A PID controller was tuned to produce the approximate range of plate temperatures of interest. Since the height of the channel is relatively low, the natural convection of air trapped inside would be minimum. Therefore, any heat introduced to the assembly will approximately equal to the heat loss. When steady state was reached for each run, the input power, the average plate temperature, $T_{s,avg}$, and ambient temperature, T_{amb}, were measured, shown in Figure 4-3, so that an overall thermal resistance for the heat loss, R_{loss}, could be anticipated according to

$$Q_{loss} = \frac{\left(T_{s,avg} - T_{amb}\right)}{R_{loss}}. \tag{4-2}$$

Consequently, while running a test, the heat loss from the test section was calculated according to the measured plate and ambient temperatures using (4-2).

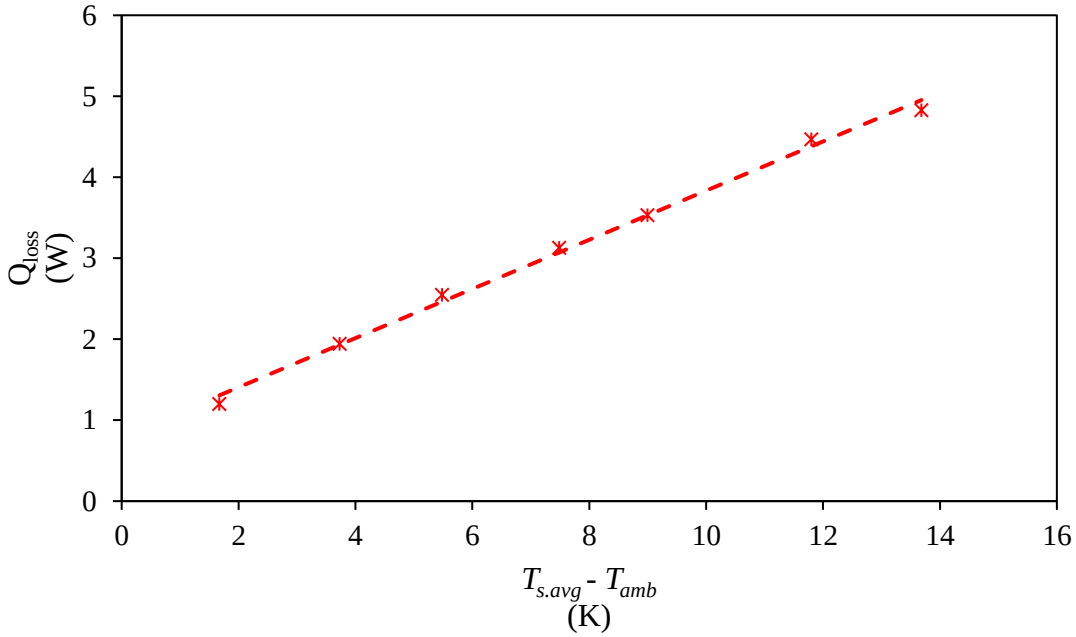

Figure 4-3 Heat loss calibration data for Standard hooks channel of C/h = 0.3

4.3 Data Reduction and Uncertainty Analysis

The heat transfer coefficient is calculated by averaging the temperature difference between the surface temperature obtained from each RTD reading, $T_{s,i}$, and its corresponding local bulk water temperature, $T_{b,i}$ as

$$\Delta T_{bulk} = \frac{\sum_{i=1}^{4}\left(T_{s,i} - T_{b,i}\right)}{4} \tag{4-3}$$

such that $T_{b,i}$ is calculated by assuming a linear rise of the water temperature along the test section and $T_{s,i}$ is obtained from 4-1). Then, the overall heat transfer coefficient of an array of hooks, h_{bulk}, is calculated as

$$h_{bulk} = \frac{Q_{elec} - Q_{loss}}{A_b \Delta T_{bulk}} \tag{4-4}$$

where Q_{elec} denotes the input electrical power to the heaters and A_b is the nominal area (101.6 x 50.8 mm²). This form of heat transfer coefficient reflects the heat transfer characteristics of the array as if there is a heat source mounted on the flat side of the plate, such as electronic-chip or plate heat exchangers. Also, it accounts for heat transfer enhancement due to both area increase and fluid dynamic effects of the arrays.

Another way of calculating the heat transfer coefficient is to use the logarithmic temperature difference ΔT_{lm} between the surface and the bulk inlet and outlet temperatures as

$$\Delta T_{lm} = \frac{\left(T_{s,in} - T_i\right) - \left(T_{s,o} - T_o\right)}{ln\left(T_{s,in} - T_i\right) - ln\left(T_{s,o} - T_o\right)} \tag{4-5}$$

where $T_{s,in}$ and $T_{s,o}$ are, respectively, the inlet and outlet surface temperatures, obtained from 4-1). The overall heat transfer coefficient of an array of hooks, h_{lm}, is calculated the same as h_{bulk}, but replacing ΔT_{bulk} with ΔT_{lm} such that

$$h_{lm} = \frac{Q_{elec} - Q_{loss}}{A_b \Delta T_{lm}} \tag{4-6}$$

The average difference between the calculated values of heat transfer coefficient using the two methods is 5%; however, the temperature difference between the plate and the water is relatively low that resulted in high uncertainties in the logarithmic difference, thus, the other method of calculating h is employed in this study.

It is common to present heat transfer results in the dimensionless form of a Nusselt number, Nu,

$$Nu = \frac{h_{bulk}\, L_c}{k} \tag{4-7}$$

where k is the thermal conductivity of water at bulk temperature, which is equal to 0.6065 W/mK, while L_c is the characteristic length, which is either the fin height, h, or the hydraulic diameter of the channel, D_h, computed as

$$D_h = \frac{2(HW)}{H + W} \tag{4-8}$$

where H and W are the height and the width of the test section channel.

For pressure drop characterization, the friction factor f is calculated as

$$f = \frac{2\ \Delta \mathrm{P}\ L_c}{L_f\ V_{in}^2\ \rho} \tag{4-9}$$

where ρ is the density of water at bulk temperature, which is equal to 997 kg/m^3, ΔP is the pressure difference across the test section measured by the DPT, and V_{in} is the mean inlet velocity to the test section.

Finally, the Reynolds number, Re, is defined based on the hydraulic diameter

$$Re = \frac{\rho\ \mathrm{V}_{in}\ D_h}{\mu} \tag{4-10}$$

where μ is the dynamic viscosity at water bulk temperature, which is equal to 0.9x10^{-3} Pas.

For a comprehensive assessment of both heat transfer and pressure drop characteristics of the hooks compared to those of the flat plate, the overall thermal performance η (proposed by Gee and Webb [63]) is evaluated as

$$\eta = \frac{\left(Nu_{D_h}/Nu_o\right)}{\left(f_{D_h}/f_o\right)^{1/3}} \tag{4-11}$$

where Nu_o and f_o are the Nusselt number and the friction factor based on D_h for flat surfaces, respectively, and Nu_{Dh} and f_{Dh} are the Nusselt number and the friction factor based on D_h for channels with hooks, respectively.

The uncertainties of the measured quantities are listed in Table 4-1. The RTDs used in this study are calibrated with respect to each other in a temperature-controlled bath of Julabo F32-HE chiller filled with water. The temperature of the bath was changed from 10 °C to 70 °C with a step of 1 °C to calibrate the RTDs. After the calibration, the uncertainties of the RTDs are within ±0.02 K of each other with a 95% confidence probability. The uncertainty of each calculated parameter is evaluated through propagation using the method proposed by Kline and McClintock [64]. It was

found that the maximum uncertainty in *Re* was 7.6%. This occurred at low flow rates and narrow channels, while at higher flow rates and wide channels the uncertainty was lower than 4%. For *Nu*, the maximum uncertainty was up to 15% that is only for some cases with high flow rates, $Re \geq 9000$, while the common value was 2%. Regarding the *f*, the uncertainty ranged between 2~7.5%. The uncertainties of the calculated parameters vary depending on the testing parameters and as such are plotted graphically using error bars.

Table 4-1 Uncertainties of measured quantities

Measured Quantity	Uncertainty
Temperature differences	0.02 K
Pressure drop	0.08% FS (FS is either 1 psi or 30 psi)
Flow rate	3% of reading
Voltage	0.1% of reading ± 2 digits
Current	0.3% of reading ± 2 digits
Tunnel's width and height	0.05 mm

4.4 Testing Procedure

Tests were conducted through a nominal Reynolds number based on the hydraulic diameter, *Re*, ranging from 1,000 to 10,000. Standard hooks were tested at nominal tip-clearance-to-hooks-height ratio, C/h = 0, 0.33, 0.5 and 1. Then, two other types of hooks arrays, (i.e., Mini and Heavy hooks) were tested at tip-clearance-to-hooks-height ratio, C/h = 0, to investigate the effect of changing the inter-fin spacings on the performance. This was achieved by changing the test section height, *H*, from 1 mm to 3 mm, by inserting the appropriate shim thickness between the top and bottom sections of the housing based on the type of hooks being tested; this corresponds to an aspect ratio, H/W, from 0.02 to 0.06. For comparison, at each test section height, a flat plate was tested.

Measurements from the RTDs, pressure transducer and power supply were monitored continuously using an Agilent 34970A data acquisition unit connected to a PC running a custom

MATLAB script to log the data simultaneously every 10 s. At each flow rate setting, temperatures were monitored to determine system steadiness. System was considered quasi-steady or steady if the temperature readings were almost consistent over time. Then for a 10 minutes periods of quasi-steady or steady operation measurments are collected then time-averaged to be used in calculating any reported parameter in the current study.

Each case of the Standard hooks was repeated after disassembling and reassembling the test section housing at approximately the same heat flux and flow rates to confirm the repeatability of heat transfer results. The resultant data were repeatable and consistent with the first trials. In addition, at C=0 and $0.33h$, three flow rates that are corresponding to Re of 2000, 5000 and 10000 were tested at different heat fluxes ranging from 2 to 15.75 W/cm². These two tip clearance values were selected as they have the highest uncertainty in the heat transfer coefficient among the tested cases. Figure 4-4 and Figure 4-5 depict the results of these tests indicating that at each flow rate the heat transfer coefficient data showed good repeatability; and hence, prove the independency of the heat transfer coefficient on the applied heat flux.

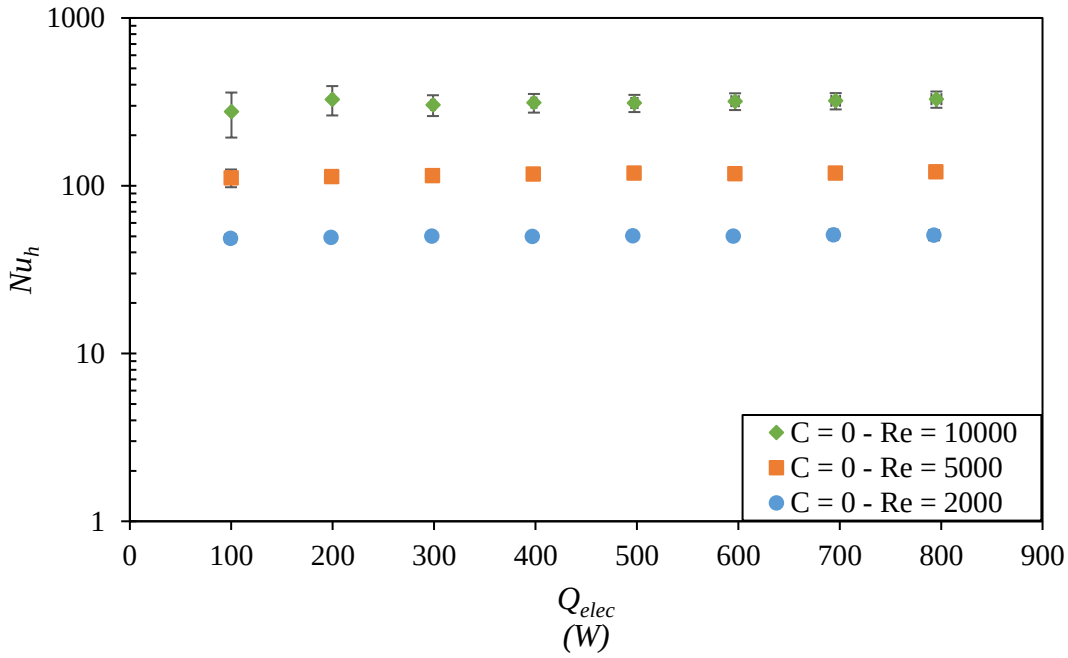

Figure 4-4 Nu_h vs Input power for rectangular channels with array of Standard hooks at C/h =0 and different Re

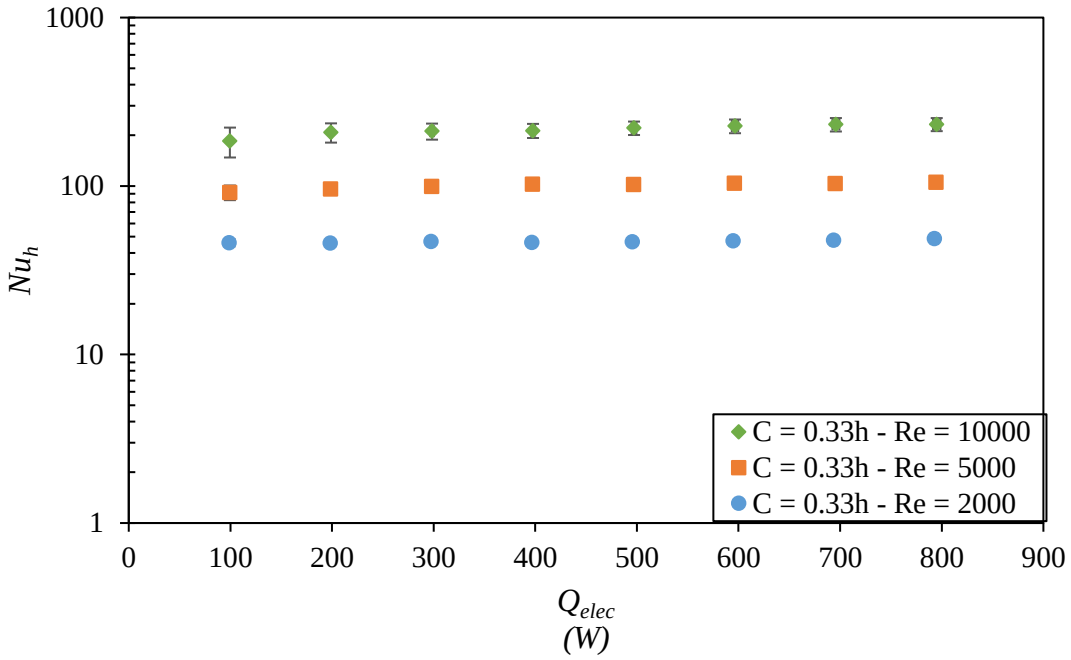

Figure 4-5 Nu_h vs Input power for rectangular channels with array of Standard hooks at C/h =0.33 and different Re

Pressure drop measurements were conducted twice, once with the heat transfer tests and the second were at zero heat flux at an inlet water temperature of 23.5°C. Also, since two differential pressure transducers were used to cover the whole test runs, measurements were taken from both sensors at the overlapping range. The resultant data showed great consistency and the measurements from both sensors were in good agreement within their uncertainties.

4.5 Results and Discussion

4.5.1 Energy Balance

An energy balance on the test section, shown in Figure 4-6, is performed to ensure the efficacy of the heat transfer performance calculations. The abscissa of Figure 4-6 is the electrical input power to the heaters, as determined by the product of the applied voltage and current minus the heat loss calculated using Eq. (4-2). While the ordinate is the power gained by the water based on the measured temperature rise of the water between the inlet and outlet minus the relatively minor viscous heating effect caused by the pressure calculated as

$$Q_{water} = \dot{m} C_p (T_{out} - T_{in}) - \frac{\Delta P \dot{m}}{\rho}. \quad (4\text{-}12)$$

where ṁ is the water mass flow rate and C_p is the heat capacity of water at bulk temperature. The agreement between the two energy values is within ±5% with an average error of ±4.35 % and a standard deviation of 2.88% for all cases.

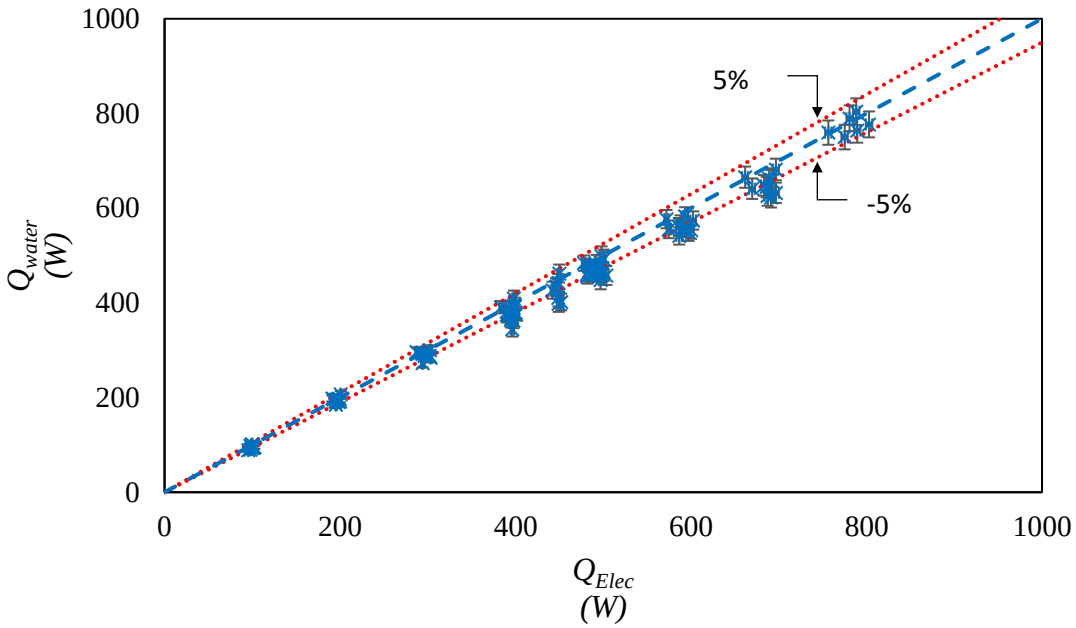

Figure 4-6 Energy balance of all experimental runs using the current fluid loop

4.5.2 Comparison of Flat Plate to Correlations

Figure 4-7 compares heat transfer results for flat surfaces at different channel heights with two correlations for laminar and turbulent heat transfer. For the turbulent flow the well-known Dittus–Boelter correlation [65] given by

$$Nu = 0.023\, Re^{0.8} Pr^{0.4}. \quad (4\text{-}13)$$

is used after multiplying it by a correction factor to account for the thermally developing flow [20,66] as

$$Nu = 0.023\, Re^{0.8} Pr^{0.4} \left[1.11 \left(\frac{Re^{0.2}}{\left(L/D_h \right)^{0.8}} \right)^{0.275} \right] \tag{4-14}$$

for $L/L_d < 1$ and

$$Nu = 0.023\, Re^{0.8} Pr^{0.4} \left[1 + \frac{0.144\, Re^{0.25}}{L/D_h} \right] \tag{4-15}$$

for $L/L_d > 1$ and such that L_d is the developing length given by

$$L_d = 0.693\, Re^{0.25} D_h. \tag{4-16}$$

While for the laminar flow, Shah and London proposed the following correlation for thermally developing flow in parallel plate under constant heat flux boundary condition [60]:

$$Nu = 2.236 \left(\frac{L}{D_h RePr} \right)^{1/3} + 0.9 \tag{4-17}$$

The experimental results showed good agreement with the corrected Dittus–Boelter correlation at high values of *Re*, (*Re* > 5000), while for lower values of *Re*, (3000 < *Re* < 5000), the maximum deviation was 17% which is reasonable within the correlation accuracy, besides, the *Nu* from the current setup is expected to deviate as the flow is not fully turbulent at this *Re* range. On the other side, the results for *Re* < 3000 didn't follow Shah and London correlation. This can be attributed to the fact that the correlation is for hydrodynamically fully developed flow which isn't the case. Also, the edges of the mating parts of the test section housing may break up the laminar boundary layer and hence, introducing some turbulence in the flow that enhance the heat transfer. It is also worth mentioning that both correlations consider the entire circumference of the channels are heated at a uniform heat flux, whereas only one side of the current channel is heated.

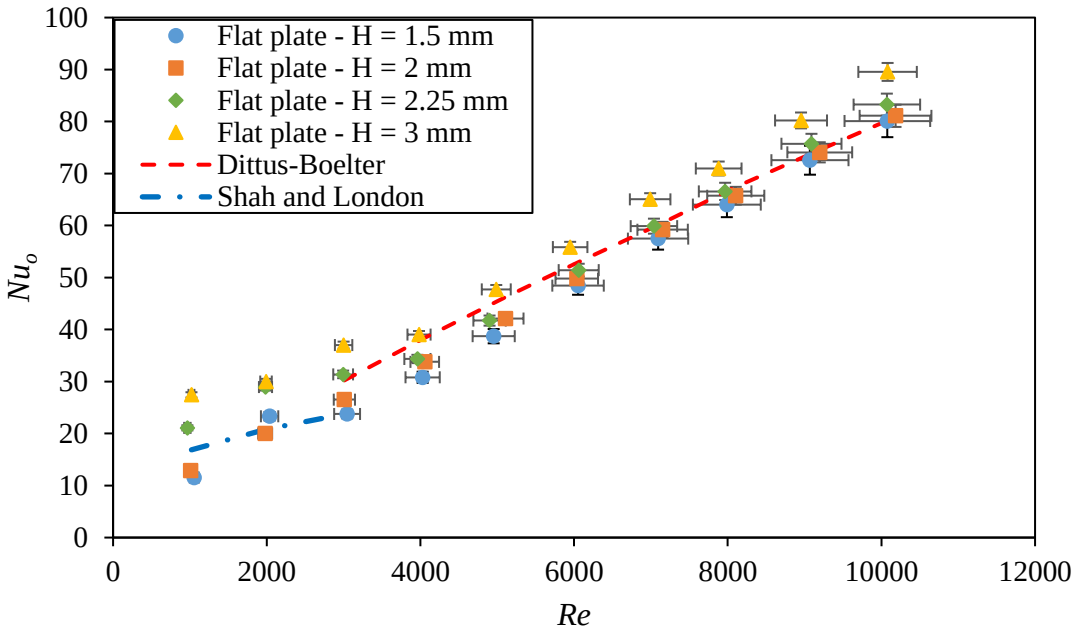

Figure 4-7: Comparison of current facility's flat plate Nu number with correlations (4-14) & (4-17)

Figure 4-8 compares the friction factor results for flat surfaces at different channel heights with Blasius correlation for smooth pipe for $Re > 3000$ [75] given by

$$f = \frac{0.3164}{(Re^*)^{0.25}} \tag{4-18}$$

such that Re^* is the modified Reynolds number proposed by Jones [70] to ensure a geometrical similarity between circular ducts and rectangular channels in calculating the friction factor given by

$$Re^* = \left[\frac{2}{3} + \frac{11H}{24W}\left(2 - \frac{H}{W}\right)\right] Re \tag{4-19}$$

and the fully developed friction factor equation for rectangular channels given by Shah and London [60] for $Re < 3000$:

$$fRe = 96(1 - 1.3553\alpha + 1.9467\alpha^2 - 1.7012\alpha^3 + 0.9564\alpha^4 - 0.2537\alpha^5) \tag{4-20}$$

such that α is the aspect ratio of the rectangular channel.

For the turbulent and transition regions, (Re > 3000), Blasius correlation overpredicted the friction factor. This discrepancy is attributed to the relatively small height of the channels that is comparable to the boundary layer thickness, and since there is large temperature gradient occurring in the boundary layer that affects the temperature dependent properties i.e., viscosity, the shear stress between the layers of the fluid and between the fluid and the channel walls is altered.

Regarding the laminar region, (Re < 3000), Eq. (4-20) underpredicts the friction factor. We conjecture that this is mainly because the flow is hydrodynamically developing while the equation requires a fully developed flow.

Overall, the heat transfer and pressure loss measurements for the flat plates are reasonable given the high-aspect ratio channel shape and the two simultaneously developing boundary layers.

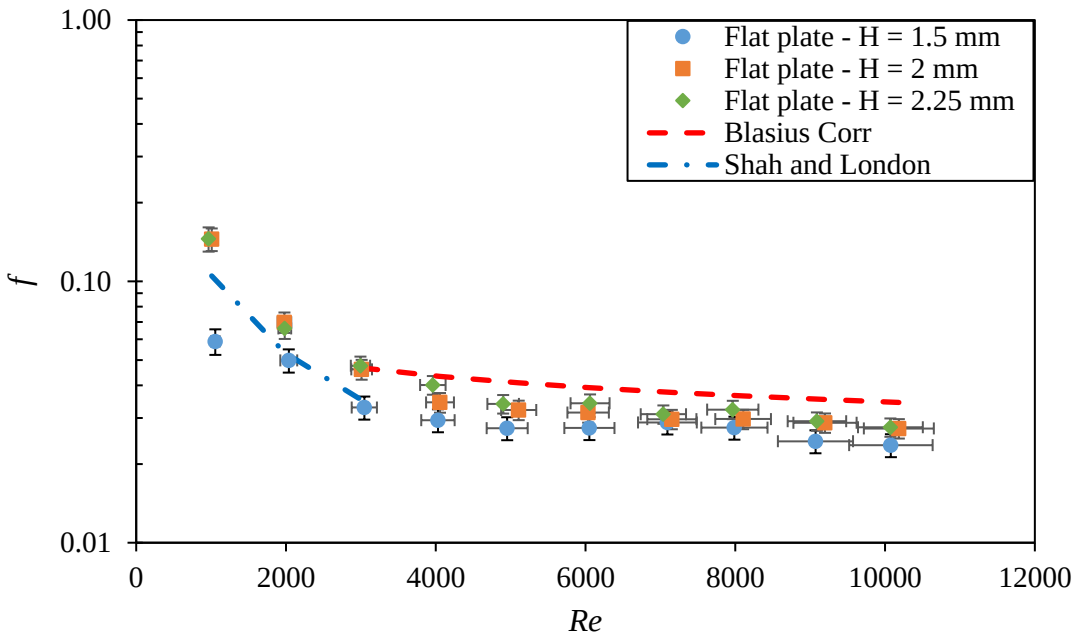

Figure 4-8: Comparison of current facility's flat plate friction factor with correlation (4-18) & (4-20)

4.5.3 Effect of Tip Clearance

Figure 4-9 compares Nusselt number, Nu_h, of the GRIPMetal Standard hooks array over the tested range of *Re* for the four tip-clearance-to-hooks-height ratios, C/h = 0, 0.33, 0.5 and 1. For all cases, Nu_h follows an increasing trend with *Re* and increasing the tip-clearance-to-hooks-height ratio, C/h, at any given *Re* decreases the Nu_h of the channel, attaining the same behavior seen in Chapter 3. It is noted that the Nu_h for C/h = 0 and 0.33 cases are very comparable for $Re < 6000$, whereas, for C/h = 0.5 and 1 the Nu_h is almost 20% and 37.5% lower than C/h = 0 on average over the same range of *Re*. This can be explained as follows; first, the presence of the clearance allows a portion of the fluid flow to bypass the array resulting in lower velocities across the array, thus lowering the heat transfer coefficient. Second, the presence of the tip clearance with the sharp end of the presented hooks generates severe vortex shedding and turbulence associated with the separated shear layers induced by such sharp end. This promotes the fluid mixing and consequently, enhances the heat transfer. These two counter-effects are the reasons for the comparable values of Nu_h for C/h = 0 and 0.33 cases.

Whereas at high tip clearance value, i.e., C/h = 1, the domination of shear layer separation over the tip clearance becomes insignificant, thus lowering the heat transfer drastically compared to no tip clearance case. While for the C/h = 0.5 the latter effect is mildly enhancing the fluid mixing, hence, resulting in less degrading of the heat transfer than the C/h = 1. For $Re > 6000$, the turbulence associated with the flow itself is the dominant factor which means that the channel whose array is exposed to relatively higher approach velocity will incur the highest heat transfer coefficient i.e., no tip clearance case. For instance, at *Re* = 10,000 the Nu_h for C/h = 0.33, 0.5 and 1 cases are 55%, 67% and 75% lower than the C/h = 0 case, respectively.

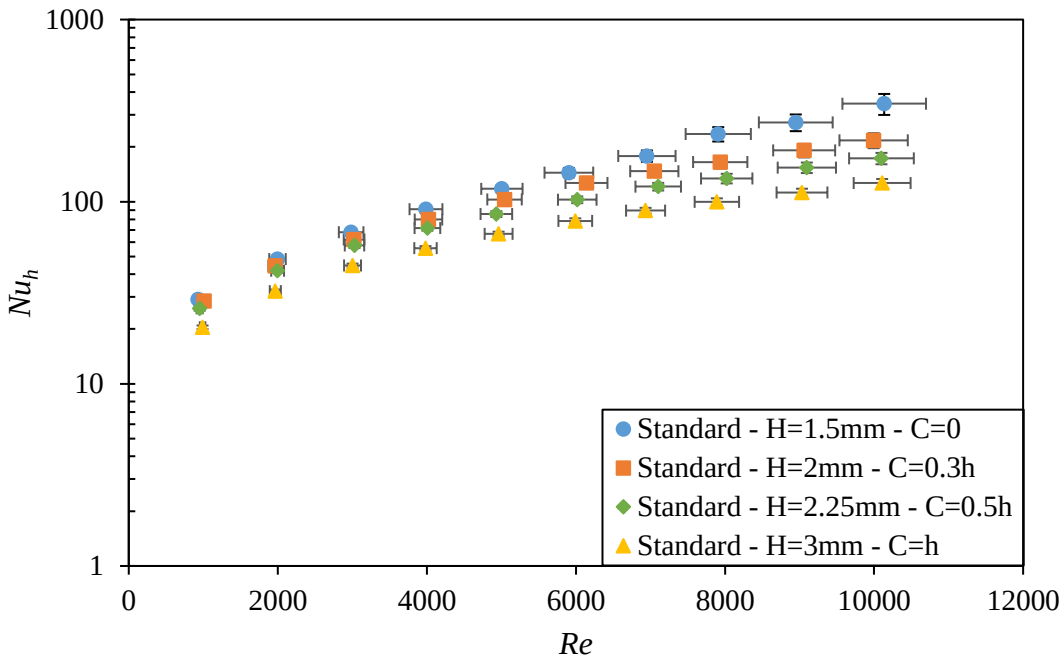

Figure 4-9:Nu_h vs Re for rectangular channels with array of Standard hooks at different values of C/h

Figure 4-10 shows the hydraulic diameter based Nusselt number, Nu_{Dh}, for the array of GRIPMetal Standard hooks at various values of *C/h* normalized by the corresponding Nusselt number for flat plate, Nu_o. The flat plate tests were conducted at the same channel height corresponding to each *C/h* value, i.e., the hydraulic diameter is constant for any given channel. This ratio represents the heat transfer enhancement factor due to the presence of the array of hooks. This enhancement is due to i) the addition of more heat transfer surface area which is 20~25% more than the flat plate area, and ii) the enhanced fluid mixing and the promoted boundary layer separation. This ratio is greater than unity for all tested channels, indicating that the presence of these arrays enhanced heat transfer.

The enhancement factor for *C/h* = 0.33 case, in fact, is generally the highest case, except when *Re* > 8000 where the no tip clearance case, *C/h* = 0, takes over which is mainly due to the superiority of *C/h* = 0 case heat transfer capabilities at the same *Re* range as shown in Figure 4-9. The enhancement factor is proportional to the *Re* with typical ranges of 5.2~ 8.4 and 5.8 ~ 7.2 for *C/h* = 0 and 0.33 respectively. While for *C/h* = 0.5 and 1 cases, this enhancement ratio is 3.5 and 2.8, respectively, at *Re* = 1000; then, it increases with increasing *Re* until it becomes independent of

Re reaching an asymptotic value of 6 and 5.4, respectively, at *Re* = 4000. This indicates that there is an insignificant change in the velocity seen by the array with further increasing of *Re* at these two values of *C/h* leading to an almost-invariant value for the heat transfer enhancement which is consistent with the findings in Chapter 3.

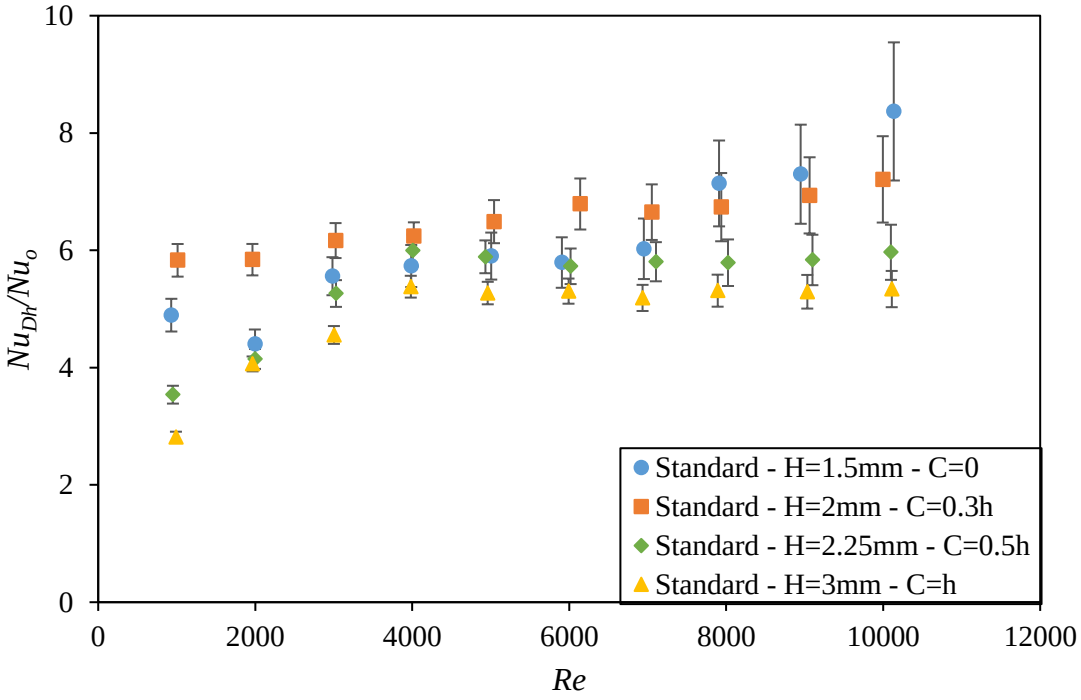

Figure 4-10: Nu_h / Nu_o vs Re for rectangular channels with array of Standard hooks at different values of C/h

Figure 4-11 depicts the friction factor, f_h, for the GRIPMetal Standard hooks array at different tip-clearance-to-hooks-height ratios over the tested range of *Re*. For *Re* < 4000, the friction factor of all cases follows a declining trend with *Re*, while for *Re* > 4000 the friction factor becomes independent of *Re*. This indicates that even for low *Re*, i.e., *Re* = 1000, the flow is already in the transition region then the flow could be considered fully turbulent for *Re* > 4000. because the frictional losses are dominant. An interesting and somewhat surprising finding in Figure 4-11 is that the f_h for *C/h* = 0.3 case is 6~56% higher than *C/h* = 0 case depending on the *Re*, besides, the f_h for *C/h* = 0.5 case is somehow comparable to the *C/h* = 0 case.

From the literal sense, increasing the tip clearance produces a gap with lower resistance to the flow, which consequently lowers the average flow velocities through the array itself and hence,

reducing the friction factor. However, as mentioned while discussing the heat transfer characteristics, there is another competing factor which is the vortex shedding and turbulence generated a top of the sharp end of the hooks. And the current observation implies that these vortices have a domain of influence beyond the vicinity of the top surface, especially for relatively small values of *C/h*. Therefore, for *C/h* = 0.3 such phenomenon has a significant effect that resulted in higher friction factor despite of the presence of a gap. On the other hand, the f_h for *C/h* = 1 case is lower than other cases. Here, further increasing of the tip clearance creates a bypass flow that lowers the average flow velocity through the array itself, hence decreasing the skin friction between the fins and the fluid.

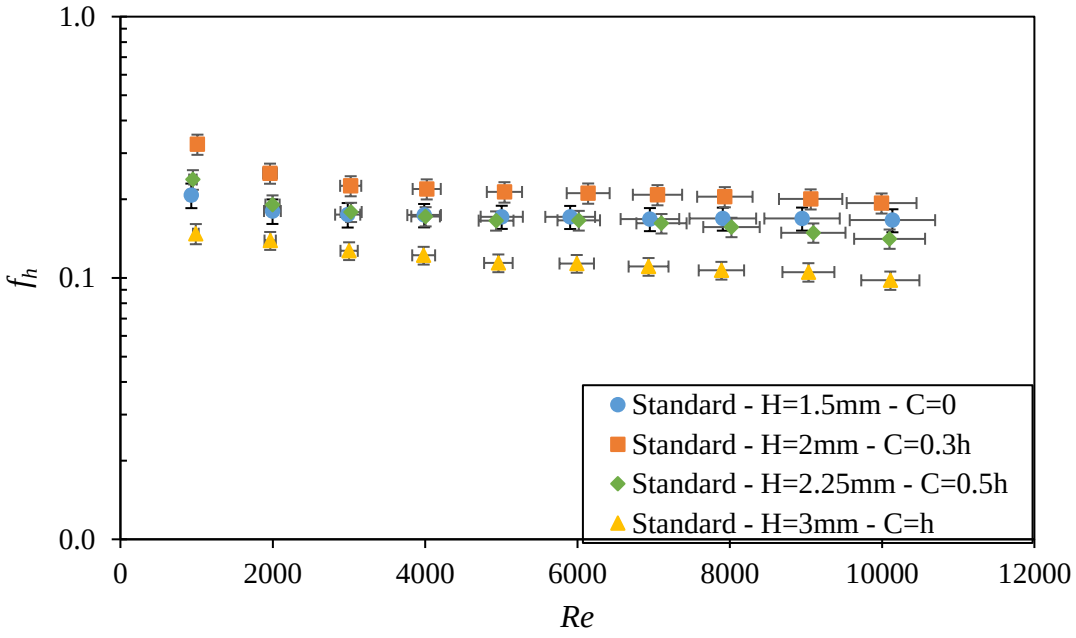

Figure 4-11: f_h vs Re for rectangular channels with array of Standard hooks at different values of C/h

The assessment of the performance of these different values of tip clearances is measured by the overall thermal performance factor, η, and shown in Figure 4-12. According to the plot, η is independent of the value of *C/h* for *Re* > 3000 except for *C/h* = 0 that shows a superior performance at *Re* = 8000 and above. This can be related to the discrepancy of Nu_h for this case from the others shown in Figure 4-9 at the same *Re* range. For *Re* < 3000, the thermal performance factor of *C/h* = 0.33 is showing a decline trend with increasing *Re*, however the factor for the other three cases fluctuates between 2.1 and 2.5. Having η greater than unity for all cases, proves that the

enhancement occurred in the heat transfer due to the presence of these arrays outweighs the added penalty of pressure drop. The maximum value of η is 3.5 for C/h = 0 at Re = 10,000, whereas the minimum value is 2.1 for C/h = 0.5 at Re = 1000 and 2000.

Since different values of C/h have comparable η, implementing a given value in a liquid cooled heat sink or a cold plate should be based on other factors such as maximum allowable temperature, pressure drop limitations and volume constraints.

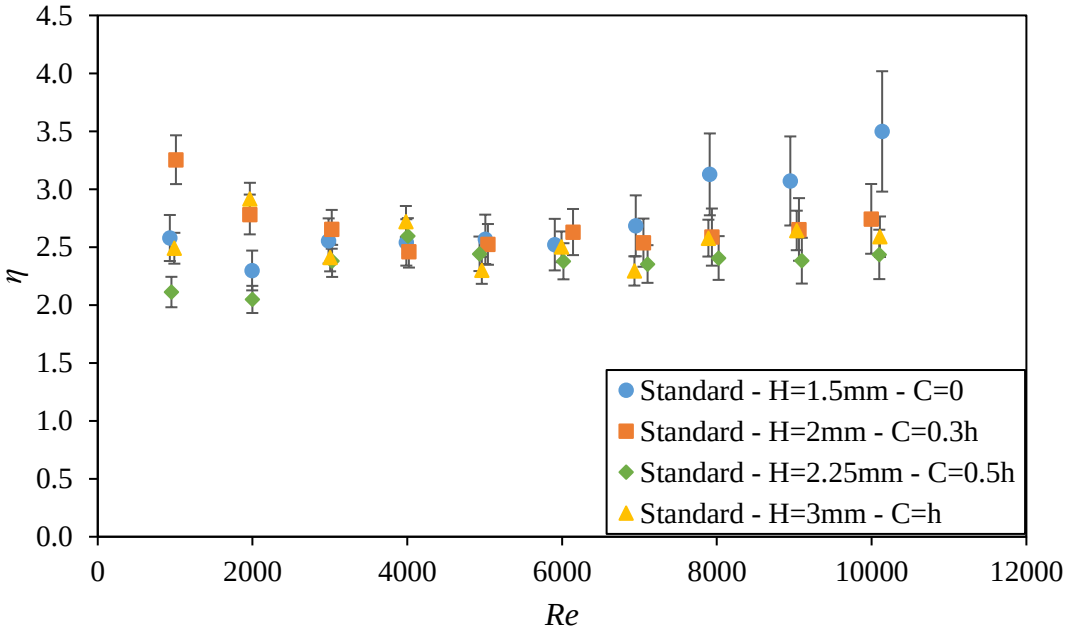

Figure 4-12: η vs Re for rectangular channels with array of Standard hooks at different values of C/h

4.5.4 Nusselt Number Correlations

The Nusselt number, Nu_h, in Figure 4-9 was correlated through a nonlinear multiple variable regression analysis. The correlation took the following form as a function of Re and C/h:

$$Nu_h = a\, Re^b \left(1 + {}^{C}/_{h}\right)^d Pr^{0.4} \qquad (4\text{-}21)$$

where *Pr* is the Prandtl number of the water at the mean bulk temperature. Including *Pr* in the correlation will allow potential users to easily assess different fluids. An attempt was made to generate a single correlation for the whole range of *Re*; however, the correlation could not predict Nu_h accurately enough for low *Re* range, *Re* < 4000 such that the root mean square error (RMSE) was 20%. This can be attributed to the fact that the flow has two different regimes along the tested *Re* range; Laminar and transitional flow for *Re* < 4000 and turbulent flow for *Re* > 4000. The reason that the flow is believed to be turbulent at *Re* > 4000 is the flattening of the friction factor curves in Figure 4-11. Therefore, two sperate correlations were developed for both regimes. The first correlation is for *Re* < 4000

$$Nu_h = 0.068\, Re^{0.7788}\left(1 + {}^{C}/_{h}\right)^{-0.6128} Pr^{0.4} \qquad \text{for } Re \leq 4000, \tag{4-22}$$

while the other correlation is for *Re* > 4000

$$Nu_h = 0.0013\, Re^{1.262}\left(1 + {}^{C}/_{h}\right)^{-1.256} Pr^{0.4} \qquad \text{for } Re \geq 4000. \tag{4-23}$$

Figure 4-13 demonstrates the comparison between the experimental data and the abovementioned correlations. The ordinate represents the Nu_h normalized by $Pr^{0.4}$ and $(1+C/h)^n$ in a log scale such that *n* is the exponent defined in correlations (4-22) and (4-23). The RMSE between predictions using these correlations and the experimental data are 5% and 9.7%, respectively.

The value of Reynolds number's exponent for (4-22) is approaching the 0.8 power dependence of the flat plate's heat transfer, supporting the claim that in this range the flow isn't laminar instead it is transitional. The Reynolds number index for correlation (4-23) is greater than unity, indicating that the flow might be turbulent as it exhibits higher dependency on *Re* than (4-22). The exponent of *C/h* for correlation (4-23) suggests that Nu_h for at this range of *Re* is becoming more dependent of the tip-clearance-to-hooks-height ratio as seen in Figure 4-9.

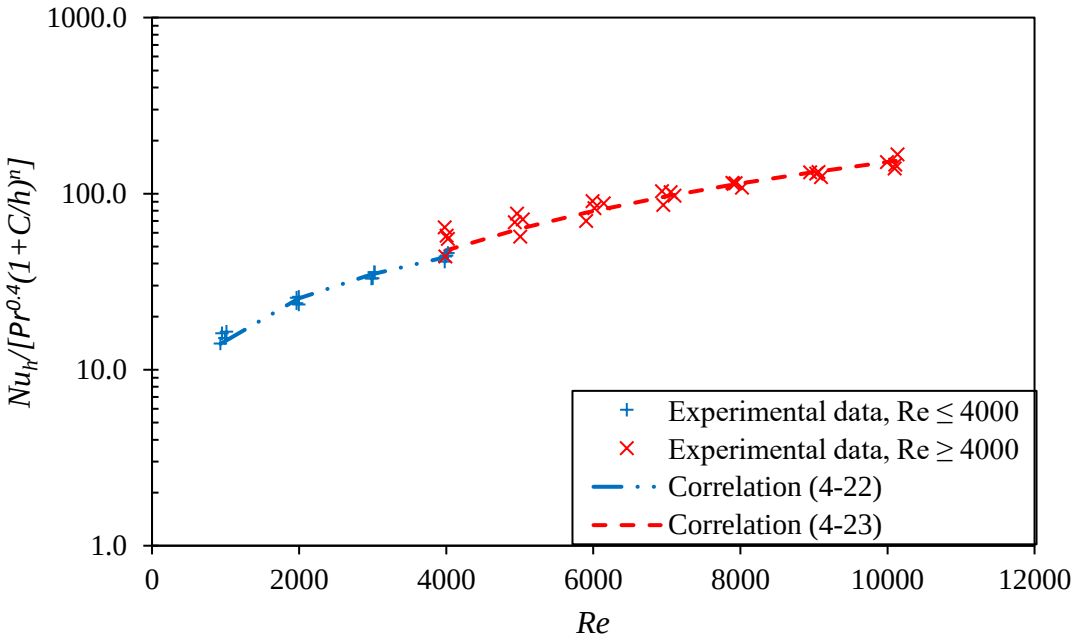

Figure 4-13: Comparison between correlations of Nu_h and experimental data for Standard hooks array

4.5.5 Friction Factor Correlations

The friction factor, f_h, shown in Figure 4-11 was also correlated through performing nonlinear multiple variable regression analysis. Inspired by the friction factor correlations in the literature, the correlation took the following form as a function of *Re* and *C/h*:

$$f_h = \left[a\,(\log Re)^b + d\left(C/h\right)^e\right]^{-2}. \tag{4-24}$$

It was impossible to correlate f_h for all channels with different *C/h* values to a single correlation. Thus, two sperate correlations were developed for the whole range of *C/h*. The first correlation,

$$f_h = \left[1.075\,(\log Re)^{0.6242} - 1.12\left(C/h\right)^{1.2}\right]^{-2} \quad \text{for } 0 \le C/h \le 0.33, \tag{4-25}$$

is for channels with *C/h* values between 0 and 0.33.

The other correlation,

$$f_h = \left[0.1029\,(\log Re)^{1.805} + 1.88\left(C/h\right)^{0.5157}\right]^{-2} \quad \text{for } 0.33 \leq C/h \leq 1, \qquad (4\text{-}26)$$

is for the with *C/h* values between 0.33 and 1. The presence of channel *C/h* = 0.33 in both correlations is to check the validity of correlation (4-25) for intermediate values of *C/h*.

Figure 4-14 shows a comparison of the experimental data of f_h with its corresponding predicted values implementing correlation (4-25) and (4-26). The RMSE between predictions using these correlations and the experimental data are 5% and 4.14%, respectively.

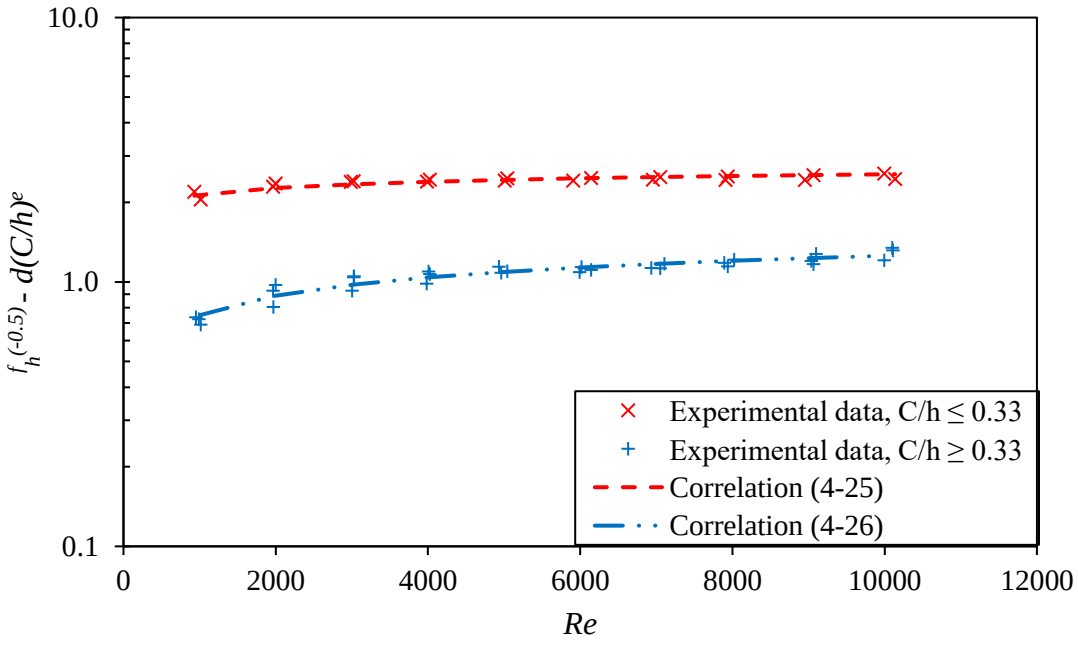

Figure 4-14: Comparison between correlations of f_h and experimental data for Standard hooks array

4.5.6 Effect of Hook Geometry

Figure 4-15 and Figure 4-16 demonstrate the Nu_h and f_h for three different arrays of hooks at *C/h* = 0 over the range of *Re*, respectively. These three arrays have different streamwise and spanwise spacings between hooks and different hook size. One of these arrays is the Standard array that was tested in the previous sections while the other two additional arrays are named "Heavy" and "Mini"

hooks (see geometrical parameters given in Table 2-1). These figures will help to understand how the geometrical parameters of GRIPMetal arrays affect the heat transfer and pressure drop characteristics. As expected, Figure 4-15 depicts that the Nu_h increases with *Re* irrespective of the hook type. Except for Heavy hooks at *Re* > 8000, results for the three types of hooks collapse onto a single straight line. This shows that the inter-fin spacings and hook shape have negligible effect on the heat transfer properties of these arrays for the tested *Re* range. In addition, the correlations provided in the previous section can be used to determine the heat transfer performance of all types of GRIPMetal array for $0 \leq C/h \leq 0.3$.

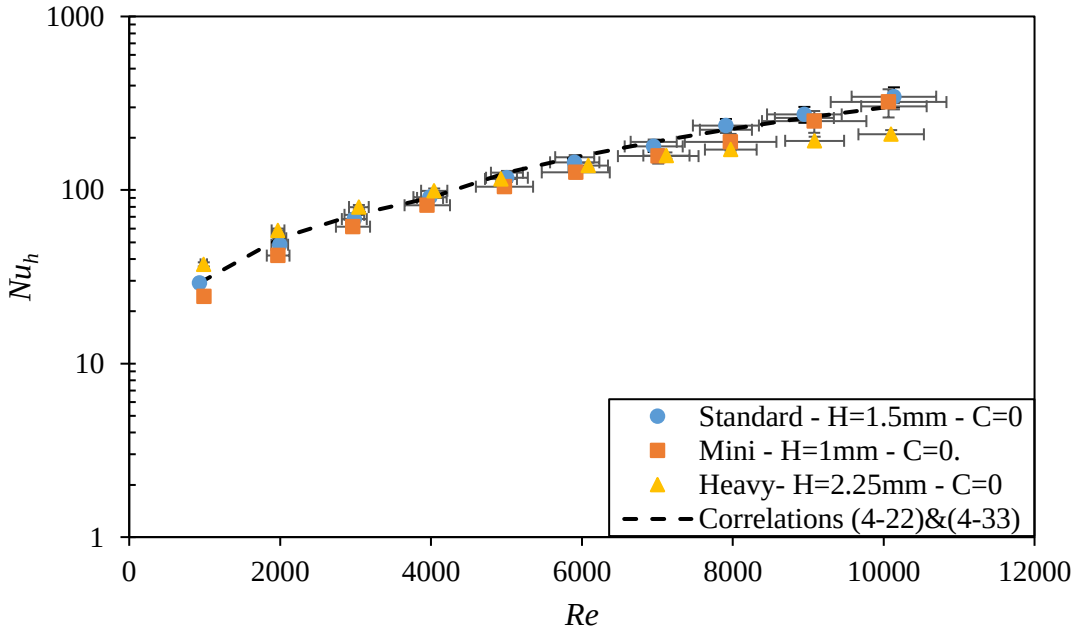

Figure 4-15: Nu_h vs Re for rectangular channels with arrays of different types of hooks at C/h = 0

On the other hand, it is noted from Figure 4-16 that f_h for the Standard and Heavy hooks is no longer a function of *Re* once *Re* is greater than 2000, while there is a slight decline with increasing *Re* observed for f_h of the Mini hooks. It should be noted that Heavy hooks yields a higher friction factor across the range of the tested *Re*. At *Re* = 1,000, the increase can be as large as 100% when compared to Standard hooks, whereas it drops to 65% for *Re* = 10,000. This dramatic increase in f_h can be attributed to the increase in the frontal blockage area of the heavy hooks, which subsequently generates larger drag to the flow when compared to other types. Although, the Mini hook array has spanwise spacings that are almost half those of the Standard and Heavy hooks that

should increase the pressure drop incurred by this array, it is thought that the inertial losses due to drag is more dominant for the current case.

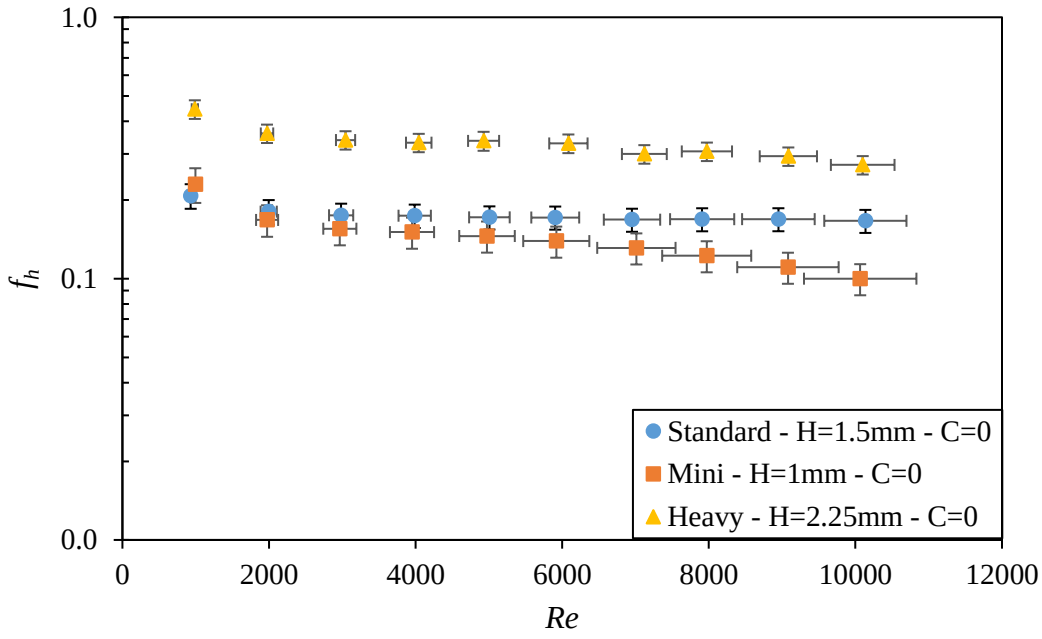

Figure 4-16: f_h vs Re for rectangular channels with arrays of different types of hooks at C/h = 0

4.6 Summary & Conclusions

In this experiment, the thermal and hydrodynamic performance of different GRIPMetal hooks arrays developed by NUCAP Industries Inc. was characterized and compared to that of flat plates. Also, predictive correlations were obtained from the resultant data to serve as design tools for liquid cooled thermal management applications. Such arrays are an attractive option for convective heat transfer enhancement due to their manufacturing simplicity and speed, low cost, and commercial availability in the market.

An evaluation of the performance for an array of GRIPMetal Standard hooks with a nominal height, h = 1.5 mm, at tip-clearance-to-hooks-height ratio, C/h, from 0 to 1 was provided. The results were obtained for Reynolds number ranging from 1,000 to 10,000 using water as working fluid. The arrays were applied to single major wall of the rectangular channel resembling most of the power electronics cooling applications such that the heat is supplied to single wall. Then at C/h

= 0, two more arrays with hooks of h = 1 mm and h = 2.25 mm, and different inter-fin spacings were tested. The results show that these hooks have good potential to serve as liquid cooled heat sinks or cold plates and the following conclusions can be drawn:

- The array of Standard hooks improved the heat transfer capabilities of the rectangular channel when compared to flat surfaces. The value of such enhancement depends on the value of tip-clearance-to-hooks-height ratio, C/h. Maximum enhancement in heat transfer was found to be for C/h = 0.33 for Re up to 8000 with a factor of 5.8 ~ 6.7. For Re > 8000, the no tip clearance case, C/h = 0, takes over with an enhancement ratio of 8.4 at Re = 10,000.
- While for C/h = 0.5 and 1 cases, the heat transfer augmentation was the lowest at low Re, then it increases with increasing Re untill it maintains a relatively constant factor of 6 and 5.4, respectively, regardless of the Re. This indicates that further increasing of Re further results in trivial change in the velocity seen by the array.
- A slight increase in tip-clearance-to-hooks-height ratio, from 0 to 0.33, results in comparable values of Nu_h from the array. The shear layer separated from the sharp edge of the top surface of the hooks and the portion of the flow bypassing the array through the clearance gap are responsible for this phenomenon.
- When the clearance gap is sufficient wide, C/h = 1, the heat transfer decreases significantly compared to no tip clearance case, which is consistent with [18]. At intermediate clearance, C$/h$ = 0.5 less deterioration of the heat transfer than the C/h = 1.
- The friction factor, f_h, of the channel with tip-clearance-to-hooks-height ratio, C/h = 0.33, is the greatest with a declining trend with Re despite of the having a small gap atop of the hooks. This can be attributed to the vortex shedding and turbulence generated a top of the sharp end of the hooks. On the other hand, the f_h for C/h = 1 case is the lowest. However, the friction factor for all channels is independent of Re. This f_h - Re curve flattening is consistent with [38].
- Four correlations were developed as a function of Re and C/h. Two of these correlations were obtained for the Nusselt number for two different ranges of Re, while the other two were for the friction factor for different range of C/h.
- The overall thermal performance factor, η, is independent of the value of C/h for Re < 8000 at which C/h = 0 begins outperforming other cases with η = 3.5 at Re = 10,000. The factor for other values of C/h fluctuates between 2.1 and 2.5 over the entire Re range. Generally, Standard

GRIPMetal arrays have $\eta > 1$ regardless of the value of C/h which confirms that the enhancement occurred in the heat transfer offsets the extra pressure drop.

- Geometrical parameters of the arrays of hooks (i.e., hook height and inter-fin spacings) are noticed to have minimal to almost no effect on heat transfer characteristics at $C/h = 0$. Consequently, the developed correlations of Nu_h for Standard hooks are recommended for the other two types for $C/h = 0$.
- The friction factor, f_h, of the Heavy hooks array were the highest for all any given Re. This can be attributed to attributed to the increase in the frontal blockage area of the heavy hooks, which subsequently generates larger drag to the flow when compared to other types.

Chapter 5 Development of a CFD Model

In this chapter, a numerical model was developed to predict the heat transfer and pressure drop characteristics for GRIPMetal Standard hooks arrays. A CAD model for the array was built based on the extracted dimensions in Chapter 4 using several microscopic images. The computational model was constructed using a commercial CFD software package, SOLIDWORKS Flow Simulations, implementing Lam and Bremhorst k-ε turbulence model for *Re* between 1000 and 10,000. Although the flow in this *Re* range may not be fully turbulent, Lam and Bremhorst k-ε turbulence model is a modified model with damping functions that can describe laminar, turbulent, and transitional flow [76] and has been implemented in fairly severe flow conditions with considerable accuracy [77,78]. This model is validated against the experimental data obtained in Chapter 4. The model aims to help understand the flow physics associated with GRIPMetal arrays, in addition to, optimizing their performance by studying a wider range of geometrical configurations.

5.1 Computational Domain

The hooks array is repetitive in the spanwise direction as depicted in Figure 5-1; Thus, only one unit-cell of the array is built using the actual dimensions of the test surfaces from Chapter 4, in which periodic conditions shall be applied to the sides to save the computational time.

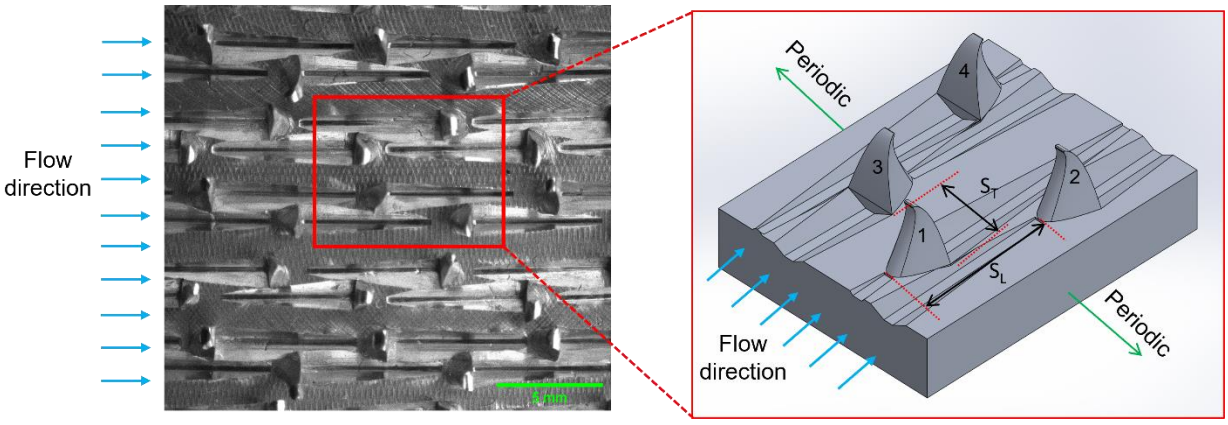

Figure 5-1 Unit cell for Standard hooks array

Figure 5-2 shows a section of the whole computational domain for the rectangular channel with *C/h* = 0. This domain resembles the test section housing used in the fluid loop facility in Chapter

4, in addition to an extra mixing region downstream of the test section in which the fluid is settled down to prevent any ambient backflow. The test section material is Al6061 alloy with a copper heater block attached to it. The test section is then surrounded by a PEEK spacer with a polycarbonate cover atop of it. The rectangular channel has a height, H, of 1.5 mm, which corresponds to $C/h = 0$ case for Standard hooks array.

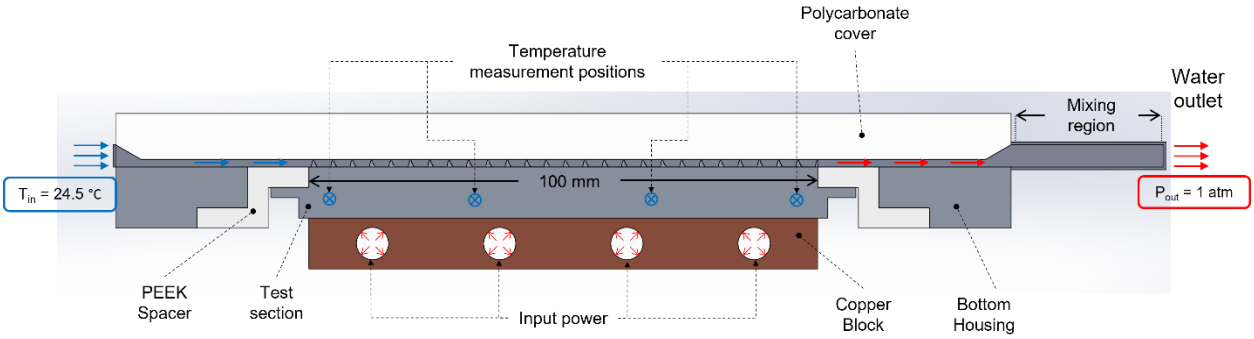

Figure 5-2 Computational domain for C/h = 0

5.2 Boundary Conditions

While the fluid across the fin array is a typical example of external convective heat transfer, the small height of the rectangular channel prohibits the development of a thick boundary layer which gives the flow the characteristics of the internal flow. Thus, the above-mentioned computational domain is solved as a steady state internal flow problem with a conjugate heat transfer. Water is used as the working fluid at atmospheric pressure with its properties being temperature dependent.

A constant temperature, T_{in}, of 24.5 $°C$ is applied at the inlet of the channel. While the inlet velocity, V_{in}, is varied to change the Reynolds number from 1000 to 10,000 with turbulence intensity of 5%. The outlet boundary condition is set as a pressure outlet at a static pressure of 1 atm for all cases and back flow of 24.5 $°C$. Periodic conditions are applied to the side walls of the domain, as shown in Figure 5-1. Constant heat flux, q_s, is applied to the surface of the cartridge heaters positions in the copper block. The heat flux is adjusted to maintain a temperature rise of 1 $°C$ in water across the domain. No slip boundary conditions are applied to all other walls with adiabatic conditions.

5.3 Solver Parameters and Turbulence Model

The governing equations used to describe the flow field are the Favre-averaged Navier-Stokes equations. These equations are discretized using a finite volume method to transform them into algebraic equations for their solution over the computational domain. Modified QUICK scheme was used to discretize both the diffusion and convective terms, while the pressure-velocity coupling problem was solved via the SIMPLE algorithm. The convergence criterion was set to 10^{-5} for all the residuals of the mass, energy and momentum balances between the inlet and the outlet. Another method for checking the solution's convergence is monitoring the behavior of important parameters such as the bulk outlet temperature, inlet pressure and solid temperature at the positions shown in Figure 5-2. Then ensuring that these parameters reach a constant value before the convergence criterion is satisfied.

The averaging step of the governing equations produces extra terms in the equations known as the Reynolds stresses. Therefore, additional information should be provided to close this system of equations. SOLIDWORKS Flow Simulation employs transport equations for the turbulent kinetic energy, k, and its dissipation rate, ε, using the modified k-ε turbulence model with damping functions proposed by Lam and Bremhorst [76].

Generally, the k-ε turbulence models were shown to be suitable for predicting the physics of the flow around pin fins with a reasonable accuracy of up to 7% error at Re = 50000 [13,45,79,80]. Whereas Lam and Bremhorst modification considers introducing damping functions that decrease the turbulent viscosity and the turbulence energy and increase the turbulence dissipation rate when the Reynolds number, based on the average fluctuations in velocity and the distance from the wall, becomes small enough. On the other hand, the damping functions wouldn't kick in, resulting in obtaining the original k - ε model [81]. In the current study, Re ranges from 1000 to 10,000, therefore, we conjecture that the flow will be in both transition and turbulent regimes.

In addition to turbulence modeling, it is also crucial to simulate fluid boundary layer near the walls correctly as the velocity and temperature gradients are very high and greatly affect the flow field parameters and consequently, affecting the overall performance of the array. SOLIDWORKDS Flow Simulation uses the two-scale wall function, *2SWF*, approach that consists of two methods

for coupling the boundary layer calculation with the solution of the bulk flow: i) a thin boundary layer approach and ii) a thick boundary layer approach [81].

The first approach is used when the number of cells across the boundary layer is not enough for direct determination of the velocity and thermal profiles. In this approach, the laminar boundary layer (viscous sublayer) is predicted through Prandtl boundary layer equations, then employing Van Driest profile instead of the well-known logarithmic profile for the turbulent layer. While the latter is used when the first cell next to the walls is small enough ($y+ \leq 1$) followed by an appropriate number of cells to resolve the boundary layer accurately. In this case the laminar boundary layers are resolved via Navier-Stokes equations as part of the core flow calculation then the turbulent layer is predicted as per the first approach.

5.4 Data Reduction

The same data reduction of Chapter 4 is employed in this chapter. Firstly, the heat transfer coefficient is calculated by averaging the temperature difference between the surface temperature, $T_{s,i}$, and its corresponding local bulk water temperature, $T_{b,i}$ as

$$\Delta T_{bulk} = \frac{\sum_{i=1}^{4}\left(T_{s,i} - T_{b,i}\right)}{4} \tag{5-1}$$

such that $T_{b,i}$ is calculated by assuming a linear rise of the water temperature along the test section and $T_{s,i}$ is determined from the temperature measurements at the positions shown in Figure 5-2 through extrapolation utilizing 1-D Fourier conduction equation

$$T_s = T_p - \frac{Q_{in}}{A_b}\left[\frac{d}{k_{Al}}\right] \tag{5-2}$$

where T_s and T_p are, respectively, the surface and the measured temperatures, Q_{in} denotes the input to the test sections, A_b is the base area (100 x 50.8 mm^2), d is the distance between the point of measuring the temperature and the surface (8 mm) and k is the thermal conductivity of Al6061 alloy, which is equal to 167 W/mK.

Then, the overall heat transfer coefficient of an array of hooks, h_{bulk}, is calculated as

$$h_{bulk} = \frac{Q_{in}}{A_b \Delta T_{bulk}} \tag{5-3}$$

It is common to present heat transfer results in the dimensionless form of a Nusselt number, *Nu*,

$$Nu = \frac{h_{bulk}\, L_c}{k} \tag{5-4}$$

where k is the thermal conductivity of water at bulk temperature, which is equal to 0.6065 W/mK, while L_c is the characteristic length, which is the hydraulic diameter of the channel, D_h, computed as

$$D_h = \frac{2(HW)}{H + W} \tag{5-5}$$

where H and W are the height and the width of the test section channel.

Secondly, the friction factor f is calculated based on the pressure drop measured at the boundaries of the test section given by

$$f = \frac{2\ \Delta \mathrm{P}\ L_c}{L_f\ V_{in}^2\ \rho} \tag{5-6}$$

where ρ is the density of water at bulk temperature, which is equal to 997 kg/m^3, ΔP is the pressure difference, and V_{in} is the mean inlet velocity to the test section.

Finally, the Reynolds number, *Re*, is defined based on the hydraulic diameter

$$Re = \frac{\rho\ \mathrm{V}_{in}\ D_h}{\mu} \tag{5-7}$$

where μ is the dynamic viscosity at water bulk temperature, which is equal to 0.9x10^{-3} Pas.

5.5 Numerical Mesh and Grid Independency

SOLIDWORKS Meshing is employed to discretize the current computational domain into hexahedral cells; Figure 5-3. For grid independence assessment, Nu_h and f_h are predicted with different element sizes at Re = 10,000. Five different meshes were examined with a total number of cells of about 0.25, 0.45, 0.89, 1.26, 1.56 and 2.8 million cells. As shown in Figure 5-4, the difference in Nu_{Dh} between the coarsest mesh (0.25 million cells) and the finest one (2.8 million cells) is 26 %, while Figure 5-5 indicates that this difference decreases to 8.6 % for f_{Dh}. Thus, a conservative value of 1.56 million cells is chosen as it has almost the same values for Nu_{Dh} and f_{Dh} as the finest mesh.

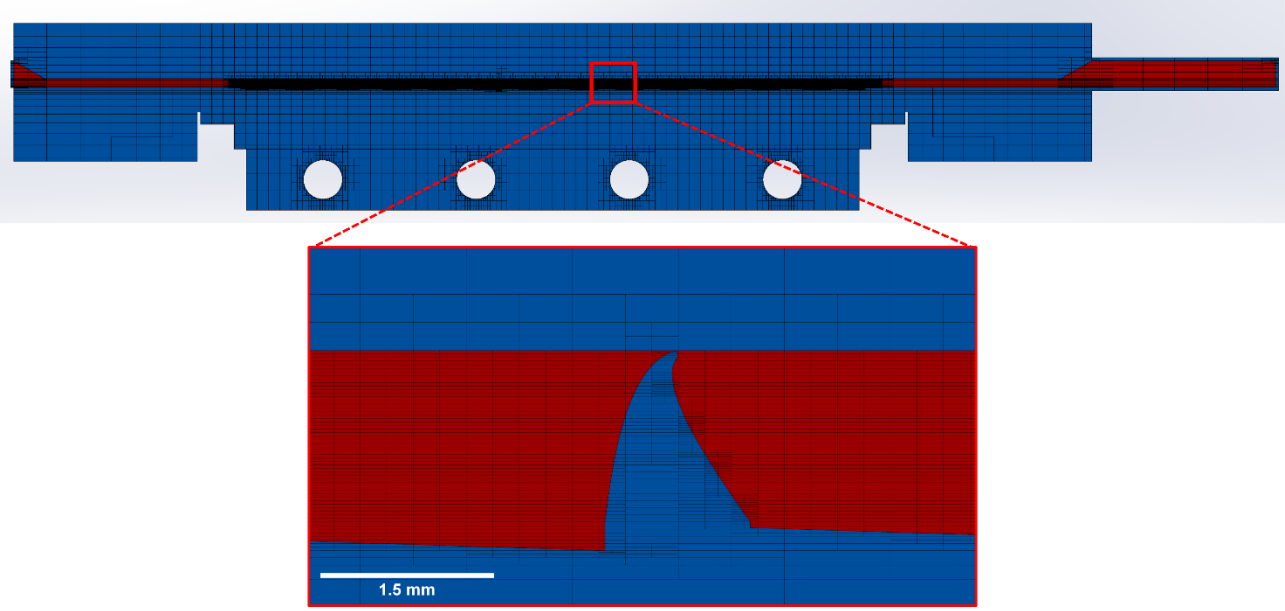

Figure 5-3 Meshing details of the fluid (Red) and the solid domains (Blue)

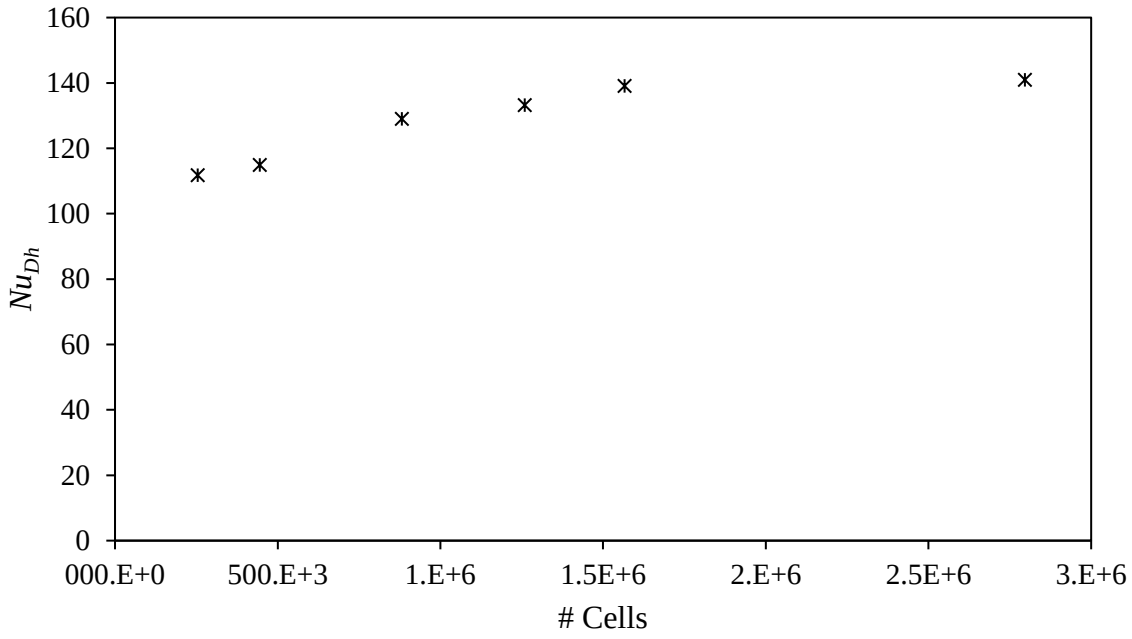

Figure 5-4 Nu_{Dh} for Standard hooks array at different grid sizes at Re = 10,000

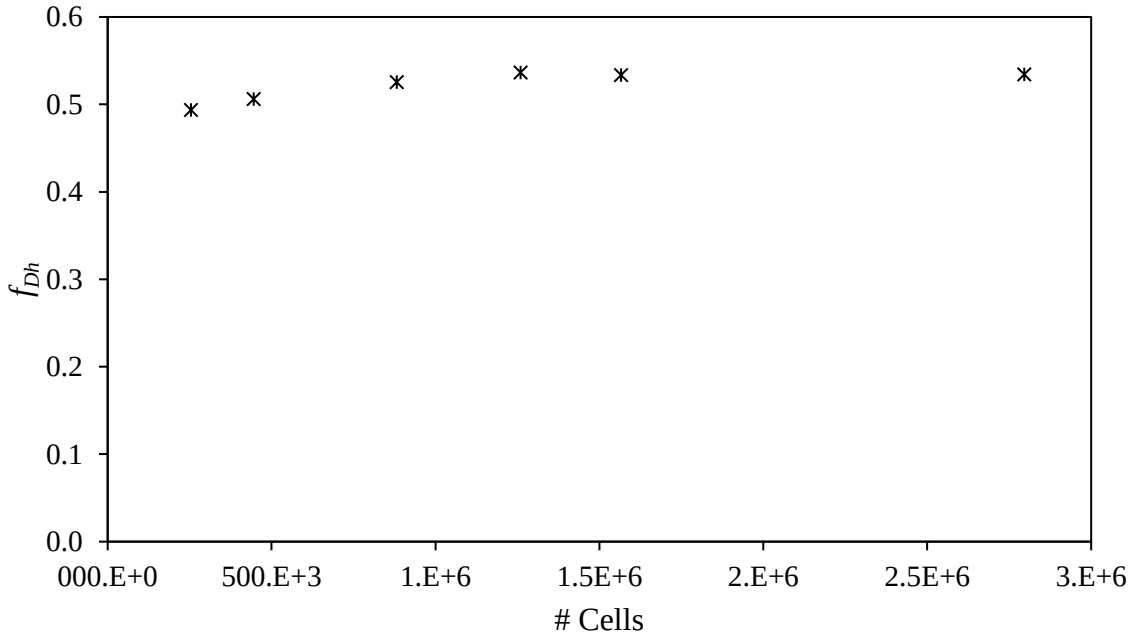

Figure 5-5 f_{Dh} for Standard hooks array at different grid sizes at Re = 10,000

5.6 Results

5.6.1 Numerical Validation

The numerical model is validated against the experimental data obtained in Chapter 4. Figure 5-6 compares the Nusselt number, Nu_{Dh}, predicted numerically and their corresponding experimental results for a flat plate and Standard hooks array at $C/h = 0$. At a low Re number of 1000, the numerical results agree with experimental data with a 9% and 2 % discrepancy for the Standard hooks array and flat plate, respectively. However, as the Re increases beyond 1000, the numerical model begins to underpredict Nu_{Dh} for both cases. The model underpredicts the Nu_h for the flat plate by an average value of 35% for $Re > 2000$. This sudden deviation is claimed to be attributed to the inaccurate resolving of the boundary layer that led to slow development of the velocities in the near-wall regions while it is sharper in the experiments[82,83]. The discrepancy between the numerical results and the experimental data is somehow consistent for the flat plate, which isn't the case for the Standard hook array. For instance, at $Re = 2000$, there is a 20% reduction in the Nu_{Dh} predicted by the numerical model compared to the experimental value for the Standard hooks array. This underprediction is further pronounced when Re increases. This is because more rigorous vortices and wakes shedding are generated in the flow field as Re increases that should led to diminish the flow reattachment length downstream of the fin, however, this length is underpredicted in the model due to overprediction of turbulent viscosity [83]. It is conjectured that this is the reason that the discrepancy is getting worse as Re increases such that at $Re = 10{,}000$ the model severely underpredicts the turbulence intensity resulting in 80% reduction of Nu_{Dh}.

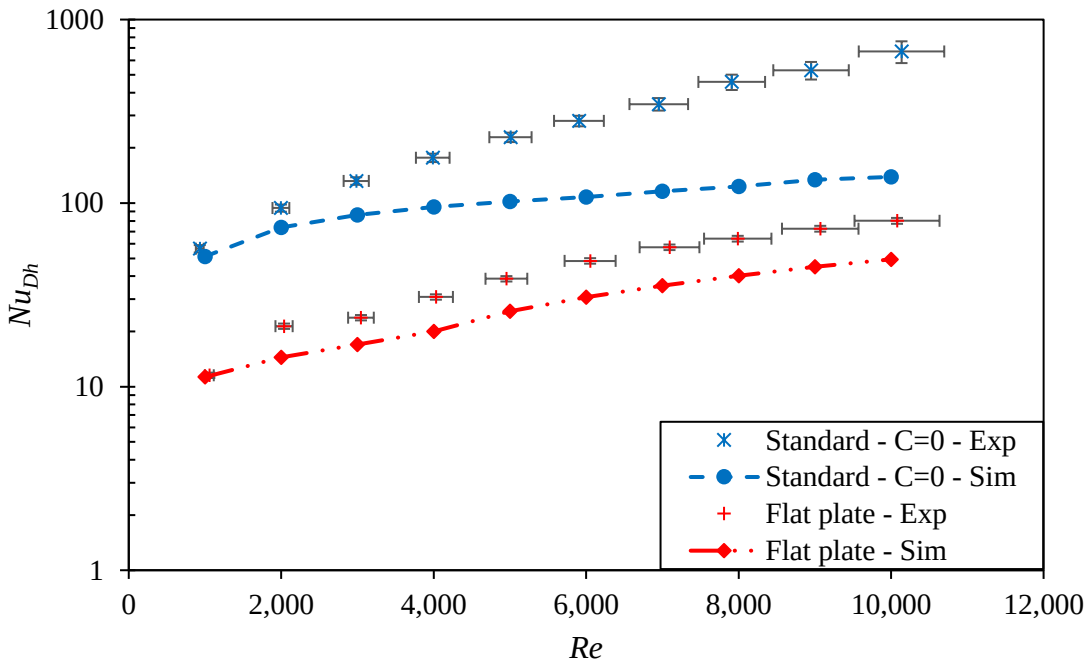

Figure 5-6 Comparison between Nu_{Dh} predicted numerically for flat plate and Standard hooks array and their corresponding values obtained from the experiments.

Figure 5-7 compares the friction factor, f_{Dh}, predicted numerically and their corresponding experimental results for a flat plate and Standard hooks array at $C/h = 0$. For the flat plate, the numerical model underpredicted the friction factor by an average of 16.6 % compared to that measured in Chapter 4. This can be attributed to the inconsistency in the surface roughness of the actual channel (different materials), which isn't captured by the simulations. In addition, the high-aspect ratio channel shape generates strong vortices at the corners and near the walls, making it hard for the model to predict the boundary layer accurately. Regarding the Standard hook array, the numerical model overpredicts the flow friction factor by an average of 68 % over the entire range of *Re* which is consistent with the finding of [84]. This discrepancy is thought to be linked to the same reason of underprediction in the $Nu_{Dh,}$. That will cause the separation of the flow around the hooks to be pulled forward, besides the backside pressure recovery due to flow reattachment will be underpredicted, causing excess drag losses to the flow.

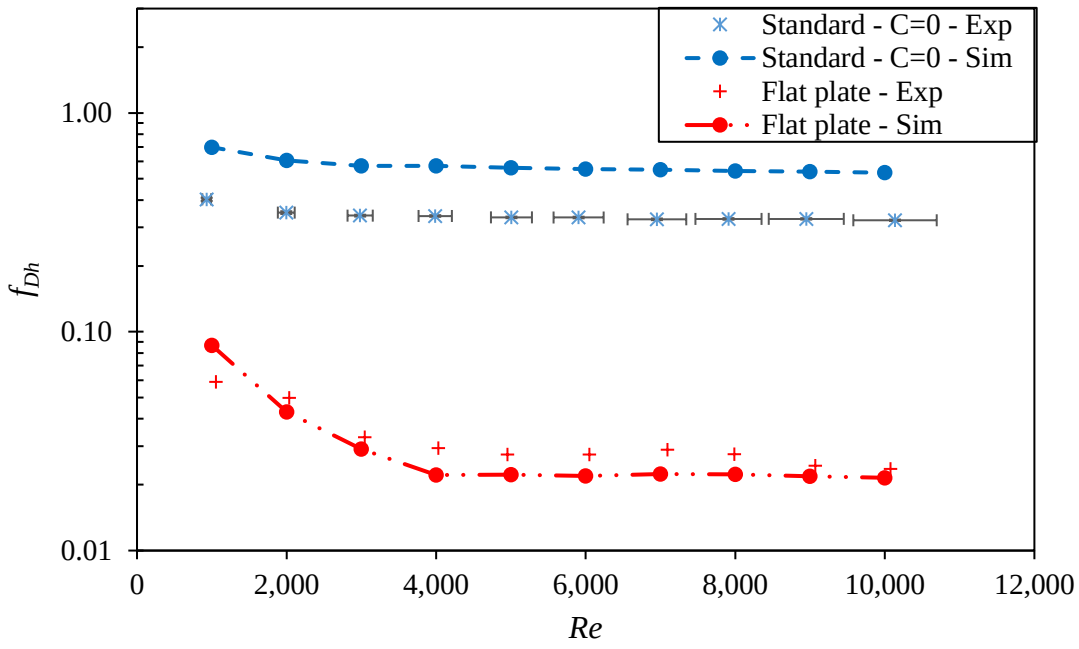

Figure 5-7 Comparison between f_{Dh} predicted numerically for flat plate and Standard hooks array and their corresponding values obtained from the experiments.

In addition, there is a potential variation between the actual and modeled geometry, i.e., the hooks profile, and the variations of interfin spacings among the same arrays. A preliminary analysis showed that such variation greatly affects the flow behaviour through these arrays. However, a more comprehensive sensitivity study should be carried out to investigate this claim further.

5.6.2 Flow Streamlines and Velocity and Temperature Distributions

Although the numerical model did not show perfect agreement with the experimental results, the velocity distribution contours might offer some physical insight into the flow field in terms of heat transfer and pressure drop.

Figure 5-8 and Figure 5-9 show the streamlines and velocity contours at the middle plane of the hooks i.e., at 0.75 mm from the endwall of the test surface at *Re* = 1000 and 10,000, respectively. First, it is noted that for both cases there is a considerable amount of the fluid flows in the gap between the two opposing groups of adjacent hooks. This is because this spanwise gap is larger than clearance between each two adjacent hooks, thus, offering less resistive flow path for the fluid. On this basis, it is recommended that this gap along with the clearance between each two

adjacent hooks is optimized to prevent such phenomenon. Second, it is clearly seen that the wake region downstream of the hooks at a given *Re* isn't the same, however, it depends on the position of the dimple with respect to the hook. When the dimple is upstream of the hook, i.e., upper group of hooks, the wake region is larger than when the dimple is downstream of the hook, i.e., bottom group of hooks. This is mainly due to two reasons: i) the hooks have a parabolic cross-sectional shape such that the flow is approaching the streamlined face in the bottom group pushing back the separation point, ii) the presence of the dimple downstream the hook allows for faster flow reattachment. Besides, the horseshoe vortex upstream of the hooks can be seen more clearly for the bottom group. This indicates that the upper region of the array exhibits lower heat transfer than the bottom one. Thus, another optimization possibility is to have only the bottom group orientation exists in the array i.e., all the dimples are downstream of the hooks.

In addition, the wake region for the whole array at *Re* = 1000 is different from the *Re* = 10,000 case which implies that the flow regimes in both cases aren't the same. That's why the model predicting a declining trend for the friction factor with increasing *Re* then at a specific *Re* the friction factor reaches an asymptotic value indicating that the flow has become fully turbulent already.

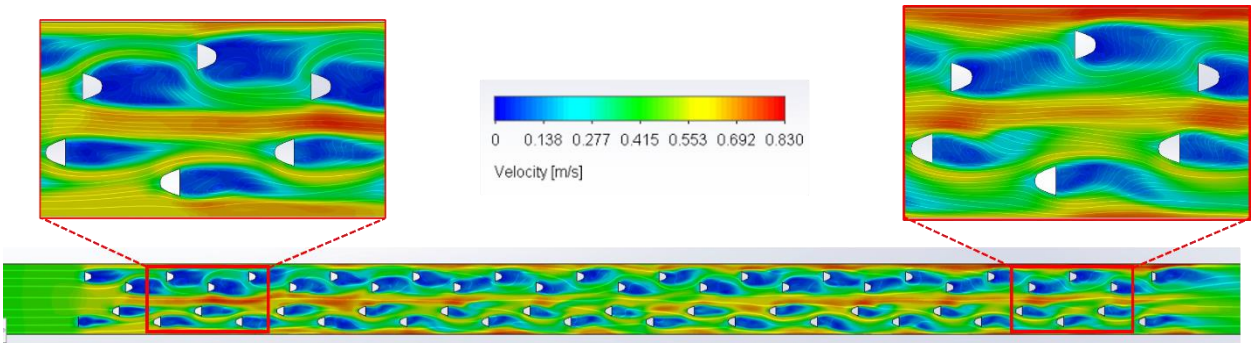

Figure 5-8 Velocity contours and streamlines for Standard hooks at Re = 1000 (flow direction from left to right)

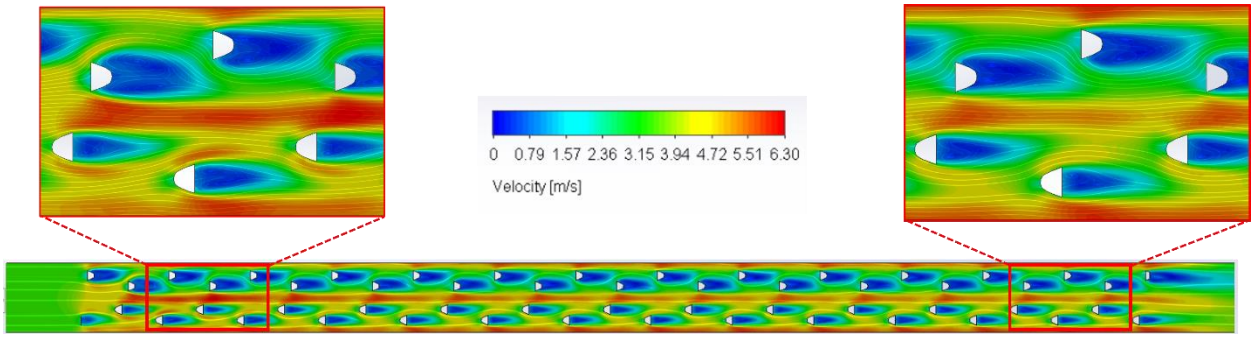

Figure 5-9 Velocity contours and streamlines for Standard hooks at Re = 10,000 (flow direction from left to right)

Figure 5-10 compares the temperature contours at the middle plane of the hooks i.e., at 0.75 mm from the endwall of the test surface between *Re* = 1000 and *Re* = 10,000 cases. The figure indicates slower development for the fluid temperature for the bottom hooks group comparable to the upper hooks group. In the latter, the large wake region downstream the hooks causes the heated fluid to be not washed away by the flow stream, thus lowering the heat transfer coefficient at such regions.

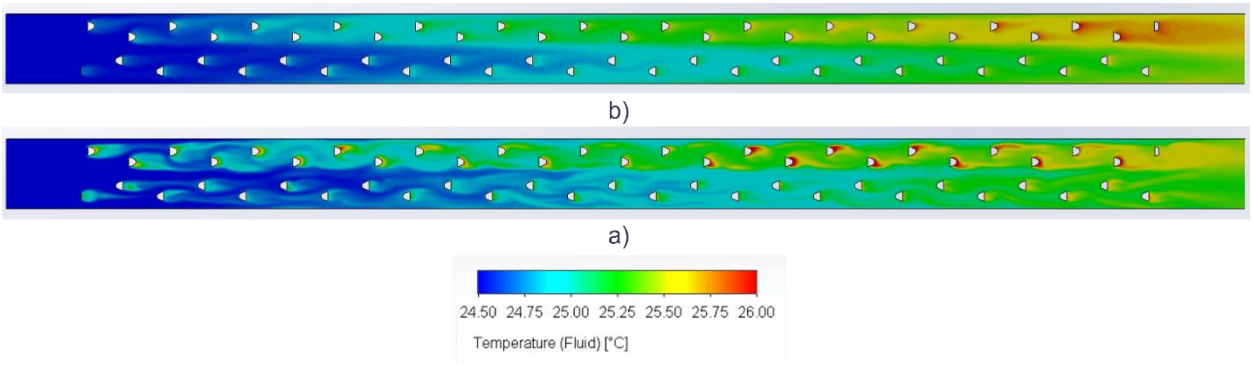

Figure 5-10 A comparison of temperature contours for Standard hooks at a) Re = 1,000 and b) Re = 10,000 (flow direction from left to right)

5.7 Conclusion

In this chapter, a numerical model was developed to assess the thermal and hydrodynamic performances of GRIPMetal Standard hooks array employed in a rectangular channel and compare them to that of a flat plate. The model aimed to help understanding the flow physics associated with GRIPMetal arrays, and leveraging their performance by optimizing their geometrical parameters (inter-fin spacings, orientations, etc.)

The computational model was constructed using SOLIDWORKS Flow Simulations software. Lam and Bremhorst k-ε turbulence model was employed for *Re* ranging between 1000 and 10,000 with water as working fluid.

The numerical results were validated against the experimental data from Chapter 4. For the flat plate, the numerical results underpredicted the Nu_{Dh} by an average of 35% for $Re \geq 2000$, while it showed great agreement with experiments at $Re = 1000$. In terms of f_{Dh}, the numerical model underpredicted the friction factor by an average of 16.6 % compared to the experimental data. On the other hand, the model severely underpredicted the Nu_{Dh} for Standard hooks array such that the maximum deviation was 80% at $Re = 10{,}000$. While it overpredicted the f_h for the array by a value of 68% on average for the whole range of *Re*.

We conjecture that the inaccurate resolving of the boundary layer, the delayed development of the velocity profile in the near-wall regions and the deviation of the manufactured array from the developed CAD model, are likely the reasons for this discrepancy.

The examination of velocity and temperature distributions indicated that the heat transfer coefficient isn't consistent throughout the whole array, however, it depends on the relative position between the hook and its corresponding dimple. On this basis, possible optimization techniques are proposed to leverage the heat transfer capabilities of such array.

Chapter 6 CONCLUSIONS AND FUTURE WORK

6.1 Summary and Conclusions

The convective heat transfer from GRIPMetal surfaces is enhanced by the means of novel arrays of hook-shaped fins and dimples on metal surfaces (trademarked as GRIPMetal) skived on the heat transfer surfaces by NUCAP Industries. The objective of this thesis was to develop models and design tools that aim to help designing GRIPMetal arrays with the optimum performance and provide a good fundamental understanding for their thermal and hydrodynamic performances. These enhanced surfaces have the potential for commercial viability, due to the ease, speed and the relatively low cost of their manufacturing process when compared to other manufacturing technologies. GRIPMetal arrays can be employed in building novel heat exchange devices such as heat sinks, cold plates, or heat exchanger.

Results showed that GRIPMetal arrays provides higher heat transfer but induces a larger pressure drop, compared to flat plate surfaces. The heat transfer is mainly augmented by i) the formation of horseshoe vortices at the fin-endwall junction downstream of the fin breaking up the wall boundary layer; ii) the presence of strong vortices and secondary vortices caused by the dimples and the adverse pressure gradients and flow separation downstream of the fin. These two phenomena produce a complex pattern of flow and strong turbulent mixing of the mainstream flow that consequently enhance the heat transfer but increases the pressure drop.

In Chapter 3, a comparative experimental study was conducted on the heat transfer and pressure drop characteristics of rectangular channels with GRIPMetal arrays of different configurations. The arrays were applied to the two opposing major walls of the channel at four different tip-clearance-to-hooks-height ratio, C/h. This study was implemented with air as the working fluid in an open circuit wind tunnel. The results yielded that these hooks have good potential for practical air-side heat transfer enhancement with the penalty of increasing the friction factor. The enhancement value depends on the Reynolds number and the value of C/h. A maximum enhancement in heat transfer of 4.6 compared to flat surfaces occurred for $C/h = 1$ case, however, it showed the greatest friction factor penalty among all cases. Four different correlations were

established for the Nusselt number and friction factor that can be used as design tools to employ these hooks in any given application.

While in Chapter 4, the GRIPMetal hooks arrays were tested for different Reynolds number range using water as working fluid. The arrays configuration in the channel were also different such that the arrays were applied to bottom major wall of the channel in which the heat is applied. The tip-clearance-to-hooks-height ratio, *C/h*, varied from 0 to 1 to investigate its effect on the thermal and the hydraulic performances of the array. The results showed a comparable heat transfer augmentation for no clearance and low level of clearance cases, however, lower heat transfer augmentation is observed as the clearance is increased further, This behavior can be credited to the production of additional vortices along the tips of the hooks and the increased wake shedding in the system, but for increased values of tip clearance, the effect of fluid bypassing the array becomes dominant, and the resulting reduction in flow rate within the array itself decreased the heat transfer capabilities of the array [36,37] . Also, predictive correlations were obtained from the resultant data to serve as design tools for liquid cooled thermal management applications. Geometrical parameters of the arrays of hooks were noticed to have minimal to almost no effect on heat transfer and a considerable effect on pressure drop.

A numerical model was developed in Chapter 5 as an attempt to better understand the thermal and the hydrodynamic performances of GRIPMetal Standard hooks array in a rectangular channel. The computational domain was built and solved using SOLIDWORKS Flow Simulation software implementing Lam and Bremhorst k-ε turbulence model. Model validation was carried out through a comparison between the data acquired in Chapter 4 and the numerical results. Generally, the model overpredicted the flow friction factor across the array and underpredicted the array Nusselt number; predictions worsen at higher Reynolds numbers. The lower estimation of turbulence intensity in the array, less aggressive turbulence in the resolved boundary layer and the difference in the manufactured surfaces and the developed CAD model likely account for such discrepancy. The examination of velocity and temperature distributions yielded that the heat transfer coefficient varies spatially through the array due to distinction in the relative position between the hook and its corresponding dimple.

6.2 Future Work

The work presented in this thesis consists of preliminary studies that demonstrate the viability of using GRIPMetal arrays in heat exchange applications and investigate the effects of some of their geometrical parameters. Nevertheless, there exist much work to be done regarding the comprehensive characterization of the thermal and the hydrodynamic performances of such arrays, for example:

- Further investigations of the GRIPMetal Heavy and Mini hooks arrays at different tip-clearance-to-hooks-height ratio.
- Expand the experiments conducted in Chapter 4 to study the performance of GRIPMetal arrays in the laminar flow region.
- Testing of different fluids such as refrigerants or oils to broaden the applicability of the correlations proposed for the Nusselt number and the friction factor.
- Exploratory experiments regarding the flow structures should be conducted and the links between the turbulence quantities and the performance of the hooks arrays need to be explored in more details.
- Development of numerical model using other available turbulence models seeking more promising accuracy. This model will help to understand the physics of the flow and allow for leverage the performance of these arrays through optimizing their geometrical parameters and configuration.

References

[1] C. Qian, A.M. Gheitaghy, J. Fan, H. Tang, B. Sun, H. Ye, G. Zhang, Thermal Management on IGBT Power Electronic Devices and Modules, IEEE Access. 6 (2018) 12868–12884. https://doi.org/10.1109/ACCESS.2018.2793300.

[2] A. Elkholy, O. Khaled, R. Kempers, Twisted Offset Strip Fin Heat Sink For Power Electronics Cooling, Intersoc. Conf. Therm. Thermomechanical Phenom. Electron. Syst. ITHERM. 2021-June (2021) 9–17. https://doi.org/10.1109/ITherm51669.2021.9503158.

[3] R. Wu, Y. Fan, T. Hong, H. Zou, R. Hu, X. Luo, An immersed jet array impingement cooling device with distributed returns for direct body liquid cooling of high power electronics, Appl. Therm. Eng. 162 (2019) 114259. https://doi.org/10.1016/j.applthermaleng.2019.114259.

[4] A. Elkholy, C. Unlusoy, R. Kempers, Thermal performance of a two-phase loop thermosyphon with an additively manufactured evaporator, Appl. Therm. Eng. 202 (2022) 117692. https://doi.org/10.1016/j.applthermaleng.2021.117692.

[5] A. Elkholy, R. Kempers, A compact integrated thermosyphon heat sink for power electronics cooling, ASME Int. Mech. Eng. Congr. Expo. Proc. 8 (2019) 1–9. https://doi.org/10.1115/IMECE2019-11777.

[6] A.J. Robinson, J. Colenbrander, T. Deaville, J. Durfee, R. Kempers, A wicked heat pipe fabricated using metal additive manufacturing, Int. J. Thermofluids. 12 (2021) 100117. https://doi.org/10.1016/j.ijft.2021.100117.

[7] M. Wong, I. Owen, C.J. Sutcliffe, A. Puri, Convective heat transfer and pressure losses across novel heat sinks fabricated by Selective Laser Melting, Int. J. Heat Mass Transf. 52 (2009) 281–288. https://doi.org/10.1016/j.ijheatmasstransfer.2008.06.002.

[8] A.J. Robinson, R. Kempers, J. Colenbrander, N. Bushnell, R. Chen, A single phase hybrid micro heat sink using impinging micro-jet arrays and microchannels, Appl. Therm. Eng.

136 (2018) 408–418. https://doi.org/10.1016/j.applthermaleng.2018.02.058.

[9] R. Kempers, J. Colenbrander, W. Tan, R. Chen, A.J. Robinson, Experimental characterization of a hybrid impinging microjet-microchannel heat sink fabricated using high-volume metal additive manufacturing, Int. J. Thermofluids. 5–6 (2020) 100029. https://doi.org/10.1016/j.ijft.2020.100029.

[10] S.C. Siw, A.D. Fradeneck, M.K. Chyu, M.A. Alvin, The effects of different pin-fin arrays on heat transfer and pressure loss in a narrow channel, in: Proc. ASME Turbo Expo, 2015: pp. 1–9. https://doi.org/10.1115/GT2015-43855.

[11] K.S. Yang, W.H. Chu, I.Y. Chen, C.C. Wang, A comparative study of the airside performance of heat sinks having pin fin configurations, Int. J. Heat Mass Transf. 50 (2007) 4661–4667. https://doi.org/10.1016/j.ijheatmasstransfer.2007.03.006.

[12] T. Yeom, T. Simon, T. Zhang, M. Zhang, M. North, T. Cui, Enhanced heat transfer of heat sink channels with micro pin fin roughened walls, Int. J. Heat Mass Transf. 92 (2016) 617–627. https://doi.org/10.1016/j.ijheatmasstransfer.2015.09.014.

[13] A. Sakanova, K.J. Tseng, Comparison of pin-fin and finned shape heat sink for power electronics in future aircraft, Appl. Therm. Eng. 136 (2018) 364–374. https://doi.org/10.1016/j.applthermaleng.2018.03.020.

[14] L. Chen, R.G.A. Brakmann, B. Weigand, R. Poser, Q. Yang, Detailed investigation of staggered jet impingement array cooling performance with cubic micro pin fin roughened target plate, Appl. Therm. Eng. 171 (2020) 115095. https://doi.org/10.1016/j.applthermaleng.2020.115095.

[15] F.Z. Bakhti, M. Si-Ameur, A comparison of mixed convective heat transfer performance of nanofluids cooled heat sink with circular perforated pin fin, Appl. Therm. Eng. 159 (2019) 113819. https://doi.org/10.1016/j.applthermaleng.2019.113819.

[16] V. Choudhary, M. Kumar, A.K. Patil, Experimental investigation of enhanced performance of pin fin heat sink with wings, Appl. Therm. Eng. 155 (2019) 546–562.

https://doi.org/10.1016/j.applthermaleng.2019.03.139.

[17] A. Žkauskas, Heat transfer from tubes in crossflow, in: Adv. Heat Transf., Elsevier, 1987: pp. 87–159.

[18] A. Žukauskas, Heat Transfer from Tubes in Crossflow, in: J.P. Hartnett, T.F.B.T.-A. in H.T. Irvine (Eds.), Elsevier, 1972: pp. 93–160. https://doi.org/https://doi.org/10.1016/S0065-2717(08)70038-8.

[19] O.P. Bergelin, Heat transfer and fluid friction during flow across banks of tubes-IV a study of the transition zone between viscous and turbulent flow, Trans. ASME. 74 (1952) 953–960.

[20] G.J. VanFossen, Heat transfer coefficients for staggered arrays of short pin fins, in: Proc. ASME Turbo Expo, 1981. https://doi.org/10.1115/81-GT-75.

[21] M.K. Chyu, Heat transfer and pressure drop for short pin-fin arrays with pin-endwall fillet, Proc. ASME Turbo Expo. 4 (1989). https://doi.org/10.1115/89-GT-99.

[22] M.K. Chyu, Y.C. Hsing, T.I.P. Shih, V. Natarajan, Heat Transfer Contributions of Pins and Endwall in Pin-Fin Arrays: Effects of Thermal Boundary Condition Modeling, J. Turbomach. 121 (1999) 257–263. https://doi.org/10.1115/1.2841309.

[23] M.K. Chyu, R.J. Goldstein, Influence of an array of wall-mounted cylinders on the mass transfer from a flat surface, Int. J. Heat Mass Transf. 34 (1991) 2175–2186. https://doi.org/10.1016/0017-9310(91)90044-F.

[24] E.M. Sparrow, J.W. Ramsey, Heat transfer and pressure drop for a staggered wall-attached array of cylinders with tip clearance, Int. J. Heat Mass Transf. 21 (1978) 1369–1378. https://doi.org/10.1016/0017-9310(78)90200-4.

[25] D.E. Metzger, R.A. Berry, J.P. Bronson, DEVELOPING HEAT TRANSFER IN RECTANGULAR DUCTS WITH ARRAYS OF SHORT PIN FINS., in: Am. Soc. Mech. Eng., 1981.

[26] J. Armstrong, D. Winstanley, A Review of Staggered Array Pin, J. Turbomach. 110 (1988) 94–103.

[27] O.N. Sßara *, Performance analysis of rectangular ducts with staggered square pin fins, Energy Convers. Manag. 44 (2003) 1787–1803. https://doi.org/10.1016/S0140-6701(03)92683-X.

[28] M.K. Chyu, V. Natarajan, Heat transfer on the base surface of three-dimensional protruding elements, Int. J. Heat Mass Transf. 39 (1996) 2925–2935. https://doi.org/10.1016/0017-9310(95)00381-9.

[29] E.M. Sparrow, J.W. Ramsey, C.A.C. Altemani, Experiments on in-line pin fin arrays-and performance comparisons with staggered arrays, J. Heat Transfer. 102 (1980) 44–50. https://doi.org/10.1115/1.3244247.

[30] S.A. Lawson, A.A. Thrift, K.A. Thole, A. Kohli, Heat transfer from multiple row arrays of low aspect ratio pin fins, Int. J. Heat Mass Transf. 54 (2011) 4099–4109. https://doi.org/10.1016/j.ijheatmasstransfer.2011.04.001.

[31] K.K. Ferster, K.L. Kirsch, K.A. Thole, Effects of geometry, spacing, and number of pin fins in additively manufactured microchannel pin fin arrays, J. Turbomach. 140 (2018) 1–10. https://doi.org/10.1115/1.4038179.

[32] M.E. Lyall, A.A. Thrift, K.A. Thole, A. Kohli, Heat transfer from low aspect ratio pin fins, J. Turbomach. 133 (2011). https://doi.org/10.1115/1.2812951.

[33] E.M. Sparrow, D.S. Kadle, Effect of tip-to-shroud clearance on turbulent heat transfer from a shrouded, longitudinal fin array, J. Heat Transfer. 108 (1986) 519–524. https://doi.org/10.1115/1.3246965.

[34] S. V. Garimella, P.A. Eibeck, Heat transfer characteristics of an array of protruding elements in single phase forced convection, Int. J. Heat Mass Transf. 33 (1990) 2659–2669. https://doi.org/10.1016/0017-9310(90)90202-6.

[35] B.A. Jubran, M.A. Hamdan, R.M. Abdualh, Enhanced heat transfer missing pin, and optimization for cylindrical pin fin arrays, J. Heat Transfer. 115 (1993) 576–583. https://doi.org/10.1115/1.2910727.

[36] M.K. Chyu, C.H. Yen, W. Ma, T.I.-P. Shih, Effects of Flow Gap Atop Pin Elements on the Heat Transfer From Pin Fin Arrays, in: Vol. 3 Heat Transf. Electr. Power; Ind. Cogener., American Society of Mechanical Engineers, 1999: pp. 0–3. https://doi.org/10.1115/99-GT-047.

[37] K.A. Moores, Y.K. Joshi, Effect of tip clearance on the thermal and hydrodynamic performance of a shrouded pin fin array, J. Heat Transfer. 125 (2003) 999–1006. https://doi.org/10.1115/1.1621897.

[38] S.C. Siw, M.K. Chyu, T.I.P. Shih, M.A. Alvin, Effects of pin detached space on heat transfer and pin-fin arrays, J. Heat Transfer. 134 (2012) 1–9. https://doi.org/10.1115/1.4006166.

[39] K.A. Moores, J. Kim, Y.K. Joshi, Heat transfer and fluid flow in shrouded pin fin arrays with and without tip clearance, Int. J. Heat Mass Transf. 52 (2009) 5978–5989. https://doi.org/10.1016/j.ijheatmasstransfer.2009.08.005.

[40] H. Tabkhi, A. Nayebzadeh, Y. Peles, Experimental and numerical local heat transfer study on micro pin fin with tip clearance, Appl. Therm. Eng. 179 (2020) 115756. https://doi.org/10.1016/j.applthermaleng.2020.115756.

[41] M. D, C. Fan, S. Haley, Effects of pin shape and array orientation on heat transfer and pressure loss in pin fin arrays, J. Eng. Gas Turbines Power. 106 (1984) 252–257. https://doi.org/10.1115/GT2010-23227.

[42] M.K. Chyu, Y.C. Hsing, V. Natarajan, Convective Heat Transfer of Cubic Fin Arrays in a Narrow Channel, J. Turbomach. 120 (1998) 362–367. https://doi.org/10.1115/1.2841414.

[43] Q. Li, Z. Chen, U. Flechtner, H.J. Warnecke, Heat transfer and pressure drop characteristics in rectangular channels with elliptic pin fins, Int. J. Heat Fluid Flow. 19 (1998) 245–250. https://doi.org/10.1016/S0142-727X(98)00003-4.

[44] Z. Chen, Q. Li, D. Meier, H.J. Warnecke, Convective heat transfer and pressure loss in rectangular ducts with drop-shaped pin fins, Heat Mass Transf. Und Stoffuebertragung. 33 (1997) 219–224. https://doi.org/10.1007/s002310050181.

[45] N. Sahiti, A. Lemouedda, D. Stojkovic, F. Durst, E. Franz, Performance comparison of pin fin in-duct flow arrays with various pin cross-sections, Appl. Therm. Eng. 26 (2006) 1176–1192. https://doi.org/10.1016/j.applthermaleng.2005.10.042.

[46] J. Xi, J. Yao, P. Su, J. Lei, J. Wu, T. Gao, Heat transfer and pressure loss characteristics of Pin-Fins with Different Shapes in a wide channel, in: Proc. ASME Turbo Expo, 2017: pp. 1–9. https://doi.org/10.1115/GT2013-95407.

[47] M.K. Chyu, Y. Yu, H. Ding, J.P. Downs, F.O. Soechting, Concavity Enhanced Heat Transfer in an Internal Cooling Passage, in: Vol. 3 Heat Transf. Electr. Power; Ind. Cogener., American Society of Mechanical Engineers, 1997: pp. 1–7. https://doi.org/10.1115/97-GT-437.

[48] Y. Rao, Y. Feng, B. Li, B. Weigand, Experimental and numerical study of heat transfer and flow friction in channels with dimples of different shapes, J. Heat Transfer. 137 (2015) 1–10. https://doi.org/10.1115/1.4029036.

[49] Y. Xie, H. Qu, D. Zhang, Numerical investigation of flow and heat transfer in rectangular channel with teardrop dimple/protrusion, Int. J. Heat Mass Transf. 84 (2015) 486–496. https://doi.org/10.1016/j.ijheatmasstransfer.2015.01.055.

[50] Y. Gao, Y. Feng, K. Tang, P. Hrnjak, Experimental study on forced convection hydraulic and thermal characteristics in a dimpled flat duct, Appl. Therm. Eng. 181 (2020) 115921. https://doi.org/10.1016/j.applthermaleng.2020.115921.

[51] H.K. Moon, T. O'Connell, B. Glezer, Channel height effect on heat transfer and friction in a dimpled passage, Proc. ASME Turbo Expo. 3 (1999) 307–313. https://doi.org/10.1115/99-GT-163.

[52] Y. Rao, C. Wan, Y. Xu, An experimental study of pressure loss and heat transfer in the pin

fin-dimple channels with various dimple depths, Int. J. Heat Mass Transf. 55 (2012) 6723–6733. https://doi.org/10.1016/j.ijheatmasstransfer.2012.06.081.

[53] R.W. Miller, Flow measurement engineering handbook, (1983).

[54] E.J. Davis, W.N. Gill, The effects of axial conduction in the wall on heat transfer with laminar flow, Int. J. Heat Mass Transf. 13 (1970) 459–470. https://doi.org/10.1016/0017-9310(70)90143-2.

[55] M. Faghri, E.M. Sparrow, Simultaneous wall and fluid axial conduction in laminar pipe-flow heat transfer, J. Heat Transfer. 102 (1980) 58–63. https://doi.org/10.1115/1.3244249.

[56] G. Maranzana, I. Perry, D. Maillet, Mini- and micro-channels: Influence of axial conduction in the walls, Int. J. Heat Mass Transf. 47 (2004) 3993–4004. https://doi.org/10.1016/j.ijheatmasstransfer.2004.04.016.

[57] G.S. Barozzi, G. Pagliarini, A Method to Solve Conjugate Heat Transfer Problems: The Case of Fully Developed Laminar Flow in a Pipe, J. Heat Transfer. 107 (1985) 77–83. https://doi.org/10.1115/1.3247406.

[58] B. Weigand, G. Gassner, The effect of wall conduction for the extended Graetz problem for laminar and turbulent channel flows, Int. J. Heat Mass Transf. 50 (2007) 1097–1105. https://doi.org/10.1016/j.ijheatmasstransfer.2006.06.047.

[59] S. Mikio, E. Kazuo, Effect of conduction in wall on heat transfer with turbulent flow between parallel plates, Int. J. Heat Mass Transf. 20 (1977) 507–516. https://doi.org/10.1016/0017-9310(77)90097-7.

[60] R.K. Shah, A.L. London, Laminar Flow Forced Convection in Ducts: A Source Book for Compact Heat Exchanger Analytical Data, 1978. http://www.sciencedirect.com/science/article/pii/B978012020051150022X.

[61] M.K. Chyu, E.O. Oluyede, H.K. Moon, Heat transfer on convective surfaces with pin-fins mounted in inclined angles, Proc. ASME Turbo Expo. 4 PART B (2007) 861–869.

https://doi.org/10.1115/GT2007-28138.

[62] G. Tanda, Heat transfer and pressure drop in a rectangular channel with diamond-shaped elements, Int. J. Heat Mass Transf. 44 (2001).

[63] D.L. Gee, R.L. Webb, Forced convection heat transfer in helically rib-roughened tubes, Int. J. Heat Mass Transf. 23 (1980) 1127–1136. https://doi.org/10.1016/0017-9310(80)90177-5.

[64] S.J. Kline, Describing uncertainty in single sample experiments, Mech. Eng. 75 (1953) 3–8.

[65] F.W. Dittus, L.M.K. Boelter, Heat transfer in automobile radiators of the tubular type, Int. Commun. Heat Mass Transf. 12 (1985) 3–22. https://doi.org/10.1016/0735-1933(85)90003-X.

[66] W.H. Mcadams, Heat Transmission: 3d Ed, McGraw-Hill, 1954.

[67] V. Gnielinski, Neue Gleichungen für den Wärme- und den Stoffübergang in turbulent durchströmten Rohren und Kanälen, Forsch. Im Ingenieurwes. 41 (1975) 8–16. https://doi.org/10.1007/BF02559682.

[68] V. Gnielinski, On heat transfer in tubes, Int. J. Heat Mass Transf. 63 (2013) 134–140. https://doi.org/10.1016/j.ijheatmasstransfer.2013.04.015.

[69] S.E. Haaland, Simple and explicit formulas for the friction factor in turbulent pipe flow, J. Fluids Eng. Trans. ASME. 105 (1983) 89–90. https://doi.org/10.1115/1.3240948.

[70] O.C. Jones, An Improvement in the Calculation of Turbulent Friction in Rectangular Ducts, J. Fluids Eng. 98 (1976) 173–180. https://doi.org/10.1115/1.3448250.

[71] G.I. Mahmood, M.L. Hill, D.L. Nelson, P.M. Ligrani, H.K. Moon, B. Glezer, Local heat transfer and flow structure on and above a dimpled surface in a channel, J. Turbomach. 123 (2001) 115–123. https://doi.org/10.1115/1.1333694.

[72] G.I. Mahmood, P.M. Ligrani, Heat transfer in a dimpled channel: Combined influences of aspect ratio, temperature ratio, Reynolds number, and flow structure, Int. J. Heat Mass Transf. 45 (2002) 2011–2020. https://doi.org/10.1016/S0017-9310(01)00314-3.

[73] P.M. Ligrani, M.M. Oliveira, T. Blaskovich, Comparison of heat transfer augmentation techniques, AIAA J. 41 (2003) 337–362. https://doi.org/10.2514/2.1964.

[74] E.M. Sparrow, V.B. Grannis, Pressure drop characteristics of heat exchangers consisting of arrays of diamond-shaped pin fins, Int. J. Heat Mass Transf. 34 (1991) 589–600. https://doi.org/10.1016/0017-9310(91)90108-Q.

[75] D. Taler, Determining velocity and friction factor for turbulent flow in smooth tubes, Int. J. Therm. Sci. 105 (2016) 109–122. https://doi.org/10.1016/j.ijthermalsci.2016.02.011.

[76] C.K.G. Lam, K. Bremhorst, A Modified Form of the k-ε Model for Predicting Wall Turbulence, J. Fluids Eng. 103 (1981) 456–460. https://doi.org/10.1115/1.3240815.

[77] A.A. Abbasian Arani, R. Moradi, Shell and tube heat exchanger optimization using new baffle and tube configuration, Appl. Therm. Eng. 157 (2019). https://doi.org/10.1016/j.applthermaleng.2019.113736.

[78] D. Korres, E. Bellos, C. Tzivanidis, Investigation of a nanofluid-based compound parabolic trough solar collector under laminar flow conditions, Appl. Therm. Eng. 149 (2019) 366–376. https://doi.org/10.1016/j.applthermaleng.2018.12.077.

[79] W. Jin, N. Jia, J. Wu, J. Lei, L. Liu, Numerical study on flow and heat transfer characteristics of pin-fins with different shapes, Proc. ASME Turbo Expo. 5A-2019 (2019) 1–11. https://doi.org/10.1115/GT2019-90520.

[80] W. Du, L. Luo, S. Wang, X. Zhang, Flow structure and heat transfer characteristics in a 90-deg turned pin fined duct with different dimple/protrusion depths, Appl. Therm. Eng. 146 (2019) 826–842. https://doi.org/10.1016/j.applthermaleng.2018.10.052.

[81] A. Sobachkin, G. Dumnov, Numerical Basis of CAD-Embedded CFD, NAFEMS World

Congr. 2013. (2013) 1–20.

[82] L.A. Dvorak, Turbulent Augmentation of Heat Transfer Off Pin and Endwall Surfaces in a Staggered Pin Fin Array, University of North Dakota, 2004. https://commons.und.edu/theses/3192.

[83] A.A. Igci, M.E. Arici, A comparative study of four low-Reynolds-number k - ε turbulence models for periodic fully developed duct flow and heat transfer, Numer. Heat Transf. Part B Fundam. 69 (2016) 234–248. https://doi.org/10.1080/10407790.2015.1097141.

[84] V.C. Patel, W. Rodi, G. Scheuerer, Turbulence models for near-wall and low reynolds number flows — a review, AIAA J. 23 (1985) 1308–1319. https://doi.org/10.2514/3.9086.